Advanced Technology Development Program for Lithium-Ion Batteries:

Thermal Abuse Performance of 18650 Li-Ion Cells

E. Peter Roth, Chris C. Crafts, Daniel H. Doughty, and James McBreen

Sandia National Laboratories

FreedomCAR

FreedomCAR & Vehicle Technologies Program

Advanced Technology Development Program for Lithium-Ion Batteries:

Thermal Abuse Performance of 18650 Li-Ion Cells

E. Peter Roth, Chris C. Crafts, and Daniel H. Doughty
Lithium Research and Development Department
Sandia National Laboratories
P.O. Box 5800
Albuquerque, NM 87185-0613

James McBreen
Energy Science and Technology Department
Brookhaven National Lab
Upton, NY 11973-5000

Abstract

Li-ion cells are being developed for high-power applications in hybrid electric vehicles currently being designed for the FreedomCAR (Freedom Cooperative Automotive Research) program. These cells offer superior performance in terms of power and energy density over current cell chemistries. Cells using this chemistry are the basis of battery systems for both gasoline and fuel cell based hybrids. However, the safety of these cells needs to be understood and improved for eventual widespread commercial application in hybrid electric vehicles. The thermal behavior of commercial and prototype cells has been measured under varying conditions of cell composition, age and state-of-charge (SOC). The thermal runaway behavior of full cells has been measured along with the thermal properties of the cell components. We have also measured gas generation and gas composition over the temperature range corresponding to the thermal runaway regime. These studies have allowed characterization of cell thermal abuse tolerance and an understanding of the mechanisms that result in cell thermal runaway.

This page intentionally left blank.

Executive Summary

The use of high-power Li-ion cells in hybrid electric vehicles is determined not only by the electrical performance of the cells but by the inherent safety and stability of the cells under normal and abusive conditions. The thermal response of the cells is determined by the intrinsic thermal reactivity of the cell components and the thermal interactions in the full cell configuration. The purpose of this program has been to identify the thermal response of these constituent cell materials and their contribution to the overall cell thermal performance. We have investigated commercial cell chemistries (Sony) as well as custom cells (Gen1 and Gen2) designed to achieve high levels of performance as well as safety. Calorimetric techniques such as Accelerating Rate Calorimetry (ARC) and Differential Scanning Rate Calorimetry (DSC) were used as a sensitive measure of the thermophysical properties. The program objectives, approach and accomplishments are summarized below.

Objectives

- Develop abuse methods which can establish cause and effect relationships between variations in abuse tolerance, thermal instabilities, or reduced lifetimes to changes in cell design or materials
- Identify mechanisms and chemical constituents leading to reduced thermal tolerance, reduced thermal stability, or reduced operational lifetime in Li-ion cells.
- Identify chemical mechanisms resulting in gas generation that leads to cell venting.
- Determine factors affecting flammability of cell vent products under abusive conditions.
- Characterize the thermal response and gas generation products of cells under various overcharge conditions.
- Develop a knowledge base of cell thermal properties leading to improved cell designs.

Approach

- Test full size cells by the method of Accelerating Rate Calorimetry (ARC) to determine cell properties leading to cell thermal runaway.
- Measure gas generation in full cells as a function of temperature and cell properties such as state of charge and aging/cycling history.
- Measure the thermal inter-reactivity of fresh cell solvents, conductive salts, and fresh/aged cell electrodes recovered from disassembled test cells by using Differential Scanning Calorimetry (DSC) and ARC.
- Measure gas-generating reactions and evolved gas species in ARC bomb capsules of electrode materials in electrolyte.
- Determine thermal response of whole cells from measurements of the thermal reactivity and interactions between the cell components leading to improved cell designs.
- Perform and video document short circuit, overcharge, and thermal heating tests on cells to benchmark the unsafe or thermal runaway behaviors seen in Li-Ion hardware.
- Video document the flammability behavior of vented cells in air and in inert gas with/without an external ignition source.

- Develop real time gas sampling and identification techniques to track rapid gas generation events during thermal abuse

Accomplishments:

Demonstrated that cell thermal runaway profiles can be characterized in three major temperature stages:

- **Stage 1: Room Temperature to 125°C – Onset of thermal runaway**
- **Stage 2: 125°C - 180°C – Venting and accelerated heating (smoke)**
- **Stage 3: 180°C and above – Explosive decomposition (flame)**

Stage 1. Room Temperature to 125°C Onset of Thermal Runaway

- Exotherms begin at anode due to SEI reactions and decomposition at temperatures as low as 50°C (possibly due to incomplete formation)
- Magnitude and onset of thermal response is highly influenced by morphology of anode carbon particles
- SEI decomposition leads to exothermic reduction of electrolyte at exposed lithiated carbon surface
- Gas generation slowly increases with increasing temperature (primarily from EMC)
- Aging reduces carbon reactivity (more stable, well developed SEI layer) leading to more thermally stable cell

Stage 2. Venting and Accelerated Heating (smoke) 125°C - 180°C

- Rate of gas generation increases above 125°C
- CO_2 is the main decomposition gas followed by CO, C_2H_4, H_2
- Cathode appears to be the major source of early gas generation along with EMC decomposition gases
- Anode reactions are the source of H_2
- Self-heating rate increases above 140°C
- Both anode and cathode participate in exothermic reactions that create a complex chemical environment within the cell.
- Electrolyte amount is critical to overall rates of heat and gas generation and ultimately dictates the full cell response
- For electrolyte decomposition reactions:
  - EMC/LiPF6 source of main gas generation but not a source of heat
  - EC/LiPF6 reaction is the main source of heat generation
  - Increased concentration of either LiPF6 or EC greatly increase rate of EMC decomposition.

Stage 3. Explosive Decomposition (flame) 180°C and Above

- In full cells, very rapid increase in heat and gas generation rate is observed, with explosive decomposition around 200°C
- Several exothermic, gas-producing reactions over narrow temperature range from 180°C to 225°C are responsible for this dramatic cell response
- High-rate decomposition reactions occur between the cathode and electrolyte materials in the 140°C -200°C range with peak in heating rate at 190°C

- High-rate decomposition reactions occur between the anode and electrolyte materials in the 200°C -225°C range with peak in heating rate at 225°C
- Electrolyte decomposition rate peaks in the 180°C -200°C range
- Sudden increase in gas evolution from anode above 200°C in addition to continued gas evolution from cathode and electrolyte decomposition
- Gases serve as propellant to eject any remaining electrolyte
- Expelled electrolyte and some of the gasses generated in the cell are flammable and can be ignited by external spark source.

This page intentionally left blank.

Acknowledgments

This page intentionally left blank.

Table of Contents

Figures

14

Tables

17

Acronyms and Abbreviations

ANL	Argonne National Laboratory
ARC	Accelerating Rate Calorimeter(ry)
ATD	Advanced Technology Development
BNL	Brookhaven National Laboratory
DEC	diethyl carbonate
DEDOHC	A dimer of 2 DEC molecules, diethyl-2,5-dioxahexane carboxylate
DMC	dimethyl carbonate
DMDOHC	A dimer of 2 DMC molecules, dimethyl-2,5-dioxahexane carboxylate
DSC	Differential Scanning Calorimeter(ry)
EMDOHC	A dimer of DEC and DMC, ethylmethyl-2,5-dioxahexane carboxylate
EC	ethylene carbonate
EMC	ethyl methyl carbonate
FTIR	Fourier Transform Infrared Reflectometer(ry)
GC	Gas Chromatography
INEEL	Idaho National Engineering and Environmental Laboratory
LBNL	Lawrence Berkeley National Laboratory
LC/MS	Liquid Chromatography/ Mass Spectrometry
MS	Mass Spectrometer (ry)
PNGV	Partnership for a New Generation of Vehicles
PVDF	poly(vinylidene fluoride)
PTC	Positive Temperature Coefficient
PEO	poly(ethylene oxide)
SNL	Sandia National Laboratories
SEI	Solid Electrolyte Interphase
SEM	Scanning Electron Microscope (py)
SOC	State of Charge
SS	Stainless Steel
STP	Standard Temperature and Pressure

This page intentionally left blank.

This page intentionally left blank.

1.0 INTRODUCTION

1.1 Purpose

The Advanced Technology Development (ATD) Program [1] was established by DOE to assist the PNGV industrial developers of high-power lithium-ion batteries to overcome key barriers in the areas of abuse tolerance, calendar life, and cell packaging cost. One goal of this project is to rapidly develop high-power lithium-ion cell chemistries, using commercially-available materials that can be shared with the industrial battery developers. A second goal is to establish the performance, life, and thermal abuse characteristics of these cells. A third goal was to study cells where all cell components and materials was clearly understood. To this end, cells were designed and built specifically for this program by commercial cell suppliers. Abuse tolerance has been a major concern limiting the application of advanced Li-ion chemistries in the consumer market. In order to study the technical barriers of abuse tolerance, it is necessary to have detailed knowledge about the cell chemistry and the cell performance under a wide range of abusive conditions. The mechanisms leading to poor abuse tolerance need to be understood to allow development of advanced cell chemistries which meet all the requirements for performance, life, cost, and safety.

The Thermal Abuse Tolerance Program at Sandia has concentrated on studying the behavior of cells and cell materials that have been specifically designed to meet these requirements. Two generations of cell chemistries (Thermal Generation 1 and Generation 2, Gen1 and Gen2) were specified and manufactured to allow detailed study and comparison of lifetime, performance, and safety. The cell chemistries were chosen to best meet the program performance requirements after screening numerous commercially available material combinations. The 18650 cell configuration was chosen to allow quick and economical cell manufacture in a meaningful cell size. The Gen1 cells were manufactured by PolyStor [2] using a crimped seal configuration while the Gen2 cells were manufactured by Quallion [3] using a laser-welded / crimp sealed can with a machined vent. Commercial Sony Li-ion 18650 cells (US18650S STG) were also measured to allow a comparison to known cell performances.

Cells were subjected to a wide range of abusive conditions to determine both qualitative and quantitative cell behavior. Poor thermal abuse tolerance results from two types of cell response; heat generation leading to thermal runaway and gas generation leading to cell venting. A range of experimental and analytical techniques was developed to enable determination of the materials and mechanisms responsible for the cell thermal response. These studies coupled with diagnostic measurements of cell materials by the other National Laboratory partners (ANL, BNL, LBNL) has resulted in a significant advancement in the understanding of cell thermal abuse tolerance.

1.2 Objectives

- Determine operational modes that lead to unsafe behavior and thermal runaway.

- Identify mechanisms and chemical constituents leading to reduced thermal tolerance and reduced thermal stability.

- Identify chemical mechanisms resulting in gas generation that leads to cell venting of flammable cell components.

- Determine effects of normal cell use and aging on cell thermal stability and abuse tolerance.

- Develop a knowledge base of cell thermal properties leading to improved cell designs.

1.3   Thermal Abuse Profile Summary

Thermal abuse testing has been performed on numerous cells of varying chemistries under a wide range of conditions. Although the performance of each cell is a function of its chemistry, construction, electrochemical state, and history, the cells have shown a common thermal abuse behavior. The cell thermal response can be generally characterized by three temperature regimes as illustrated in Figure 1-1. The information summarized in this report outlines the experimental testing that went into characterizing the thermal response of these cells and identifying the underlying chemical mechanisms.

Three stages of thermal runaway:

Stage 1:   **Room Temperature to 125°C – Onset of thermal runaway**

Stage 2:   **125°C - 180°C – Venting and accelerated heating (smoke)**

Stage 3:   **180°C and above – Explosive decomposition (flame)**
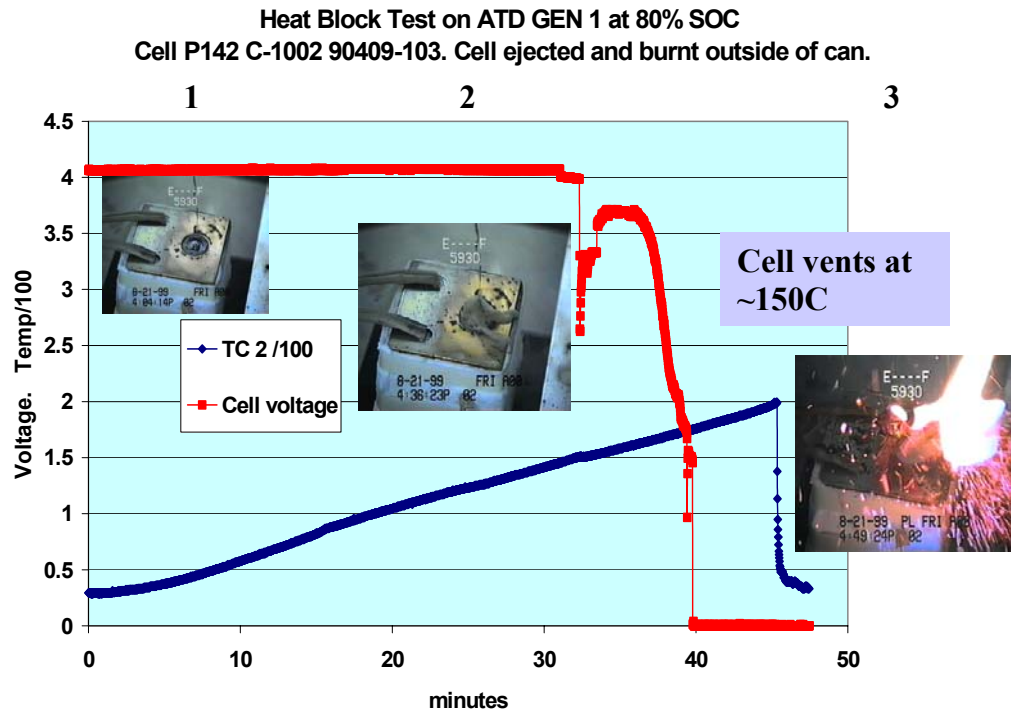
Figure 1-1.   Thermal block ramp of Gen1 cell to destructive runaway.

1.4   Sony and Gen1 Cell Testing

Initial measurements were performed on commercial Sony 18650 cells (1.2Ah) to develop measurement techniques for the following Gen1 cells and to establish a baseline of comparison for cell thermal abuse behavior. A thermal abuse test plan was developed that integrated several methods to establish thermal runaway and degradation characteristics of the cells.   The plan was comprised of thermal block, microcalorimetry, accelerated rate calorimetry, and other safety tests, using cells at various stages of life.   The thermal block test is a quick screening test for catastrophic failure, as well as a technique for quenching the thermal processes before catastrophic failure occurs.   DSC, microcalorimetry, and ARC techniques are used to supplement the thermal block tests, to examine specific combinations of cell components and/or achieve enhanced sensitivity.

The Sony cells were screened for fundamental safety response including short circuit, overcharge, and high-temperature thermal block ramp. These cells were also measured under more controlled conditions in the Accelerating Rate Calorimeter (ARC) to determine the effects of state of charge (SOC) on the thermal runaway behavior of these cells. The cells were disassembled to obtain samples of the anode and cathode materials for thermal analysis using Differential Scanning Calorimetry (DSC). Degradation reactions in the cells, which affect aging and lifetime, were measured as a function of temperature and state of charge using microcalorimetry.

Gen1 cells also underwent destructive safety tests and video recordings were obtained of the cell behavior. Gen1 cells were measured using the same techniques developed for the Sony cells and for most of the same conditions. However, the Gen1 cells were subject to an additional set of calendar and cycle aging over a range of temperatures, cycling profiles, and states of charge. The life test matrix on the Gen1 cells distributed 135 cells over three States-of-Charge (80%, 60%, and 40% SOC), four temperatures (40°C, 50°C, 60°C, and 70°C), and four life-cycle profiles (0%, 3%, 6%, and 9% ΔSOC pulse profiles).   The thermal abuse tolerance of these aged cells were measured and compared to the original "as received" cells. Aged cells were also used to obtain materials for subsequent thermal analysis and comparison to the original material measurements. Prior to any cell testing or electrochemical cycling all starting materials used in construction of the electrodes were measured by DSC. Coated electrode materials for the Gen1 cells were also provided and electrochemically cycled using three-electrode T-cells. The T-cells allowed Gen1 electrode materials to be placed in known states of charge and then subsequently measured by DSC for comparison to actual cell materials. These measurements formed the basis for the understanding of thermal abuse tolerance in these and the following Gen2 Li-ion cells.

1.5   Gen2 Cell Testing

Gen2 cells were subjected to the same initial safety screening tests as was used for the Gen1 cells. Electrical, thermal, and video recordings of the cell responses were made during these destructive abuse tests. The cells were also measured in a sealed bomb apparatus that allowed gas sampling of the vent gases. Flammability of the vent gases was measured using an external ignition source for cells venting in both air and inert gas.

Controlled thermal runaway experiments were performed using the ARC to fully characterize the cell response in each of the three major temperature regimes. Modifications were made to

the ARC system using a sealed capsule cell and manifold that allowed measurement and collection of the evolved gases. Cells were measured at two states of charge and in both "as received" and "aged" conditions.

Fundamental cell material reactions were measured to determine the contributions of the cell materials to the overall cell thermal performance. Sealed ARC "bomb" runs were made of anodes, cathodes, and electrolyte under the same conditions experienced by a cell during thermal runaway. A gas collection and measurement system was constructed to allow quantitative determination of total evolved gas volume and later determination of the evolved gas species. These measurements were used in determining the sources of heat and gas evolution in each of the temperature regimes. Cell materials were obtained both from disassembled cells and from materials cycled in the T-cell apparatus. Both ARC and DSC analytical techniques were used to characterize the material properties.

2.0   CELL CONSTRUCTION INFORMATION

ANL screened a large number of commercially available positive electrode, graphite negative electrode, electrode additive, and binder materials as potential candidates for use in Gen1 and Gen2 high-power cells. Electrode and additive materials were characterized for their particle shape, size distribution, and chemical homogeneity. Promising electrode, additive, and binder materials were processed into electrodes and evaluated in 32 cm^2 laboratory cells that employed conventional electrolytes. Reversible and irreversible capacity density, rate capability, and reactivity with the electrolytes (via DSC) were established for each material and used to design the test cells.

The Gen2 cell chemistry was chosen based on the performance of the Gen1 cells. The chemistries selected for use in these ATD cells, as well as basic design data for the Sony cells, are summarized in Table 1 below. Gen1 cells were constructed by PolyStor Corp. [2] using a negative steel case design with crimped seals while the Gen2 cells were constructed by Quallion Corp. [3] using a laser-welded positive Al case design with a machined vent. Figure 2-1 below shows photos of the two cell assemblies.

Table 1. Cell Chemistries and Electrode Compositions

Sony Cells: (commercial)	Anode Cathode Electrolyte:	Coke-Based Carbon + unknowns $LiCoO_2$ + unknowns $PC:DMC/LiPF_6$
Gen1 Cells: (Argonne National Laboratory Design)	Anode: Cathode: Electrolyte:	75% MCMB-6-2800 Carbon 16% SFG-6 Graphite 9% PVDF Binder 84% $LiNi_{0.85}Co_{0.15}O_2$ 4% Carbon Black, 4% SFG6 Graphite 8% PVDF Binder 1M $LiPF_6$ in EC:DEC (1:1)
Gen2 Cells: (Argonne National Laboratory design)	Anode: Cathode: Electrolyte:	92% MAG10 Graphite 8% PVDF Binder 84% $LiNi_{0.80}Co_{0.15}Al_{.05}O_2$ 4% Carbon Black, 4% SFG6 Graphite 8% PVDF Binder 1.2M $LiPF_6$ in EC:EMC (3:7)

Gen1 Crimped Sealed   Gen2 Laser Welded/Machined Vent

Figure 2-1.   Photos of ATD Gen1 and Gen2 Cells.

3.0 EXPERIMENTAL METHODS

The thermal abuse study integrates several methods to determine the thermal runaway and degradation characteristics of 18650-size lithium-ion cells. Test assemblies have been designed to measure cell performance under destructive abuse conditions as well as under increasing levels of control. Destructive techniques are used to test and observe the limits of cell abusive response while more controlled methods are used to quantify cell behavior during the thermal excursions. Detailed analytical methods are also used to identify and quantify the thermal activity of the cell materials as well as the chemical products of these reactions. The following sections outline these experimental techniques.

3.1 Destructive Cell Testing – Thermal Block

For rapid screening tests (including tests to catastrophic failure), a thermal ramp test block has been constructed. This apparatus has the capability to heat cells at rates of 1°C per minute and faster to temperatures in excess of 200°C. Venting of these cells occurs near 125°C, and further heating can lead to cell roll expulsion in the range of 175-225°C. Two types of experiments are carried out as a function of state-of-charge, cell age, and cycle history. These are a rapid thermal ramp to catastrophic failure (venting) and a slower thermal ramp to just below the catastrophic failure point, which allows the application of in situ diagnostics and recovery of the cell for further analysis and postmortem before it is damaged by a full-fledged thermal runaway. The heating block is well suited for fairly rapidly screening the effect of different thermal environments and for generating a group of cells for further postmortem analysis. The thermal block assembly is shown if Figure 3-1.

A test assembly was also constructed for determination of inherent flammability of vented cell gases. External spark ignition sources were placed around the cell thermal block and the block assembly was monitored and recorded by video camera. The cell voltage and temperature were recorded and correlated with the video record of the runaway event. In addition, an inert gas chamber was constructed to house this test assembly and record the possible ignition of vent gases with and without the presence of a surrounding air supply. This assembly is shown in Figure 3-2.

A steel bomb enclosure was used to capture and monitor in real-time the vent gases during the thermal ramps. A gas chromatography (GC) system was used to measure the vent gases during the run and the gas species were correlated with the measured cell thermal events.

Figure 3-1. Cell Mounted in thermal ramp heat block.

Figure 3-2. Thermal heat block in inert gas enclosure.

3.2   Cell and Cell Component Measurements

3.2.1   *Calorimetric Methods*

3.2.1.1 DSC

A technique that is being applied to understand the effects of thermal abuse is differential scanning calorimetry (DSC). This enables the thermal response of individual and selected combinations of cell components to be measured over a broad temperature range. In favorable cases, this information allows identification of the components participating in thermal activity. The DSC technique also allows qualitative measurement of the local charge state of the electrodes, which impacts the cell thermal reactivity leading to cell thermal runaway as well as cell self-discharge. Measurements can be made on disassembled cells as well as laboratory half-cells enabling detailed characterization of individual electrode changes under controlled conditions.

DSC measurements were performed using a TA Instruments Model 2910 (TA Instr., New Castle, DE). Typical DSC runs are performed using crimped Al pans prepared in an Argon glove box. Only a few milligrams of material are measured to minimize gas evolution at higher temperatures. Even so, these pans usually vent gas at high temperatures with an accompanying endothermic peak in the measured signal. Hermetic, high-pressure steel pans have also been used which contain the evolved gases but these pans have high mass and are less sensitive to low thermal events compared to the Al pans. The appropriate pan was used to give the greatest sensitivity in the region of interest. A scan rate of 10°C/min was typically used for the low-mass Al pans and 5°C/min for the higher mass hermetic steel pans.

3.2.1.2 ARC

For experiments conducted at slower heating rates under adiabatic conditions, the Accelerating Rate Calorimeter (ARC) is the method of choice. The ARC apparatus used in these experiments is an Arthur D. Little Model 2000 (AD Little, Acorn Park, Cambridge, MA 02140). The ARC allows more precise control of temperature and exposes the cell to more uniform conditions over longer periods of time. A typical experiment requires a few days rather than a few hours as in the case of the heating block. Because of the adiabatic environment, the onset of self-heating due to chemical reactions in the interior of the cell can be detected with greater sensitivity. The ARC operates in a heat, wait, search mode to allow determination of the onset of self-heating. The ARC increases the temperature in discrete steps, waits for the thermal transients to decay and then monitors the temperature of the cell for a fixed time period. If the cell temperature is not increasing above a threshold value, typically 0.02°C/min, the temperature is increased by another step and the process repeated. If the cell temperature is increasing at rate equal or above the threshold value, the ARC switches to the exotherm mode during which the ARC temperature closely matches the cell temperature, thus maintaining the adiabatic state. The ARC matches the rate of temperature rise of the cell even at quite high heating rates. The normal mode of operation of the ARC terminates an experiment by cooling the sample once it reaches a set upper temperature limit. The ARC experiment more closely simulates a thermal abuse environment that includes moderately high temperatures for relatively long periods of time.

The ARC apparatus can be used for measurements of full cells as well as cell component materials. Cells can be measured either in the open ARC enclosure or can be placed in a pressure vessel which allows good thermal contact to the cell while also containing and measuring the evolved cell gas. The gas pressure rise during the run can be used to determine the cell vent temperature and to calculate the amount of evolved gas. A gas manifold allows collection of grab samples of the vent gases for later analysis. In addition, sealed feed-thrus allow monitoring of the cell voltage during these runs. Figure 3-3 shows a picture of the ARC apparatus with the sealed 18650 cell holder.

The ARC can also be used to measure cell components in a high-pressure "bomb" which allows sensitive measurement of heat generation and gas evolution. Gas samples can be collected at the end of the run for later analysis. These ARC bombs are 1-inch spherical capsules made from thin-wall titanium. The capsules are loaded with electrode/electrolyte material in an Argon glove box to preserve the inert environment found in the cell interior.

Top   Cell Holder   Clam Shell   Heating Unit
Blast Shield
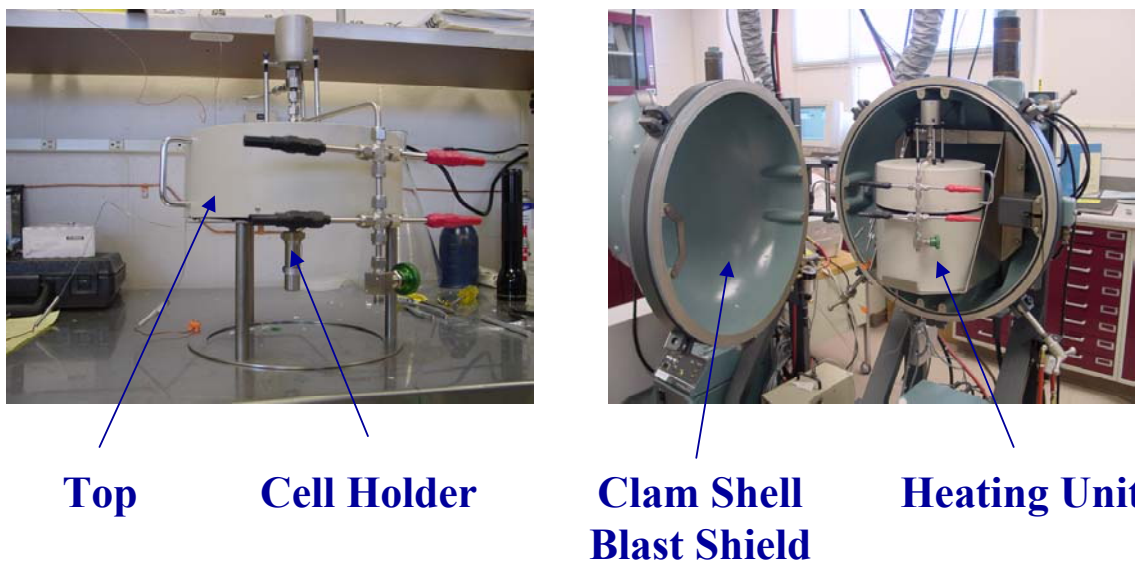
Figure 3-3.   ARC 18650 cell holder and ARC assembly.

3.2.1.3 Microcal

Microcalorimetry was used to measure the heat generation of the cells under open circuit conditions at various states of charge and temperatures. The microcal can measure heat output at the microwatt level and is useful for determining low-level reactions that affect cell lifetime and aging reactions. A CSC2000 microcalorimeter (Calorimetry Sciences Corp., American Fork, UT) was used in these measurements that allowed simultaneous measurement of up to three cells at temperatures from –40°C to 80°C.

3.2.2 Gas Analysis

Gas analysis was performed on cells and cell materials throughout the thermal abuse testing study. The gas species were identified using both gas chromatography (GC) and mass spectrometry (GC/MS). Cell head-space gases were measured using a special puncture fixture that allowed direct sampling of the gases into the GC and also allowed measurement of total gas volume. Gases from cells that vented during the ARC runs were accumulated in the sealed gas manifold system and collected with grab sample cylinders for later analysis in the GC. Grab sampling was also used for gases that vented from the cells into the surrounding space during thermal block ramps. In some runs, a real-time GC system was used to monitor gases periodically during the thermal ramps.

Whenever possible, the individual gas species were represented as effective gas volume at standard temperature and pressure (STP). These calculations were performed for the non-vented cells that were punctured for GC analysis. However, for many runs meaningful gas volumes could not be calculated, so these gas species were presented as relative percentages of evolved gas.

Gas volumes were also calculated for ARC bomb runs of electrode/electrolyte samples using the calibrated gas manifold system. The moles of evolved gas were calculated as a function of temperature and normalized by the moles of solvent in the ARC bomb. These measurements were used in developing a quantitative chemical reaction mechanism for these decompositions. GC analysis of grab samples from these runs was then used to calculate the relative number of moles of each gas species produced by these reactions.

4.0 THERMAL ABUSE TESTING

4.1 Destructive Cell Testing

Basic electrical safety and handling tests have been performed for each new test group of cells in the ATD program. These tests involved destructive testing of the cells during overcharge, short circuit and thermal ramp. The 18650 cell types used in the program have been changed to make them a better experimental vehicle, and many of the safety features inherent in commercial 18650 cells have been removed. The basic safety tests are designed to characterize the intrinsic safety response of these cells and cell materials. Beyond the standard electrical tests, thermal ramp testing has been developed to watch and record how cells behave during heating, which also happens to be an abuse mode for these cells. Cells wrapped in heat tape were cumbersome, so a method of mounting a cell vertically in a heated copper block became a better way of controlling and monitoring the cells during forced thermal ramp. These thermal blocks served as a better way to hold, heat, eject and cool down a cell before it went too far into thermal runaway. As interest has rightfully shifted to getting more quantitative results, the gas analyses which started out with a variant of the thermal ramp test in a He bomb is now part of the more precise ARC cell test.

During abuse testing the cells typically vent internal generated gases in a sometimes very energetic manner. A critical safety performance response for these cells concerns the flammability of the vented gas species. The flammability of the vent gases depends on the composition of the gases and on the external environment. The presence of an external

oxygen source and a source of ignition determines if the cell gases will ignite. Therefore, the cells were measured under controlled atmospheric conditions including air and inert gas both with and without an external spark ignition source while undergoing thermal ramp to temperatures above the vent regime. The safety test matrix is given below in Table 2 for the three cell chemistries.

Table 2. Sony, Gen1 and Gen2 Test Matrix

	Sony	**Gen1**	**Gen2**
Safety/Handling			
Short Circuit	**2**	**2**	**2**
5C Charge	**2**	**2**	**2**
5C Discharge	**2**	**2**	**Not required**
Heat to 200°C (100% SOC)	**2**	**2**	**2**
Heated to 120°C With complex impedance	**2**		
Thermal Ramp		**2 20%SOC**	
		2 50% SOC	**1 60% SOC**
		2 80% SOC	
Open Spark Tests in Air with Video	**Not developed at this time**	**1 100% SOC done with ramp to 200°C**	**1 100% SOC done with ramp to 200°C**
Open Spark Tests under N2 Gas with Video	**Not developed at this time**	**1 100% SOC done with ramp to 200°C**	**1 100% SOC done with ramp to 200°C**

4.2   Thermal Characterization and Mechanism Study

4.2.1   Sony and Gen1 Test Matrices

Objectives of Sony and Gen1 Thermal Abuse Study:

- Develop and demonstrate calorimetric methods useable in the identification of construction factors or chemical constituents leading to reduced thermal tolerance, reduced thermal stability, or reduced operational lifetime in Li Ion cells.

- Determine the effects of aging on cell thermal stability.

- Develop a knowledge base of cell thermal properties leading to improved cell design.

Testing of the Sony and Gen1 cells was carried out in accordance with test matrices that obtained the maximum information from the limited number of test cells available. Each subsequent cell study was designed upon the information obtained in the previous studies to build a comprehensive understanding of the basic mechanisms contributing to the cell

thermal abuse tolerance and behavior. Table 3 below lists the tests performed on the commercial Sony cells that were designed to develop the basic test protocols for the following ATD cells. ARC testing was performed as a function of SOC for fresh cells and for cells that experienced various levels of accelerated aging. Microcalorimetry was used to measure the isothermal self-generated heating of the cells at increasing SOCs and temperature. The results of these tests and the preliminary hypotheses of cell reaction mechanisms are discussed in the following sections.

Table 3. Sony Cell Thermal Test Matrix

No. Cells	Cell Condition	Cell Temp Max	Cell SOC	Thermal Test Performed
6	fresh	25°C	0%, 20%, 50%, 80%, 100%	Microcal
3	fresh	60°C	90%	Microcal
1	fresh	140°C	0%	ARC
1	fresh	140°C	50%	ARC
1	fresh	140°C	75%	ARC
1	fresh	140°C	90%	ARC
2	fresh	140°C	100%	ARC
1	aged 25°C/6 months	140°C	100%	ARC
1	Microcal: 60°C /90%SOC/2 weeks	140°C	100%	ARC
1	Microcal: 60°C /90%SOC/2 weeks	140°C	90%	ARC
1	Calendar Life: 70°C /80% SOC/ 6 weeks	140°C	100%	ARC
Total: 19				

The Gen1 test matrix concentrated on establishing the thermal performance baseline for this advanced cell chemistry and on studying the effects of aging on thermal abuse tolerance. ARC testing was performed at several SOCs and compared to the Sony results. Several cells were also abuse tested that had been either calendar or cycle aged. Cycling was performed according to the ATD test protocols that subjected the cells to charge/discharge pulses that resulted in a change of SOC of 3%, 6%, or 9% around an 80%SOC baseline and at temperatures of 40°C, 50°C, and 60°C. Microcalorimetry was also performed on a few cells at a limited number of SOCs for comparison to the other cell chemistries. The Gen1 test matrix is listed in Table 4 below.

Table 4. Gen1 Cell Thermal Test Matrix

		Cycle Life Cells: ARC			
delta SOC	40°C, 80%SOC	50°C, 80%SOC	60°C, 80%SOC		
3%	2	2	1		
6%	1	1	1		
9%	2	2	1		
		Uncycled Cells: ARC			
100+%SOC	100%SOC	90%SOC	75%SOC	50%SOC	5%SOC
1	1	1	1	1	1
		Uncycled Cells: Microcal/ARC			
	25°C, 0-100%SOC		60°C, 0-100%SOC		
	1		1		
	1		1		
	1		1		
		Total Number Cells: 25			

4.2.2 Gen2 Test Matrix

Objectives of Gen2 Thermal Abuse Study:

- Identify mechanisms for thermal abuse intolerance for Gen2 baseline cell chemistry.

- Identify gas-generating reactions leading to cell venting.

- Determine the effect of cycle aging on cell thermal stability.

- Develop fundamental description of thermal abuse mechanism variables

Gen2 cell testing concentrated on more quantitative measurements of cell abuse performance and material reactions. Gas analysis of cell gases from vented and non-vented cells was expanded to determine the degradation process throughout the thermal runaway profile. ARC runs were performed at only two SOCs but the runs were quenched from several intermediate temperatures to measure the progress of the decomposition reactions. A limited microcalorimetry study was performed to determine the activation energy of the open circuit self-generated heating reactions for this cell chemistry. The Gen2 cell test matrix is listed in Table 5 below.

Table 5. Gen2 Cell Thermal Test Matrix

Test Type	Description	SOCs	# Cells	Total # Cells
Handling Characterization a. **Safety (overcharge/short)** b. **Thermal block ramp**		 60, 100	 2 1	 4 2
Initial Thermal Scans a. **ARC – New cells** b. **ARC – Tested cells (45ºC)** c. **Thermal Block Ramp in Bomb w/gas collection @ 6 different temps**	**Establish thermal runaway onset temp & thermal runaway temp**	 60, 100 60,100 60	 2 2 2	 4 4 2
Chem. Anal. a. **ARC – unaged** b. **ARC – cycle @ 45ºC**	 **120ºC, 140ºC, 160ºC, 180ºC** **120ºC, 140ºC, 150ºC, 180ºC**	 60, 100 60	 2 2	 16 8
Microcal	**25ºC, 35ºC, 45ºC, 55ºC, 65ºC**	**80**	**2**	**2**
Total				**42**

5.0   THERMAL ABUSE RESULTS

5.1   Destructive Cell Testing Results

Safe handling/standard electrical tests, and thermal ramp tests showed the merits and deficits of the PTCs found in the standard Sony cell, the shutdown separators found in Gen1 and Gen2 cells, and the vents found in all three designs. While these cells are too small to find too much trouble in short circuit, they seem to uniformly need thermal and overcharge protection help.

5.1.1. Sony and Gen1 Cells

Short circuit, charge, and reversal tests were performed on commercial Sony and on ATD Gen1 18650 cells. Thermal ramp tests on the Sony cells in air and in a SS bomb under argon were performed to the point of thermal runaway with in-situ EIS. Testing showed that the commercial Sony cells were safety protected by the presence of a built-in PTC, but were still dangerous in overcharge or when heated near 200°C. ATD Gen1 cells, built without PTCs, were always dangerous under charge conditions, and ran away thermally at progressively lower temperatures (again near 200°C) as the SOC was increased.

5.1.2   Gen2 Cells

Gen2 cells showed themselves to be better experimental quality cells, with superior leak tightness compared to Gen1 cells. This was not an advantage in the thermal ramp destructive tests during which the cells often underwent explosive disassembly due to build up of high internal gas pressures. Video records were obtained for the short circuit, overcharge, and

heating tests in air on cells at 100% SOC and also at 60% SOC. The shutdown behavior in short circuit, vent behavior on overcharge, and vent behavior in thermal heating tests were determined as a safety reference for future cell testing.

Safety tests on Gen2 hardware showed Gen2 chemistry to behave in a similar fashion to Gen1. The Gen2 cells showed differences in these tests not due to the chemistry, but due to the considerable difference in cell hardware. Gen1 cells used conventional steel 18650 drawn tube/crimp seal hardware while Gen2 hardware was custom made of aluminum with welded closures. Gen2 cells showed better leak tightness, and appeared to be a better experimental hardware design. However, in thermal block heating tests, Gen2 cell machined vents did not open, and did not successfully protect the cell case from damage.

Two cells at 100% SOC were each separately short-circuited through a 0.050 ohm load. Figure 5-1 shows the typical results of these tests. The cell's high current was apparently cut off by the response of the cell roll's shut-down separator, leaving the cell vent unopened and the resulting cell safe and leak free.

Two cells at 100% SOC were each overcharged separately at a 5°C rate. In both cases the cell vent opened successfully to save the cell hardware from over-pressurization. The cell interior appeared to be very hot and glowed orange, but the can remained intact as can be seen in the sequence shown in Figure 5-2.

Two cells at 100% SOC and two cells at 60% SOC were run in heating tests to 200°C. In these tests, two cells vented, saving the respective cans, and two cells did not, causing the can lid to fail and the roll to eject. There was a result each way, at each SOC. It appears that in instances where there was can, or seal, or vent damage which could cause the cell to leak prematurely, then the cell did leak prematurely, and the cell was eventually observed to vent through the machined vent, and the can was saved from overpressure. In the other two, normal cases where there was no premature leakage, the machined vent never opened, and the case and roll were destroyed by overpressure. It is this result for the 100% SOC case that is shown in Figure 5-3.

0.050 Ohm Short Circuit on Gen 2
Sandia Cell 412 Quallion SOOl211 023 No Venting, Reinforced Leads
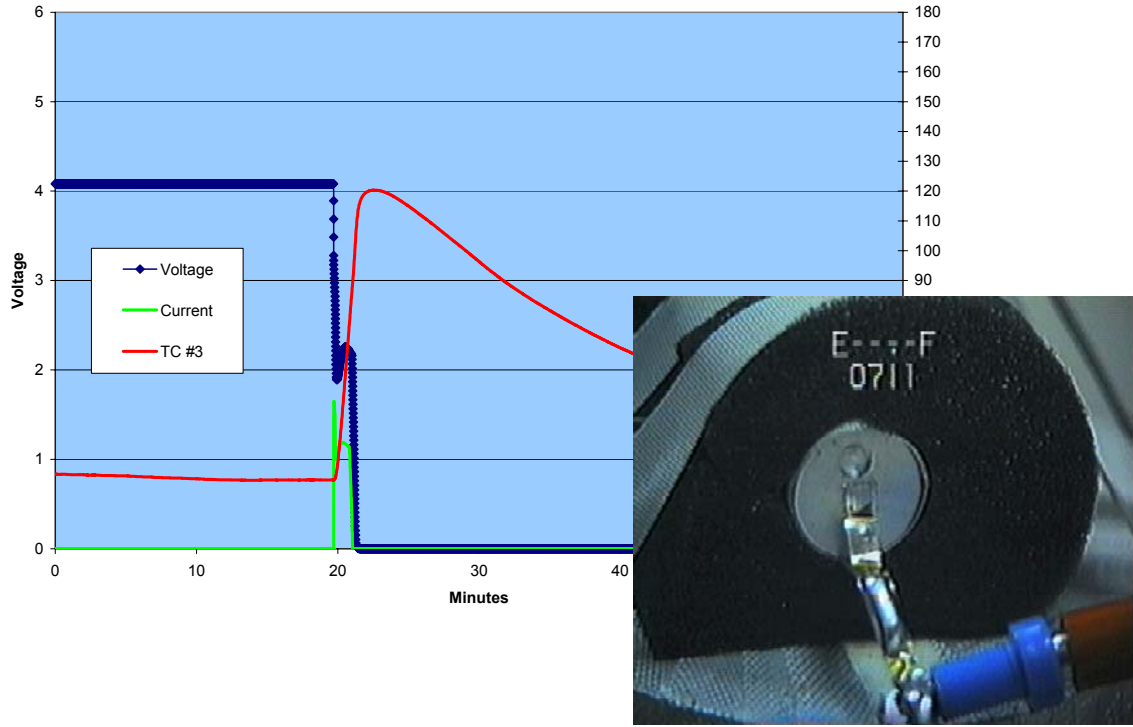
Figure 5-1. **Observed Successful Gen2 Cell Non-Venting during Short Circuit.**
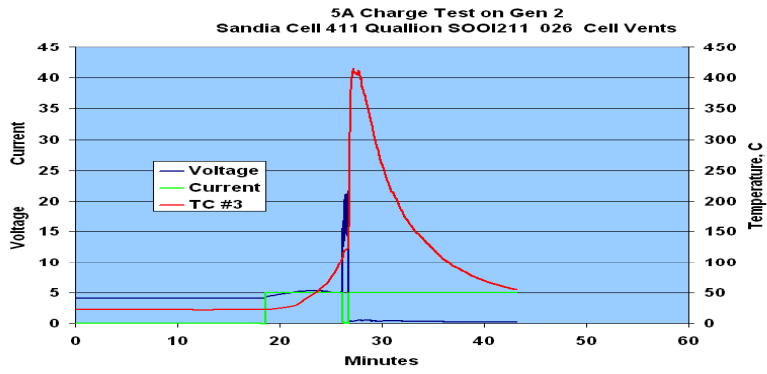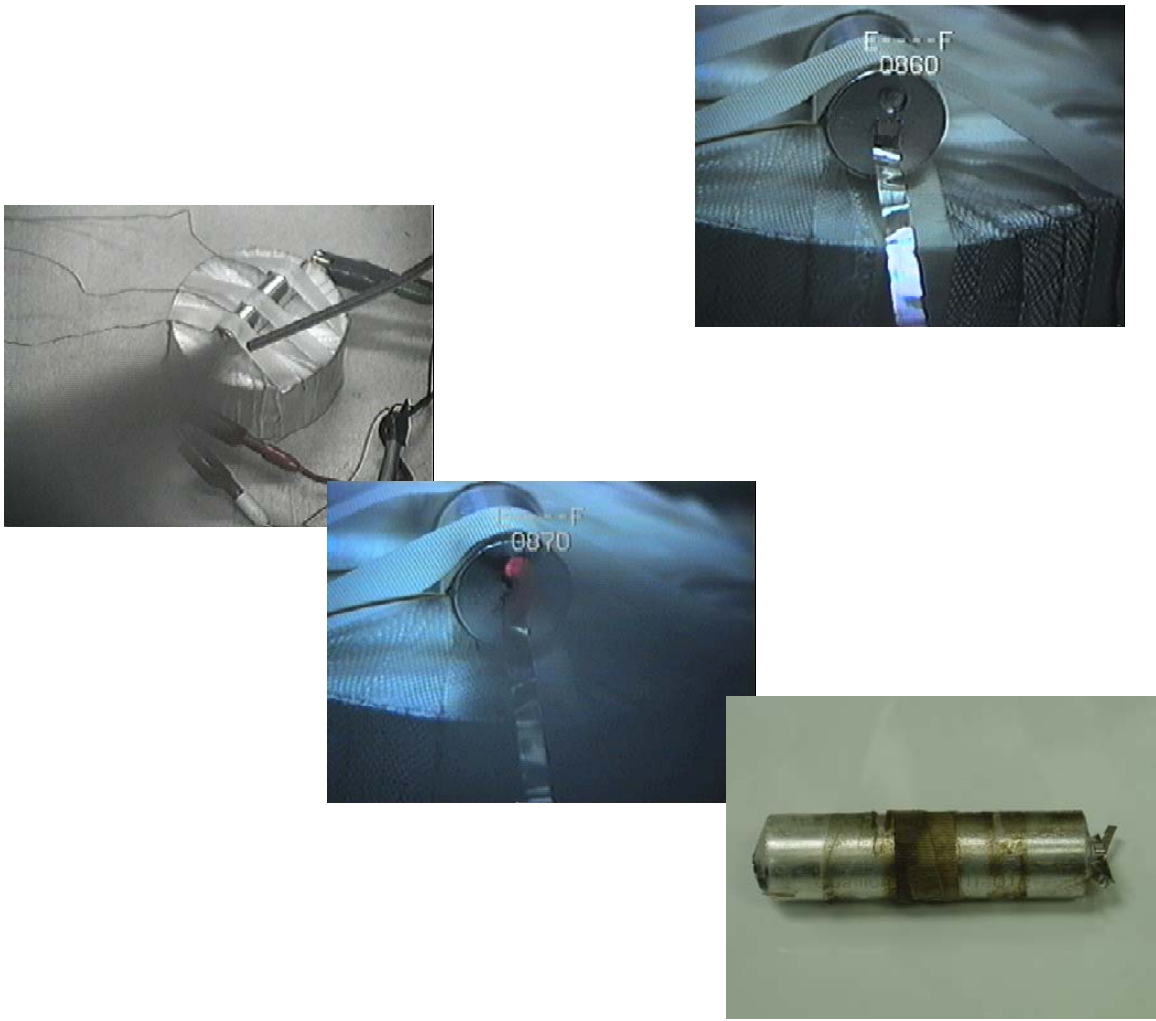
Figure 5-2.   Observed Successful Gen2 Cell Vent during 5C Overcharge.
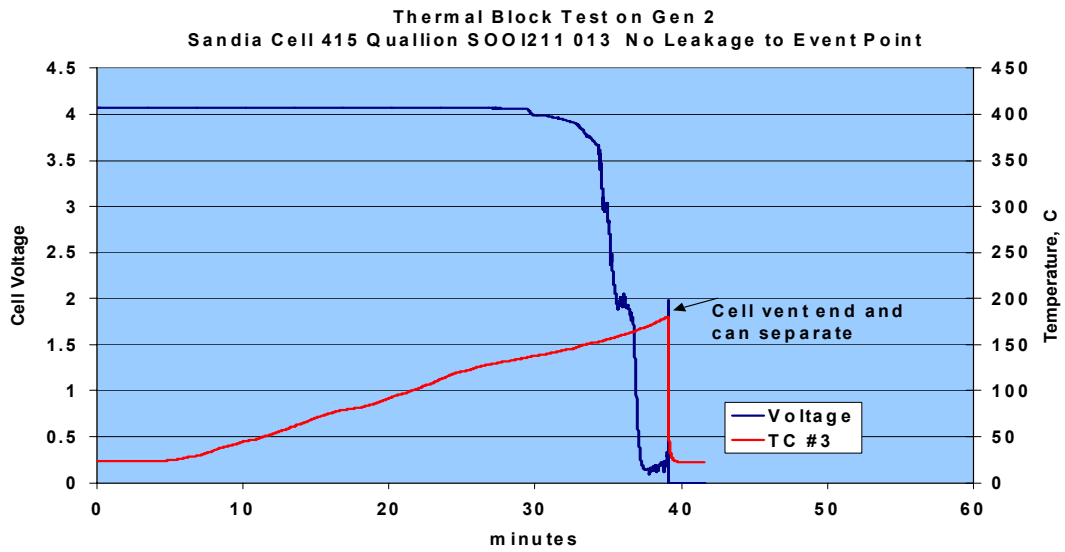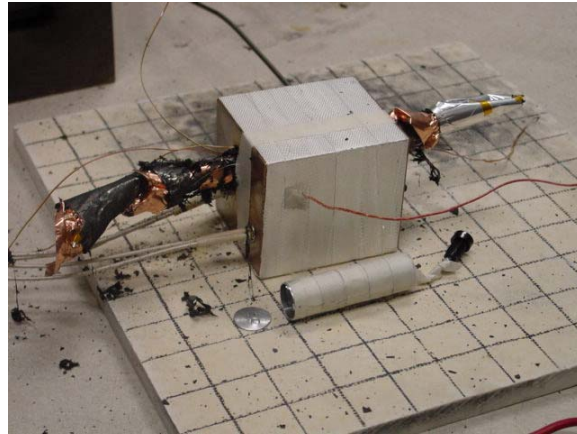
Figure 5-3. **Observed Unsuccessful Gen2 Cell Vent during Heat Test of Cell at 100% SOC to 200°C.**

5.1.3 Flammability Study

A study was conducted to test the inherent flammability of vented cell gases and electrolyte under controlled conditions. Thermal block ramps were performed on Gen1 and Gen2 cells in air and in a newly developed inert gas (N_2) container in the presence of a spark source. Previously, we have shown that both Gen1 and Gen2 cell vent products can ignite if an ignition source is present. A new containment system was developed which consists of a Lucite enclosure (3'x2'x2') through which N_2 gas flows at a rate of 20 std. cu. ft./hour. Spark ignition sources were present near the top of the cell fixture. The cell was placed in a heated copper block that was ramped from 3-4°C/min to the point of cell venting and thermal runaway. Gen1 cells vented around 160°C followed by thermal runaway near 200°C. Large quantities of smoke were observed venting at high rates from the cell. However, the generated gases did not ignite in the inert gas enclosure even in the presence of the spark ignition source. Similar behavior was seen for the Gen2 cell which also went into thermal runaway around 200°C with large quantities of vented gas.

A separate run was performed using a Gen2 cell (80% SOC) in a steel bomb enclosure to allow grab sampling of the evolved gases and an estimation of the evolved gas volume. The bomb enclosure had been flooded with He prior to starting the thermal ramp. A total of six samples were taken during the ramp to 200°C and were taken at the temperatures indicated in Figure 5-4. An initial sample was taken around 130°C prior to any indication of major venting. Venting occurred around 150°C at which point two more gas samples were taken. Two more samples were taken around 170°C immediately prior to thermal runaway (200°C) and one sample was taken after thermal runaway. Figure 5-5 shows the evolved gas analysis from GC. The vent gases measured below thermal runaway were primarily CO_2 and CO as seen for all of the previous cells measured. These gases increased with increasing temperature. After thermal runaway and cell temperatures above 250°C larger portions of CO_2 were generated along with new gas species of H_2 and O_2. The quantities of these gases apparently did not reach the explosive limit during the spark source runs. A rough value of one liter of evolved gas was obtained from pressure measurements.
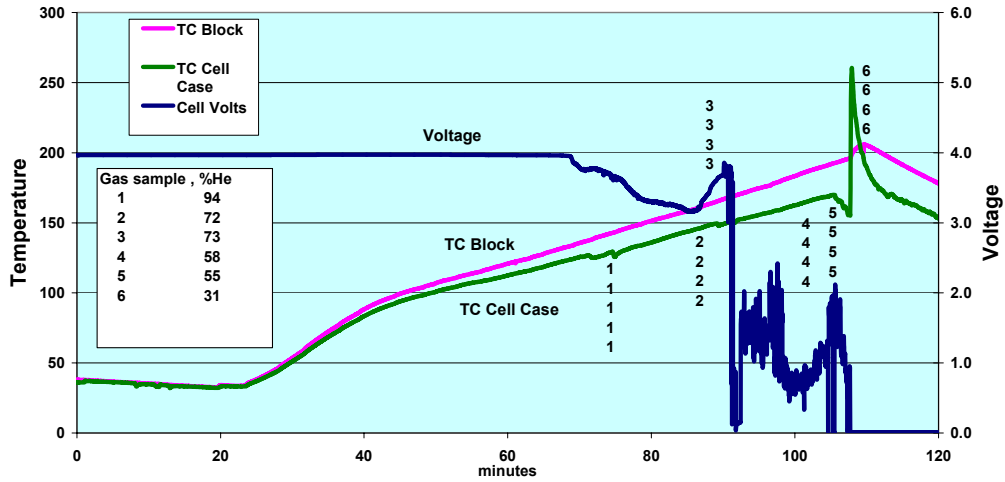
Figure 5-4. Temperature and voltage data for Gen2 cell in steel bomb.
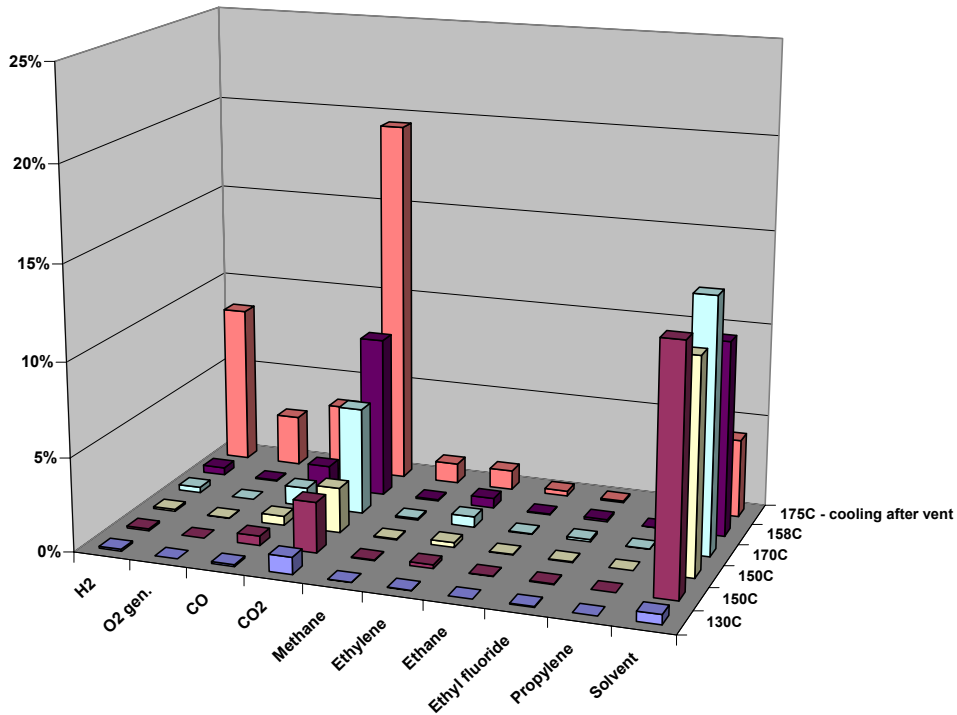
Figure 5-5. GC gas analysis (vol. %) of sequential bomb grab samples shown in Figure 5-4.

5.2   Thermal Characterization and Mechanism Results

5.2.1   *Thermal Decomposition Reactions - Sony and Gen1Cell Summary*

- ***Onset of self-heating begins below 100°C.*** ARC testing showed that the onset temperature for self-sustained self-heating in Sony and Gen1 cells began as low as 50°C at higher SOCs. The magnitude of the heating rate was not SOC dependent.

- ***Accelerated self-heating is dependent on SOC and occurs for greater than 50%SOC.*** ARC measurements of Sony cells showed accelerating heating only above 140°C for discharged cells but decreased to 60°C at 75%SOC. The magnitude of the heating rate increased with increasing SOC. The Gen1 cells showed two reaction temperature regimes: a non-accelerating region below 80°C and an accelerating region above 80°C. For the Gen1 cells, the heating rate increased only slightly with increasing SOC.

- ***Anode is the initiator for low-temperature thermal runaway.*** DSC measurements of the Sony and Gen1 anodes showed low-level exothermic reactions beginning below 100°C.

- ***Anodes (Sony and Gen1) show exothermic peaks around 125°C independent of SOC.*** These reactions have been reported to result from conversion of the solid electrolyte interphase (SEI) layer from metastable to stable products [4-6].

- ***Anode reactions (Sony and Gen1) increase steadily with temperature and show high-rate exotherms above 180°C that are strongly SOC dependent.***

- ***Discharged anodes show little reactivity above 150°C.***

- ***Gas generation increases with increasing SOC***

- ***Gen1 anodes do not show as sharp an SEI decomposition peak as seen for Sony anodes.*** ARC and DSC data of Gen1 cells below 140°C show evidence of relatively stable SEI layer.

- ***Cathodes show sudden onset of exothermic reaction* in the 200°C-300°C range *with reaction temperatures slightly below anode peak reaction temperatures.*** Exothermic cathode reactions were observed by DSC in the 200°C-300°C range for Sony and Gen1 materials. Reactions decreased quickly with decreasing SOC.

- ***Gen1 cathodes have lower decomposition temperature than for Sony cathodes.*** Gen1 $LiNiCoO_2$ cathodes are less stable than Sony $LiCoO_2$ cathodes.

- ***Aging/cycling accelerate low-temperature SEI formation reactions in fresh cells, thus raising the onset temperature for thermal runaway.***

- ***Isothermal microcalorimetry at 25°C and 60°C have self-heating rates that are high at both high and low SOCs with a minimum at intermediate SOC.*** Rates decline asymptotically with time. The cells exhibited the lowest self-heating around 50% SOC.

- *Low-temperature heat generating reactions do not depend on electrical charge/discharge cycling but are dependent only on SOC, temperature, and time at temperature.*

5.2.2   Thermal Decomposition Reactions – Gen2 Cell Summary

- *Thermal runaway initiates at anode as a low-rate exothermic reaction*
- *Gen2 cells show earlier onset of thermal runaway compared to Gen1 cells due to flake-like morphology of Gen2 anode carbon particles*
- *High-rate exothermic reactions from cathode in 150°C -200°C range*
- *High-rate reactions from anode in 200°C -225°C range*
- *Effects of aging - Cells show signs of continued SEI formation and passivation*
- *Three regions of gas formation: Initial formation gases, RT-125°C, 125°C - 210°C*
- *No effect of aging or SOC on high-temperature gas species*
- *EMC/LiPF$_6$ as a source of gas generating reactions (mostly CO$_2$) but not source of heat generating reactions*
- *EC/LiPF$_6$ reaction with EMC source of heat generation*
- *Gas evolution reduced in presence of lithiated anode material*
- *Gas evolution from cathode beginning at 140°C*
- *EC/EMC decomposition reduced at low LiPF$_6$ molarities (below 1.2M)*
- *Maximum EC/EMC decomposition at 1.2M LiPF$_6$ and above*

5.2.3   Sony and Gen1 Cell Measurements

5.2.3.1 ARC Measurements (Unaged Cells)

ARC measurements allow determination of adiabatic cell response to increasing temperature and thus measure the onset and development of thermal runaway under controlled conditions. Figure 5-6 shows the ARC results for the "as received" Sony cells from 0%-100%SOC. These cells were measured in an open cell holder configuration. The onset temperature of self-generated heating decreased with increasing SOC while the magnitude of the self-generated heating rate increased. Figure 5-7 shows the ARC data vertically offset for easier comparison. Self-generated heating occurred as low as 50°C, but accelerating heating rate was not observed until above 100°C. At 100°C a sharp increase in the heating rate was observed for cells at 50%SOC or greater. A "knee" in the heating rate around 110°C has been associated with breakdown of the anode solid electrolyte interface (SEI) layer followed by exothermic reduction of the electrolyte by the lithiated carbon [5-6]. The increase of this reaction with increasing SOC indicates only a moderately effective SEI layer. A dip in the heating rate around 130°C resulted from the endothermic melting of the separator material. In addition, cell venting often occurred slightly above this temperature region with resultant cell cooling. Cell voltage drops in the 115°C-130°C range, also shown in Figure 5-7, were similar

to those seen in the heating block runs. The voltage drops did not result from internal shorting of the cells since no sudden increase in heating rate was observed. The ARC runs limited the maximum temperature to 140°C (160°C for the 0%SOC cell) to prevent uncontrolled, explosive decomposition of the cell in the ARC chamber.

ARC runs were performed on Gen1 cells at several SOCs while monitoring the cell voltages. The maximum temperature was again set at 140°C. The ARC data, shown in Figure 5-8, show that theGen1 cells have greater thermal stability than seen for the commercial Sony cells. Figure 5-9 shows the ARC data vertically separated for ease of comparison. The cells with 50% or lower SOC showed no accelerated heating, only transient heating spikes. The cells with higher SOC showed a low-temperature constant heating rate whose onset temperature decreased with increasing SOC to as low as 40°C. Above 80°C a sustained but low-level heating rate was observed up to 130°C at which point separator melt occurred with a resultant decrease in the heating rate. Above this temperature, the heating rate began to accelerate until termination of the measurement. Cell voltage dropped upon separator melting but no discontinuities in the heating rate were observed indicating that no short circuits occurred within the cell. The Sony and Gen1 ARC behavior are compared Figure 5-10. The Gen1 cells had significantly improved thermal stability compared to the Sony cells.
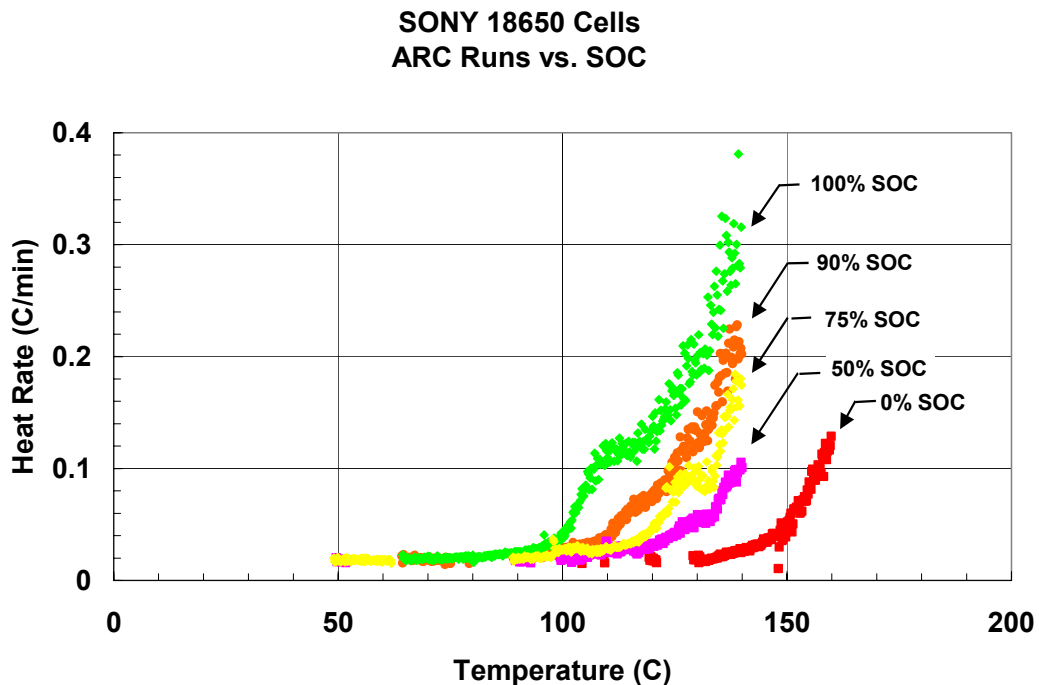
Figure 5-6.   ARC runs for Sony 18650 cells vs. SOC.

SONY 18650 Cells ARC Runs vs. SOC
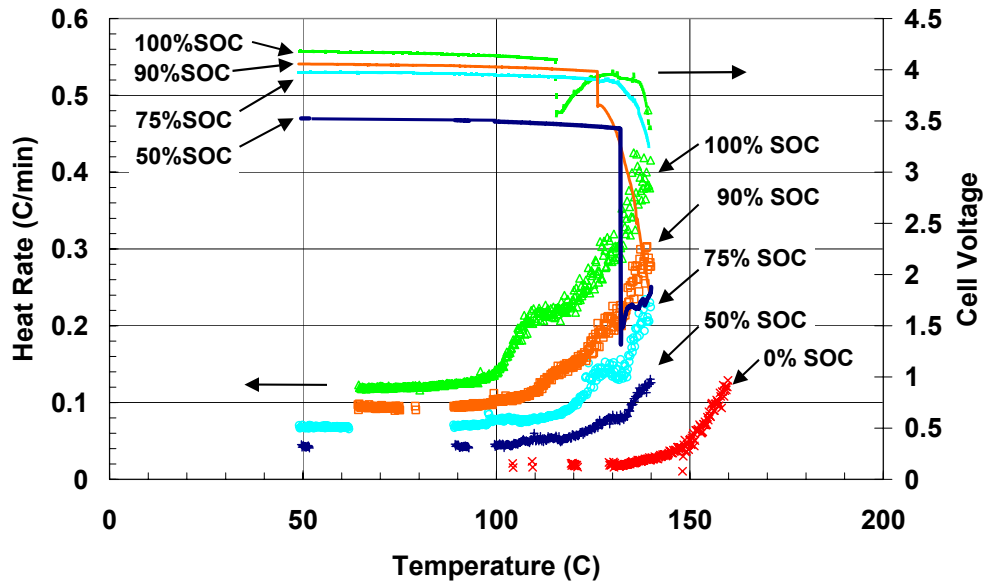
Figure 5-7.   ARC runs for Sony 18650 cells with cell voltage vs. SOC.

GEN1 Cells: 5%, 50%, 75%, 90%, 100%, 100+% SOC
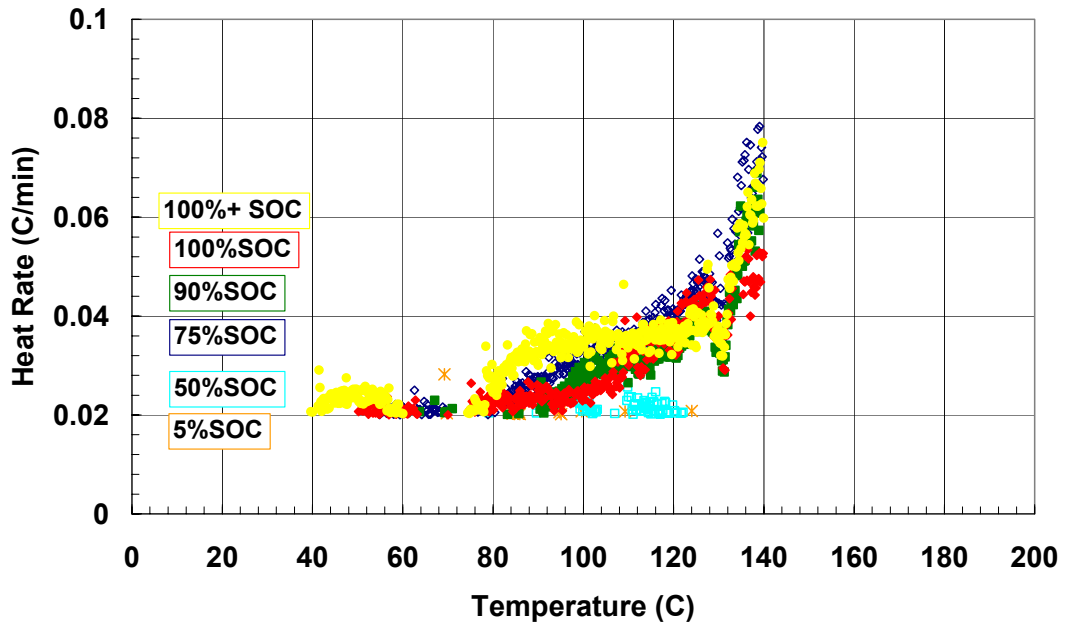
Figure 5-8.   ARC runs for Gen1 cells vs. SOC.
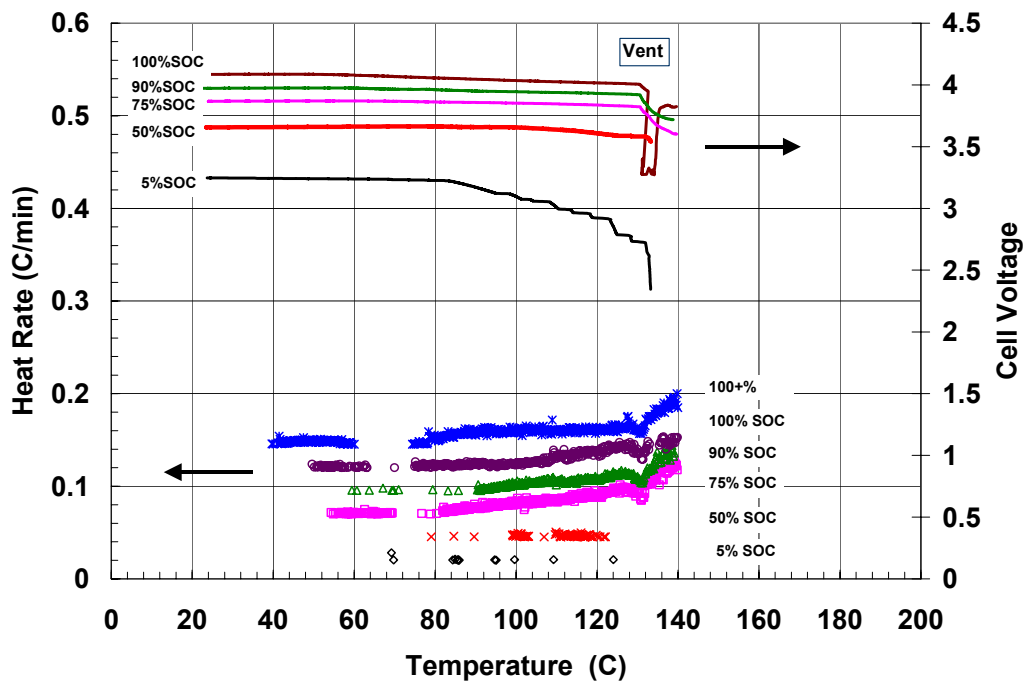
Figure 5-9. ARC runs of Gen1 cells with cell voltage vs. SOC.
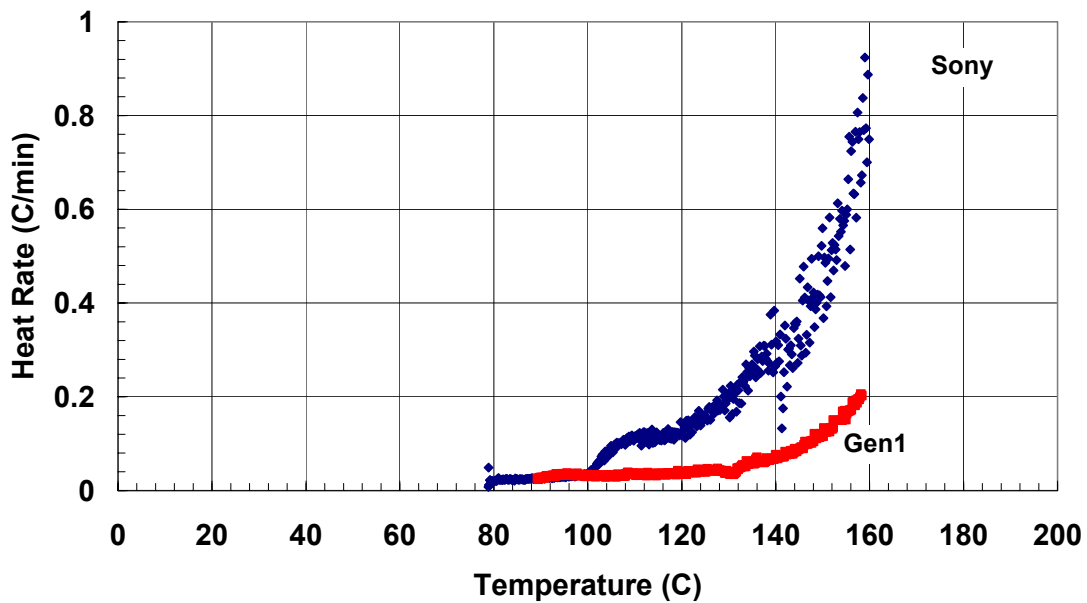
Figure 5-10. ARC runs of Sony and Gen1 cells at 100% SOC

5.2.3.2 Sony and Gen1 Cell Components -Differential Scanning Calorimetry (DSC)

DSC measurements of disassembled Sony cells were performed for cells in both charged and partially discharged states. Full cells that had been electrically cycled were disassembled and the electrodes measured up to 400°C. The cells were disassembled in an Ar glove box and electrode material sealed in Al crimped-sealed pans in the presence of cell electrolyte. Calculations of heat flow are based on estimates of the dry film weight in each electrode sample. DSC measurements are performed at a much faster temperature rate (5-10°C/min) than for the ARC runs and give a sensitive measurement of low heat-rate reactions. The measurements are useful for comparing reaction events between materials but give reaction temperatures that are higher than observed in the equilibrium ARC runs. Figure 5-11 shows the results for the Sony anodes from cells disassembled at full SOC and in a partially discharged (less than 50%SOC) state. A low-temperature region from about 100°C-200°C shows an exothermic reaction that has been found to involve SEI decomposition from a metastable species formed during initial cycling to more stable inorganic reaction products followed by further electrolyte reduction [4-6]. This reaction has been seen to start as low as 80°C. The exact temperature range of these reactions depends on the particular solvent and salt species used for the electrolyte [7,8]. The Sony anodes showed an exothermic peak starting at 120°C that was not sensitive to SOC but the reactions following this peak decreased at lower SOC. Exothermic peaks occurred at temperatures above 250°C that have been reported to result either from reactions involving the intercalated Li with the PVDF binder [9,10] or with the electrolyte [11]. Decreasing SOC significantly reduced the highest temperature (350°C) peak. This high-temperature peak may result from reaction with the PVDF or possibly with additives that are used in these commercial cells.

Figure 5-12 shows the results of the Sony cathode DSC measurements. The major cathode exotherms occurred above 200°C (at a 10°C/min scan rate) and are reported to result from interaction of the active metal oxide with the electrolyte possibly through the release of atomic oxygen [12-15]. The cathode exotherm decreased significantly with decreasing SOC. The DSC profiles of the anode and cathode materials are compared in Figure 5-13. These measurements indicate that cell thermal runaway initiates as a low-rate reaction at the anode followed by high-rate anode and cathode reactions at higher temperatures. The DSC scans show that the first peak reaction occurs at the cathode followed by the anode exothermic peaks. In an ARC thermal runaway environment these peak reactions will occur at lower temperatures and can account for the explosive cell decomposition seen around 200°C in the heat block experiments.

46

Sony Anodes: EC:DMC/LiPF$_6$ Electrolyte
Disassembled Full Cells (estimated film wt.)
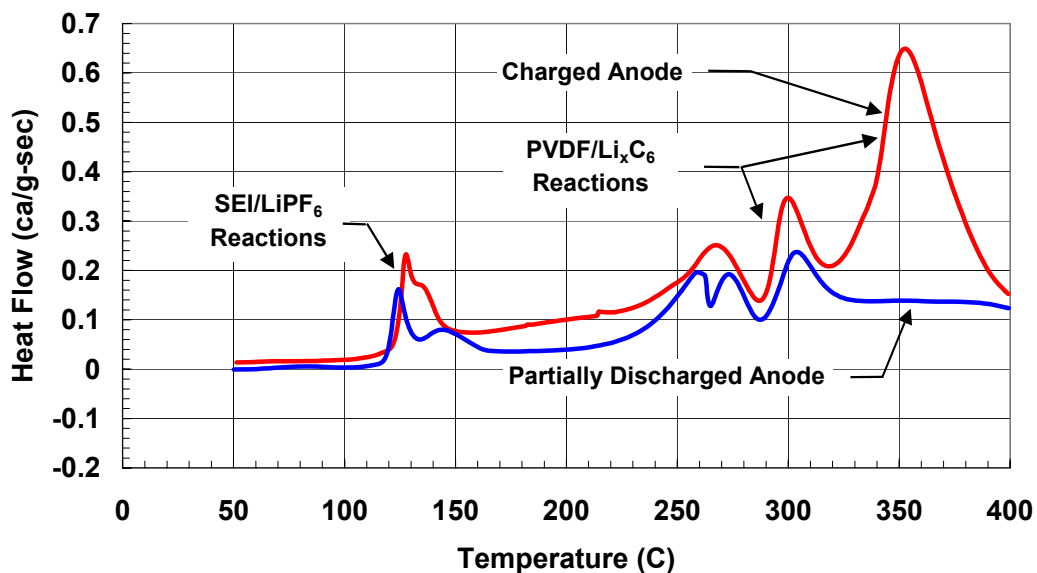
Figure 5-11.　DSC runs of Sony anodes charged/discharged in electrolyte.

SONY 18650 Disassembled Cell
Based on estimated film wt.
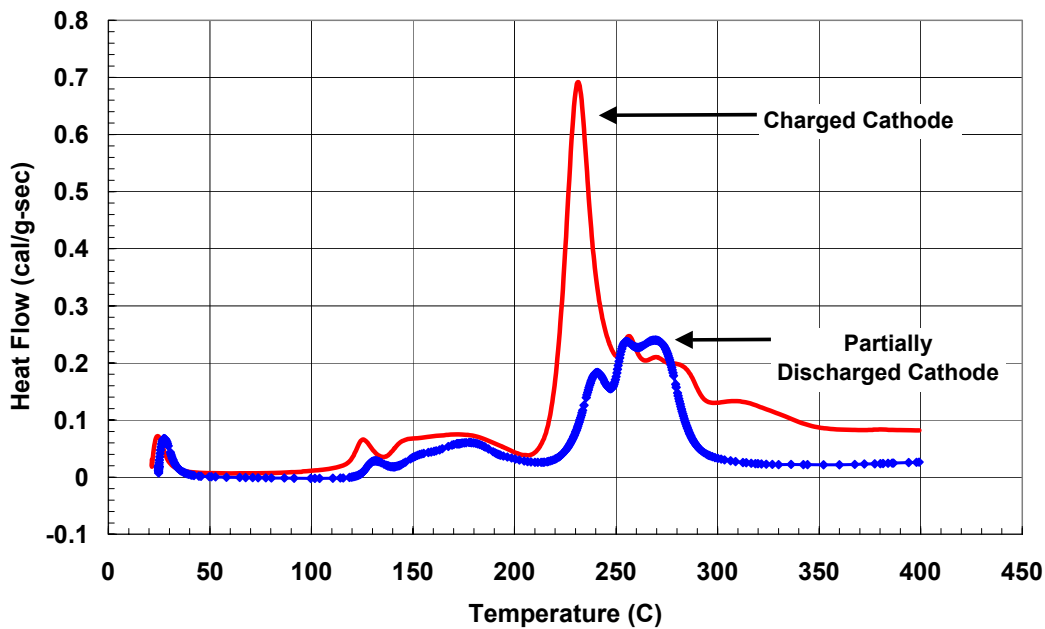
Figure 5-12.　DSC runs of Sony cathodes charged/discharged in electrolyte.

Charged Sony Anodes/Cathodes (Cell 110)
(Based on estimated film wt.)
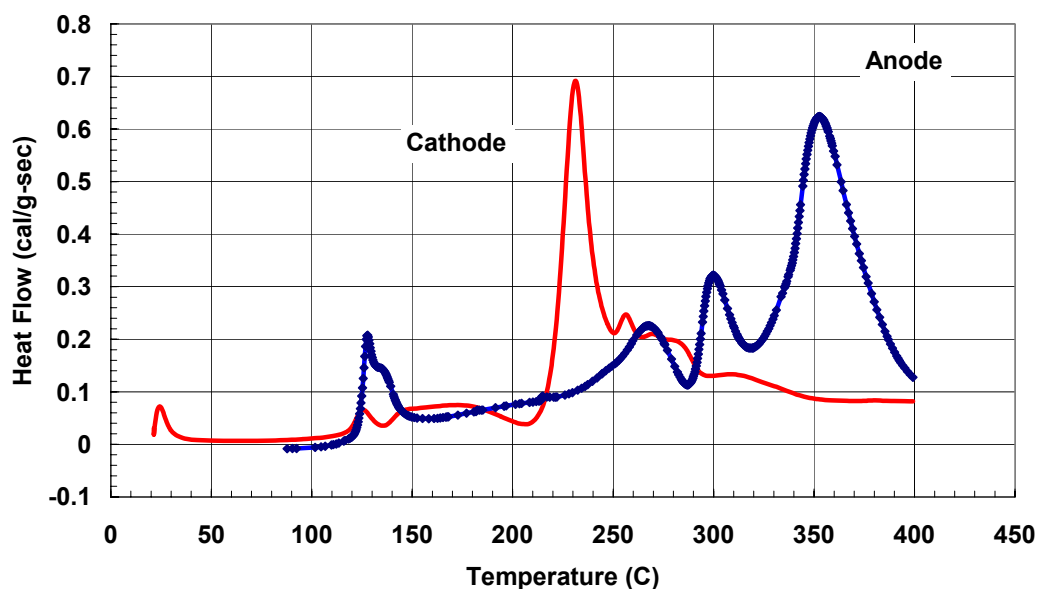
Figure 5-13.   DSC comparisons of Sony anode and cathode at 100% SOC.

The full cell thermal response is determined not only by reaction of the cell electrode materials but also by reaction of the cell electrolyte [16,17]. Figure 5-14 shows the DSC data for the thermal reactivity of the Gen1 electrolyte components. A hermetically sealed steel high-pressure pan was used to contain the released gases at high temperatures. $LiPF_6$ salt was measured and showed the expected melt endotherm at 190°C. No other thermal reactions were observed. The EC:DEC (1:1) solvents were measured and showed no exothermic reactions up to 300°C. An endotherm around 35°C resulted from melting of the frozen solvent which had been cooled to below 0°C before the onset of the DSC scan. The EC:DEC/1M $LiPF_6$ electrolyte was then measured and showed an exotherm beginning around 225°C and peaking at 250°C. These runs show that the $LiPF_6$ salt is a necessary component in the exothermic decomposition of the EC:DEC solvent species. The peak in the electrolyte decomposition is in the same region of exothermic reactions of the anode and cathode material seen for the Sony cells and thus will contribute to the violent cell reactions seen at these high temperatures. The relative contribution to the total cell reaction depends on the cell mass balance for a particular cell design. The gas decomposition products resulting from electrolyte reaction and vaporization may contribute more to the cell behavior than just the heat generation term.

Full Gen1 cells were likewise disassembled and the electrode materials measured by DSC. Uncycled, unaged baseline cells were measured as well as cells that had undergone elevated temperature and cycle aging. The measured baseline cell had undergone calendar aging at 25°C at 80% SOC. Anode material was also measured that had been cycled in a T-cell against Li foil and set at known SOCs.

DSC Gen1 Electrolyte Components
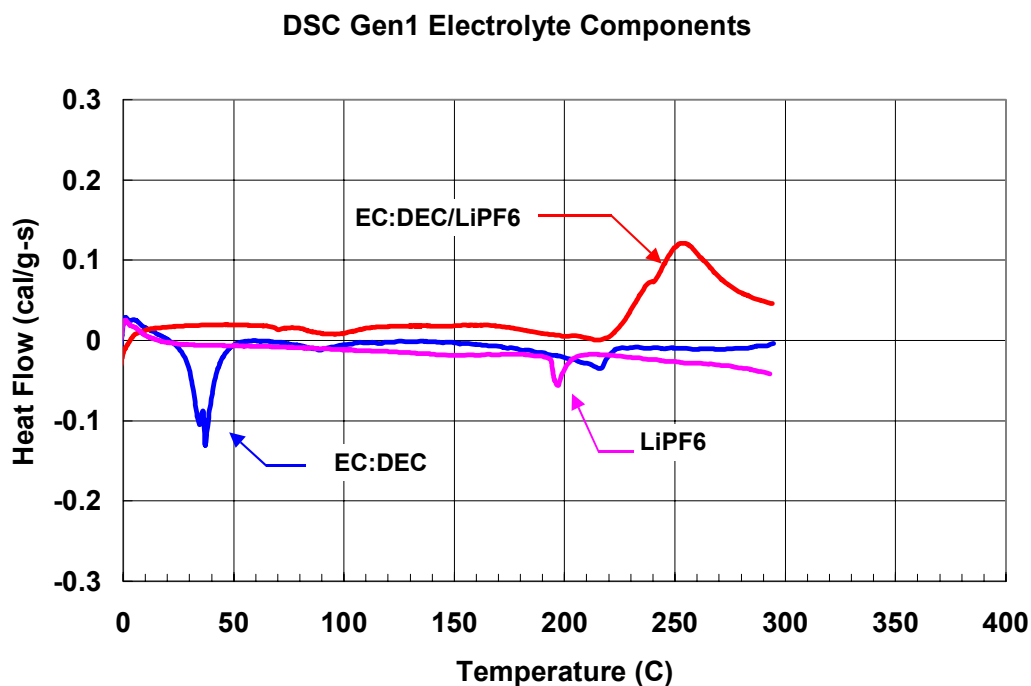
Figure 5-14.   **DSC runs of Gen1 electrolyte components.**

DSC data for the Gen1 anode material in the charged (100%SOC) and partially discharged (50% SOC) state are shown in Figure 5-15. The disassembled sample cells had been held at 25°C at 80% SOC and had not undergone any cycling. The samples were run in the presence of the Gen1 electrolyte and showed a strong vent endotherm around 275°C for the charged material. The charged anode material showed an exotherm beginning at 100°C and continuing to increase steadily with increasing temperature. A slight peak around 125°C can be attributed to the SEI layer decomposition but was overlapped by the rising exothermic reaction due to reduction of the electrolyte by the lithiated carbon through the steadily decomposing SEI. The endotherm resulted from a sudden increase in gas pressure that caused the cell to vent. The increase in gas pressure could result from a high-rate reaction of the anode material that would have given an exothermic peak around 275°C but was masked by the vent cooling. The discharged cell showed a sharp SEI decomposition peak around 125°C but showed no further exothermic reactivity since there was no intercalated Li to reduce the solvent species. A slight endotherm around 270°C resulted from a low-level gas release from the electrolyte. Since similar amounts of electrolyte were used in each sample, this data indicates that gas evolution from the electrode/electrolyte reaction increases with increasing SOC.

The $LiPF_6$ salt has been seen to play an important role in the exothermic decomposition reactions. The role of the salt in the anode decomposition reactions was investigated by performing DSC measurements of charged/discharged anode materials in the presence of full

49

electrolyte or with just the solvent species. The reactions at the anode surface can depend sensitively on the composition and structure of the SEI protective layer. Initial measurements were performed on the undisturbed cycled anode surfaces with added electrolyte or solvent. Although salt remained as part of the electrolyte entrapped in the anode pores, the addition of solvent reduced the concentration of the salt and helped determine the role of the salt in these reactions. Figure 5-16 shows the DSC data for the discharged anode material. Analysis of discharged anodes allows a more clearly defined measure of the SEI reactions without the confounding electrolyte reduction exotherm, which overlaps the SEI decomposition peak. The discharged anode material run in the presence of the full electrolyte showed a sharp SEI decomposition exotherm beginning around 110°C after which no further reactions occurred, as discussed previously. However, the "undisturbed" anode material run with only added EC:DEC solvent showed only minor exothermic reactions. This data indicates that the $LiPF_6$ salt is necessary for decomposition of the "undisturbed" SEI layer and that the SEI exotherm does not result from self-reaction of the SEI layer species. These reactions were further investigated by washing the anode material with DEC to remove the entrapped salt-containing electrolyte and measuring again in the presence of electrolyte or solvent. Washing can remove the more soluble and less adhered SEI species, exposing portions of the anode surface as well as the base layers of the SEI. The washed material will have significantly lower salt levels that will further clarify the role of the salt in the observed exothermic reactions. Figure 5-17 shows the washed anode with added electrolyte and solvent as well as the unwashed anode with added electrolyte for reference.
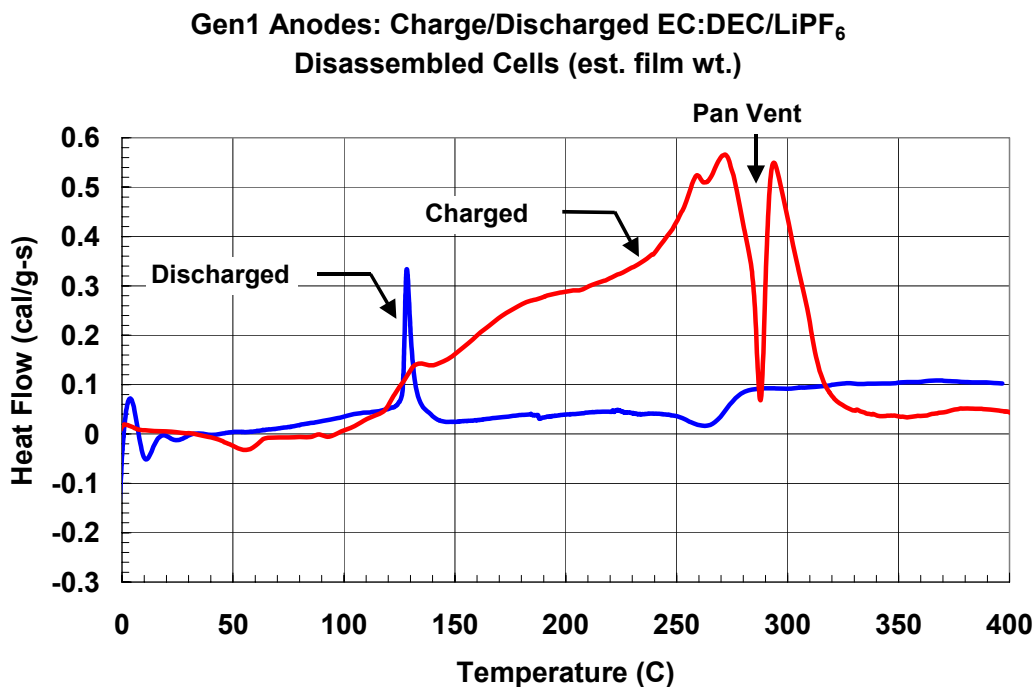
Figure 5-15. **DSC runs of Gen1 anodes in charged and discharged states with electrolyte.**

50
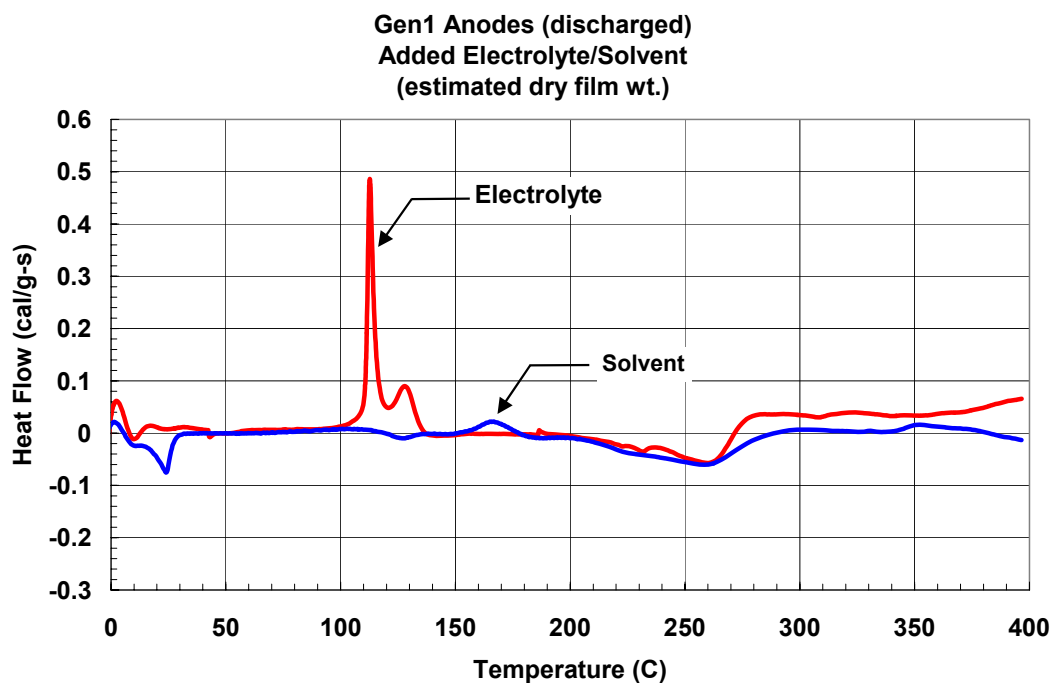
Figure 5-16. DSC runs of discharged Gen1 anodes with electrolyte and solvent.
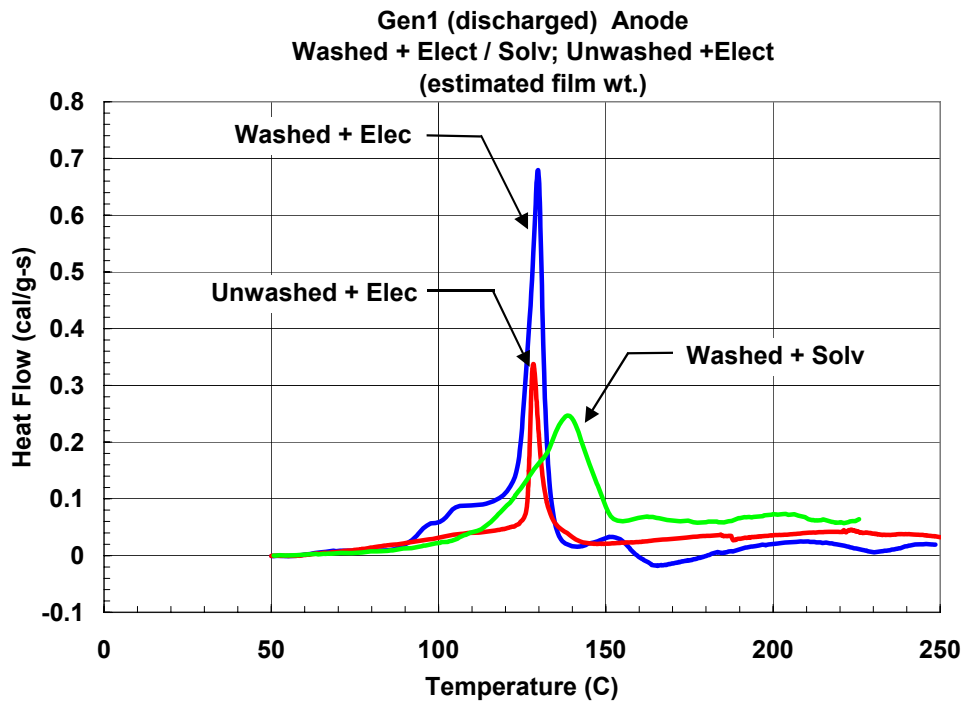
Figure 5-17. DSC runs of discharged Gen1 anodes washed and with added electrolyte and solvent.

These measurements show that the washed anodes with added electrolyte started reacting at lower temperatures and with a higher peak reaction rate than the unwashed anode which indicates that washing did indeed remove part of the protective SEI layer. The washed anode with added solvent had a higher onset temperature and a lower reaction rate peak than the washed anode with electrolyte indicating that although the washed anode surface can react with the solvent species only, the reaction is increased in the presence of the $LiPF_6$ salt.

The same experiments were performed on fully charged anode material as shown in Figure 5-18. These anodes also had been rinsed with DEC to remove the entrapped salt containing electrolyte. Below 125°C the reactions followed the same pattern as seen for the discharged anodes. An exothermic reaction occurred in the presence of the full electrolyte but was absent with only solvent species present. Again, this indicates that the $LiPF_6$ greatly enhances the decomposition of the SEI layer. Above 125°C the washed anode with the added electrolyte continued to react exothermically but only at a moderate rate. However, the washed anode material that had only solvent species present showed a high-rate reaction over a broad temperature range (125°C-225°C). This reaction can be explained by thermal breakdown of the SEI layer followed by reduction of the solvent species by the highly lithiated anode carbon. The washed anode material reacted in the presence of the electrolyte showed a lower reaction rate at temperatures above the SEI decomposition reaction. This reaction rate could be reduced since some of the lithium had been consumed in the reactions below 125°C and also could be reduced if the reaction products in the presence of the salt are forming a partially protective layer on the anode surface even as the SEI layer breaks down.

DEC Washed Gen1 Anode (4.1V)
with added Gen1 Elect. or Solvent
(estimated film wts.)
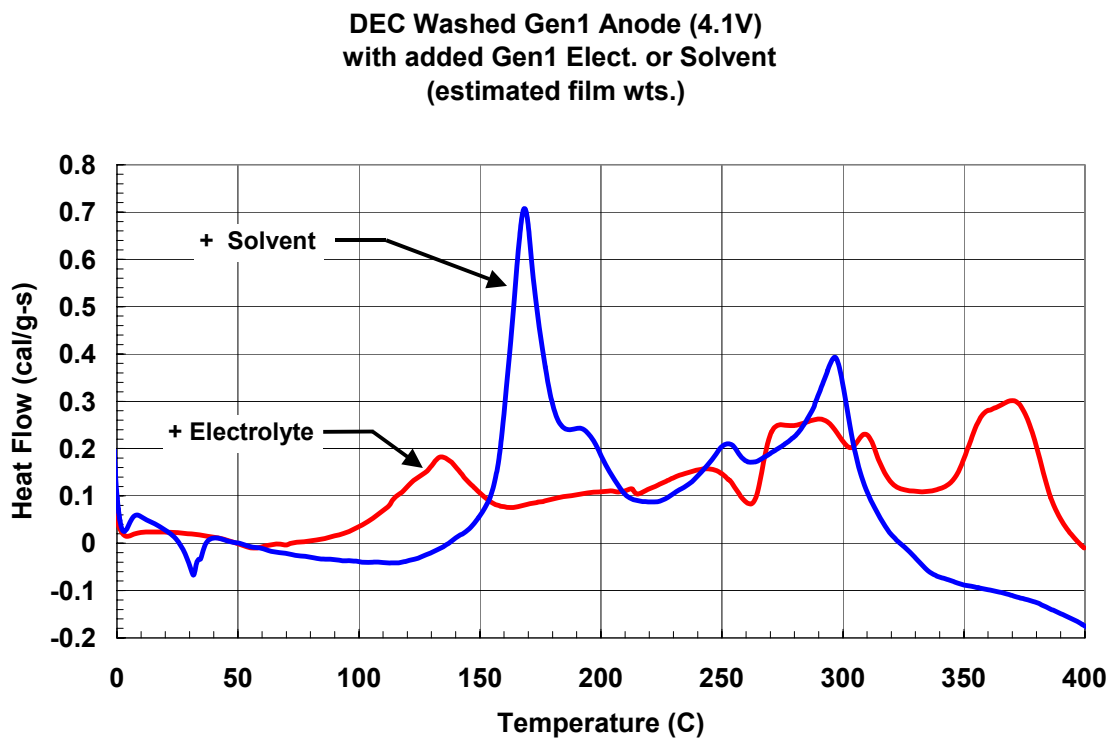
Figure 5-18. DSC runs of charged Gen1 anodes washed and with added electrolyte and solvent.

DSC data for the Gen1 cathode material in the charged and partially discharged (50%SOC) state are shown in Figure 5-19. Material was obtained from the same cells as was the anode material. The cathode material showed little low-temperature reactivity but exhibited a sharp exothermic peak in the 200°C to 250°C region. The discharged cathode showed a much lower exothermic peak reaction rate that occurred almost 50°C higher in temperature than for the peak reaction seen in the high SOC cathode. Obviously, the cathode decomposition reaction is highly state of charge dependent.

The anode and cathode DSC data for 100% SOC materials are compared in Figure 5-20. The anode shows low-level exothermic reactivity beginning just above 100°C as was seen for the Sony anodes. The high-rate reaction peaks occur first at the cathode and then are followed by the anode high-rate reaction peaks. This is the same sequence of reaction peaks observed in the Sony cell material. The reaction peaks will occur at lower temperatures in an actual cell since during the DSC measurements the temperature is being ramped at a fixed high rate.

Some of the aged Gen1 cathode materials showed a low-temperature exotherm around 120°C very similar to the one seen in the discharged anode materials. The sensitivity of this exotherm to the presence of the electrolyte salt was investigated by performing measurements in the presence of the full electrolyte or solvent species as was done for the anode materials. A sample of the cathode material was washed with DEC and measured by DSC with either added electrolyte or solvent. Figure 5-21 shows the data for the cathode material with electrolyte. Also shown is a curve of unwashed material that shows that washing did not significantly affect the state of the cathode material. The 120°C exotherm was seen for both samples. Figure 5-22 shows the washed cathode with added solvent and clearly shows that no exothermic reaction occurred at 120°C although the peak at 200°C remained. These measurements suggest that the cathode may form surface products similar to the anode SEI film and the decomposition of this film results from reactions involving the electrolyte salt. The higher temperature exotherm is believed to result from solvent combustion with evolved oxygen from the decomposing cathode and is not sensitive to the presence of the salt

The Gen1 and Sony anode materials at 100%SOC are compared in Figure 5-23. The Sony anode material showed a much more defined SEI decomposition reaction than was seen for the Gen1 anode material. This reaction peak can account for the knee seen in the ARC heating rate data for the Sony cells. At high temperatures the Sony anodes showed three reaction exotherms while only two were seen for the Gen1 anodes. This difference could arise from different binder materials, which are not known for the Sony cells, or possibly from some other cell additive component. The data for the Sony and Gen1 cathodes are compared in Figure 5-24. The $Li_xNi_{0.85}Co_{0.15}O_2$ cathodes from the Gen1 cells were markedly more exothermic than the Li_xCoO_2 Sony cathodes at similar SOC and the reactions initiated almost 50°C lower in temperature.

Gen1 Cathodes: Charged/Discharged EC:DEC/LiPF$_6$
Disassembled Cells (estimated Film wt.)
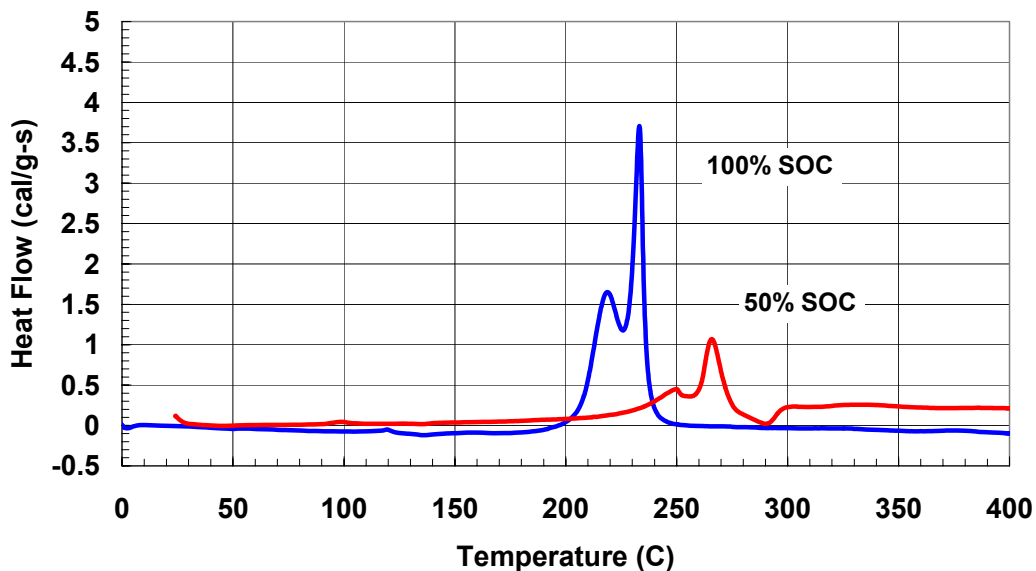
Figure 5-19. DSC run of Gen1 cell cathodes at 50% SOC and 100% SOC.

Gen1 Anodes/Cathodes: Charged EC:DEC/LiPF$_6$
Disassembled Cells (estimated film wts.)
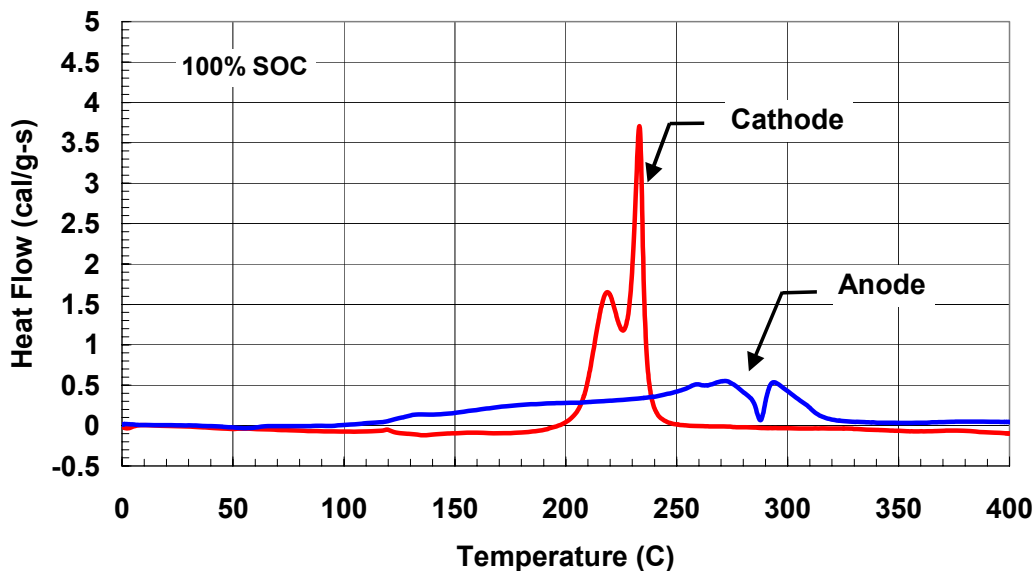
Figure 5-20. DSC comparison of Gen1 Cell anodes and cathodes at 100% SOC.

Gen1 (aged 50C, 80% SOC 9% delta 4 weeks)
Cathode+ Elect. / Charged Cell
(estimated film wts.)
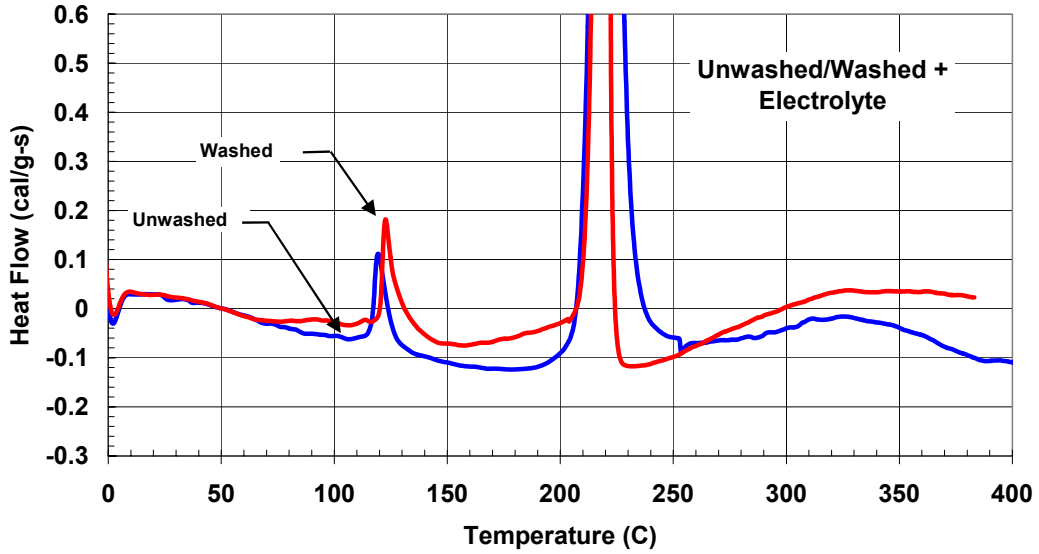
Figure 5-21.   DSC runs of washed and unwashed Gen1 cell cathodes with Gen1 electrolyte.

Gen1 (aged 50C, 80% SOC 9% delta 4 weeks)
Cathode+ EC:DEC solvent /Charged Cell
(estimated film wt.)
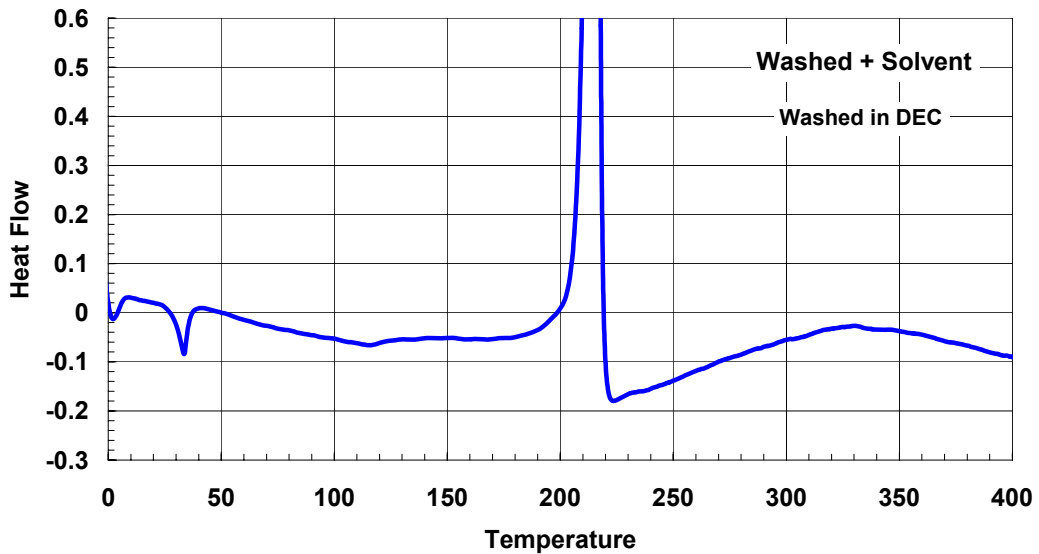
Figure 5-22.   DSC run of washed Gen1 cell cathode with EC:DEC solvent.

Gen1/Sony Anodes Charged
(est. film wt.)
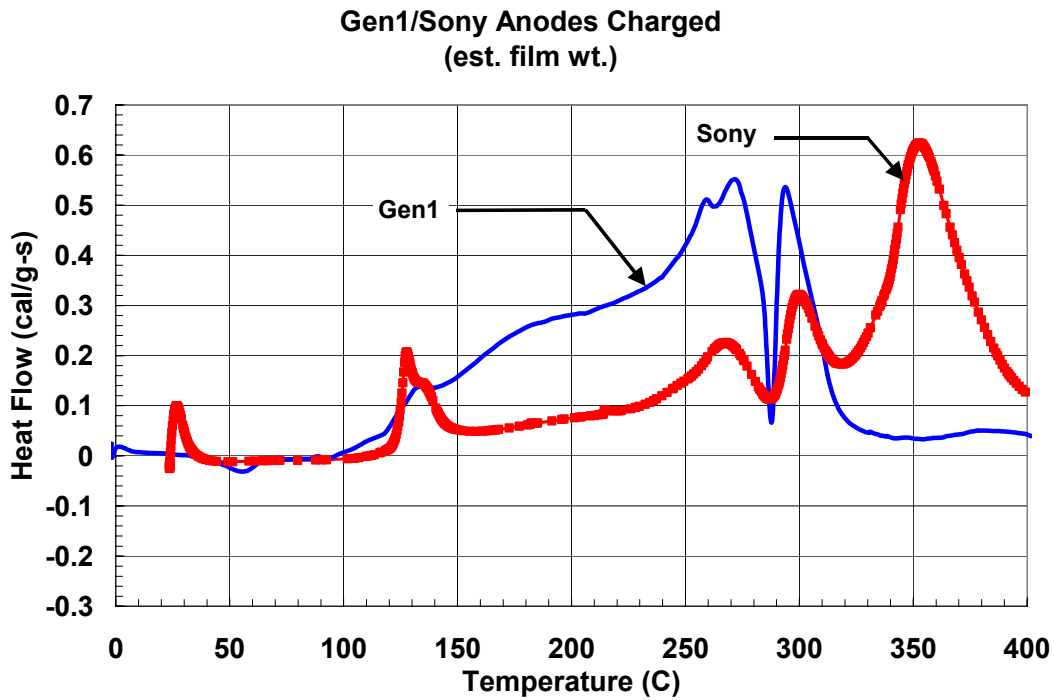
Figure 5-23.   DSC run of Sony and Gen1 cell anodes at 100% SOC.

Charged Sony/Gen1 Cathodes
(est. film wt.)
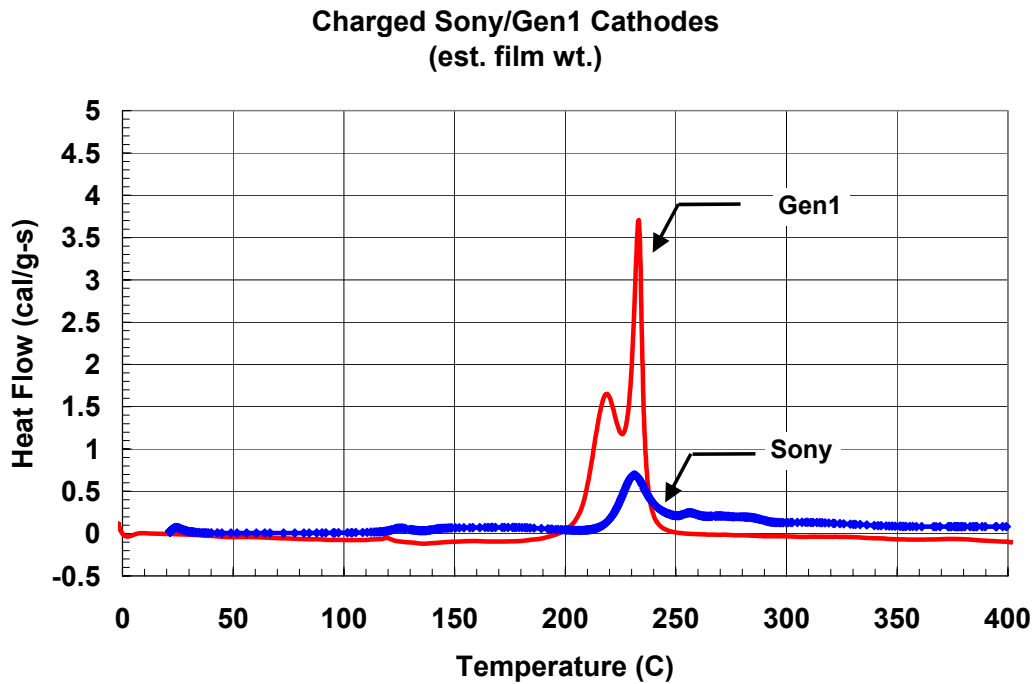
Figure 5-24.   DSC runs of Sony and Gen1 cathodes at 100% SOC.

5.2.3.3 Gen1 Electrolyte and Electrode Reactions – ARC Bomb Runs

The contribution of the cell components to the full cell thermal runaway profile as seen by ARC can best be determined by measuring the components under similar conditions. The Gen1 cell materials from the disassembled cells were measured in the ARC using high-pressure bombs using the same threshold criteria (0.02°C/min) for self-generated heating as was used for the full cell measurements.

Initial measurements were performed on the Gen1 electrolyte (EC:DEC/1M LiPF$_6$). Figure 5-25 shows the heat rate and pressure data for an ARC run to 400°C. This electrolyte began to show decomposition reactions at 220°C with both heat and gas generation. This reaction temperature agrees with the onset of exothermic reaction seen by DSC (Figure 5-14).

Anode and cathode materials were also measured in the presence of the Gen1 electrolyte. Figure 5-26 shows the ARC data for these measurements. The anode material showed transient, un-sustained reaction peaks over the whole temperature range. A sharp exotherm was observed at 225°C followed by a limited but more sustained reaction at 300°C that may have resulted from electrolyte or binder decomposition. Reactions of the partially reacted cathode with electrolyte have also been reported in this temperature region for similar metal oxides [13,14]. The cathode material showed a strong exothermic between 170°C and 190°C, which corresponds to the explosive decomposition regime seen in the thermal ramp experiments. A strong exothermic region was also observed starting at 325°C and peaking at 350°C. This reaction would not initially contribute to the thermal runaway reactions that result in the 200°C explosive decomposition but could contribute to the energetics of the complete cell decomposition.

Bomb Run 79.2 mg EC:DEC/LiPF$_6$
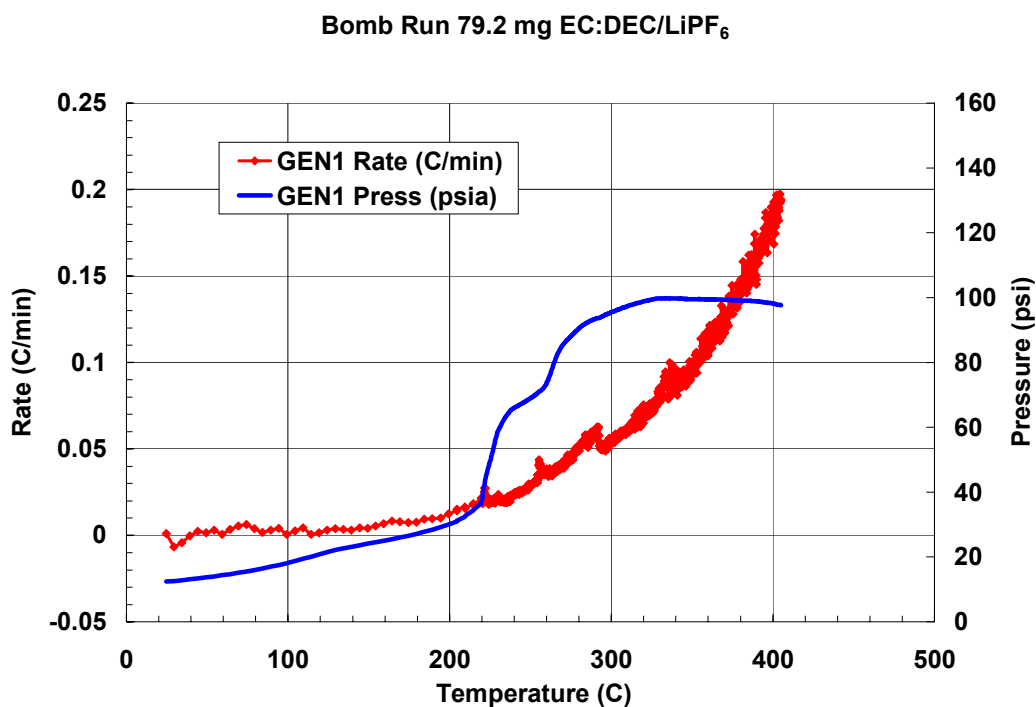
Figure 5-25.   ARC bomb run of Gen1 electrolyte.

57

Gen1 Charged Anodes/Cathodes/EC:DEC/LiPF$_6$
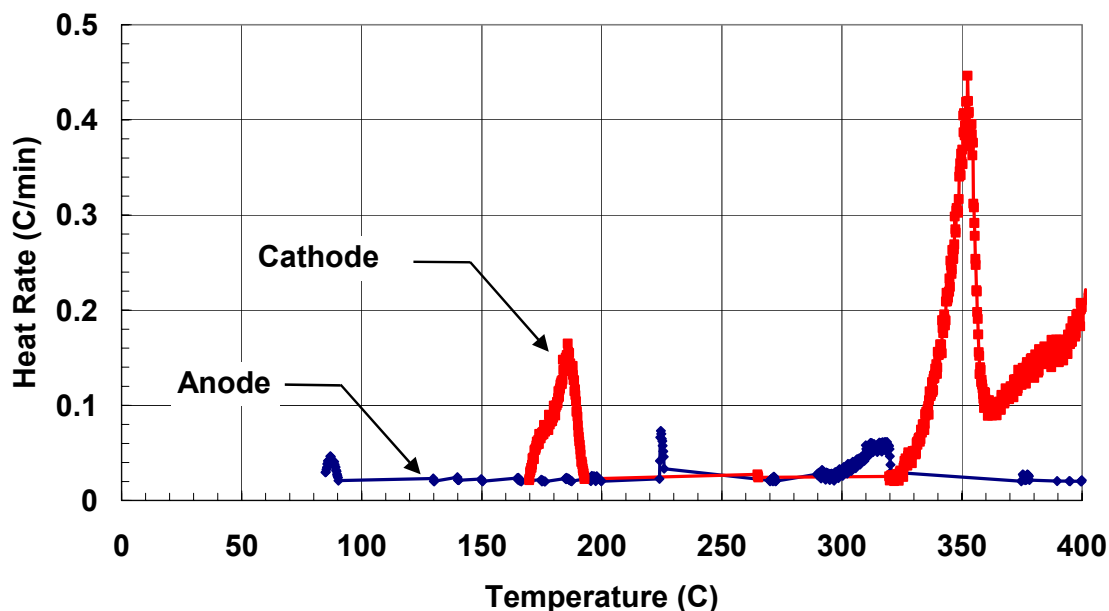
Figure 5-26. ARC bomb run comparison of charged Gen1 anodes and cathodes in Gen1 electrolyte.

5.2.3.4 Aged Sony and Gen1 Cells – ARC Measurements

The effects of aging at elevated temperatures were measured by performing ARC runs of thermally aged Sony and Gen1 cells. Figure 5-27 shows the results for the Sony cells which had been aged for 6 months/25°C, 11 days/60°C and 6 weeks/70°C. The cells showed a loss of low-temperature reactivity with increased aging. All cells were measured at 100% SOC. The data show that aging resulted in loss of the low-temperature heat output with increasing time and temperature. The onset temperature of sustained heat output increased with increased time/temperature aging. These measurements suggest that the SEI layer is undergoing partial conversion from the metastable species to the stable inorganic species even at these low temperatures. The majority of this conversion takes place relatively quickly (less than two weeks) even at 60°C since little further change was noticed for the 70°C/6 week cell. After decomposition of the SEI layer the exothermic heating rates are similar regardless of the previous aging history.

ARC measurements were also performed on Gen1 cells that underwent accelerated cycle aging at elevated temperatures of 40°C, 50°C, and 60°C. The cycle consisted of a discharge/charge profile resulting in a decrease in SOC of 3%, 6%, or 9% from a baseline of 80%SOC. The details of this cycling protocol are given in the PNGV manual [18]. All cells were placed at 100%SOC for ARC measurements up to 160°C.

The ARC profiles for the cells aged at 40°C, 50°C, and 60°C are shown in Figure 5-28, Figure 5-29, and Figure 5-30, respectively. The cells cycled with 3%, 6% and 9% delta SOC

are shown along with the unaged baseline cell data. The 40°C aged cells (Figure 5-28) showed the greatest affect of aging. These cells showed a reduction in the low temperature heating rates such that only transient, unsustained heating occurred. Accelerated heating did not occur until above 140°C. No difference was seen between the cells cycled at increasing delta SOCs. This response indicates that the Gen1 anodes were developing a more effective SEI layer at this relatively low temperature. The cells aged at 50°C and 60°C showed a reduction in the low temperature heating rates such that self-sustained heating did not occur until above 80°C. Above 80°C the heating rates were very similar to the heating rates of the unaged cell. The dip in the heating rate at 130°C resulted from the melting of the separator material. The temperature dependence of the data at each delta SOC are shown in Figure 5-31, Figure 5-32, and Figure 5-33 for the 3%, 6% and 9% cycles respectively. These figures show that the 40°C aged cells, although more passivated at temperatures below 140°C, experienced a sharper increase in the heating rate once the cells went into thermal runaway. This behavior could result from the increased level of lithiation of the anodes at this temperature that had been protected by the enhanced SEI layer that had developed during aging. An enhanced SEI layer apparently did not develop at the higher temperatures indicating that the effectiveness of SEI formation is a complicated function of temperature, chemistry, and particle morphology.
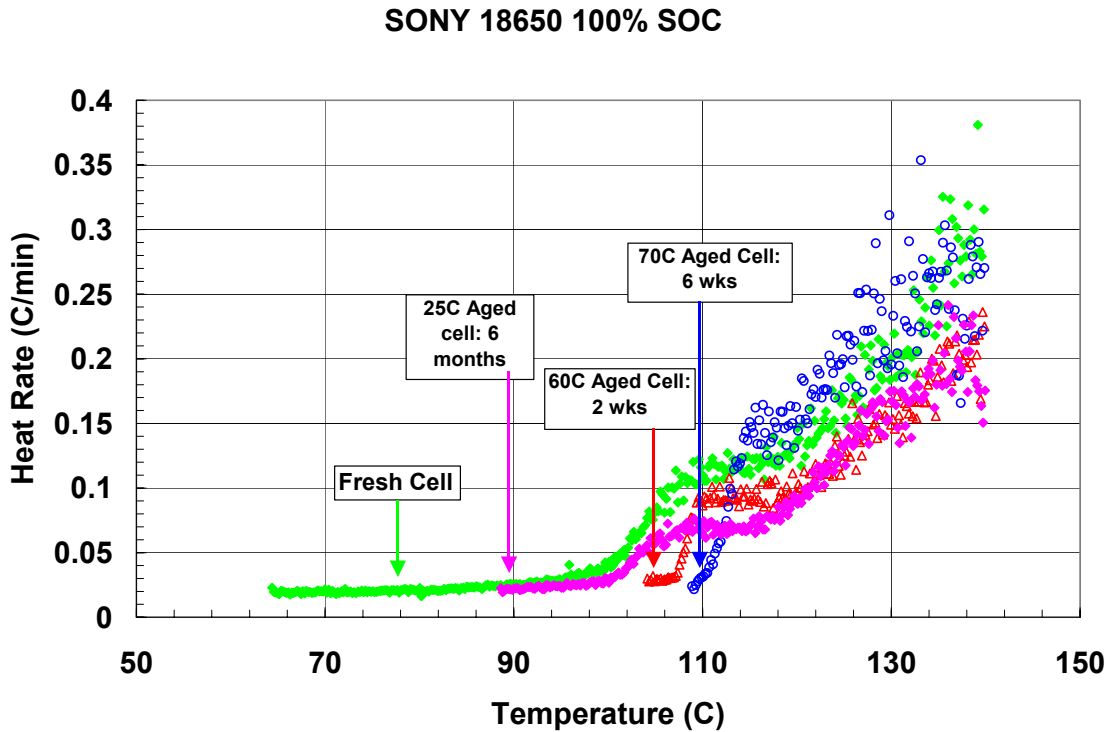
Figure 5-27.   ARC runs of fresh and aged Sony cells at 100% SOC.
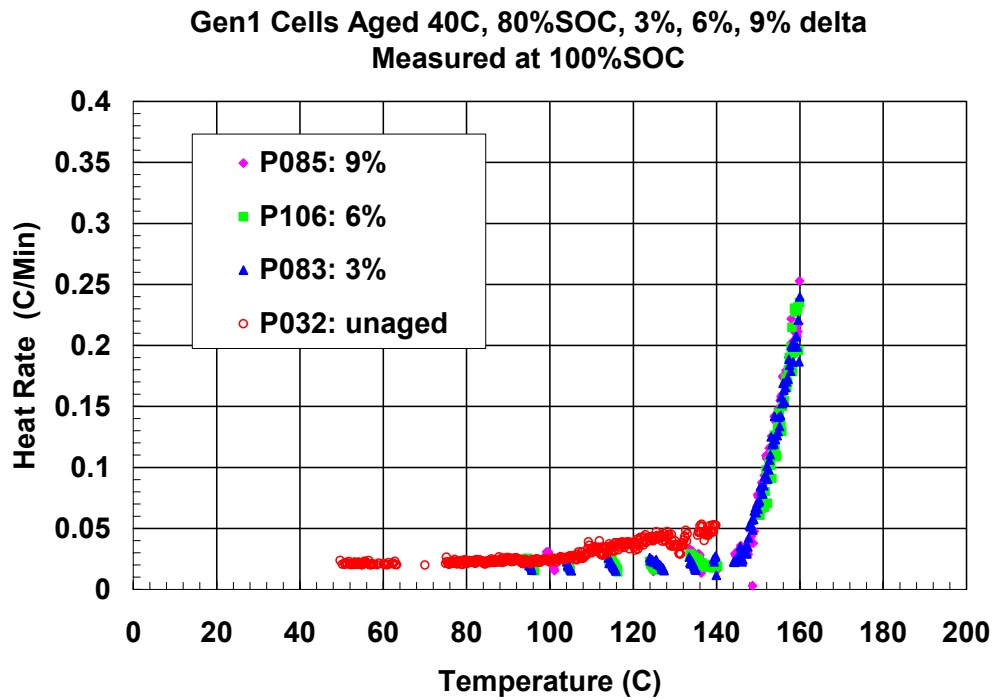
Figure 5-28. ARC runs of Gen1 cells (100% SOC) aged at 40ºC, 8% SOC, at 2%, 6% and 9% delta
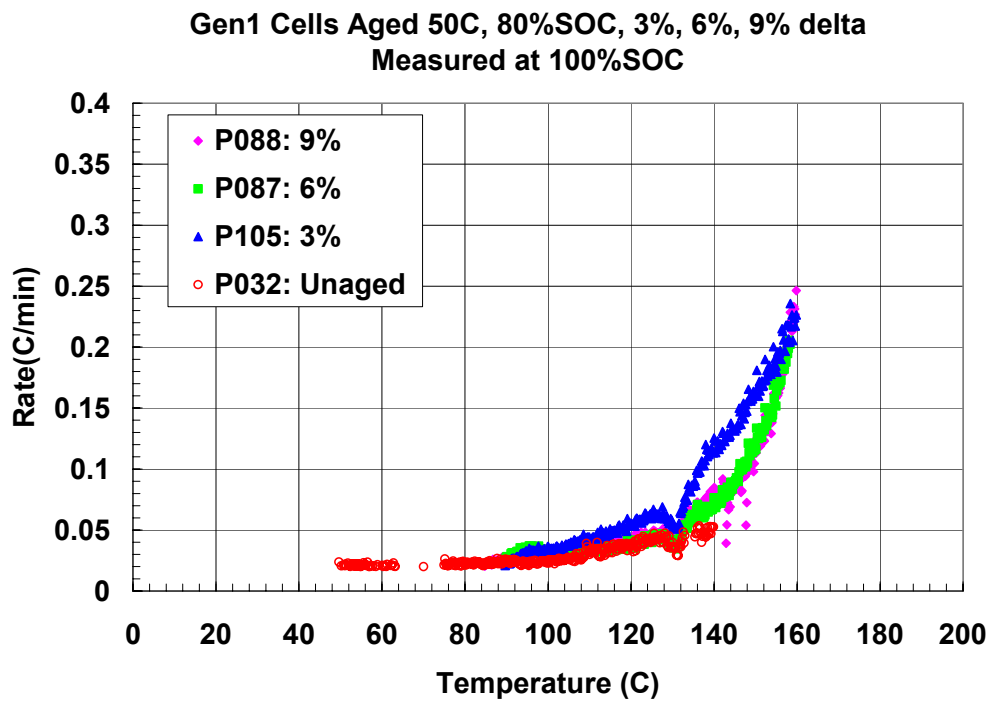
Figure 5-29. ARC runs of Gen1 cells (100% SOC) aged at 50ºC, 8% SOC, at 3%, 6%, and 9% delta.

Gen1 Cells Aged 60C, 80%SOC, 3%, 6%, 9% delta
Measured at 100%SOC
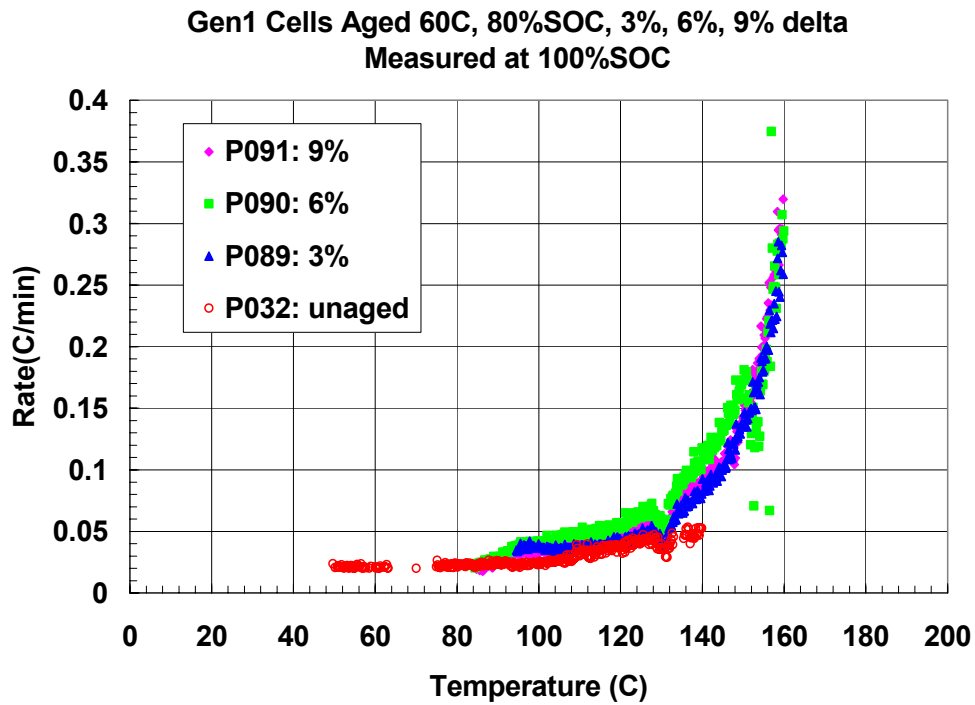
Figure 5-30. ARC runs of Gen1 cells (100% SOC) aged at 60ºC, 80% SOC, at 3%, 6%, and 9% delta.

Gen1 Cells Aged 80%SOC, 3% delta: 40C, 50C, 60C
Measured at 100%SOC
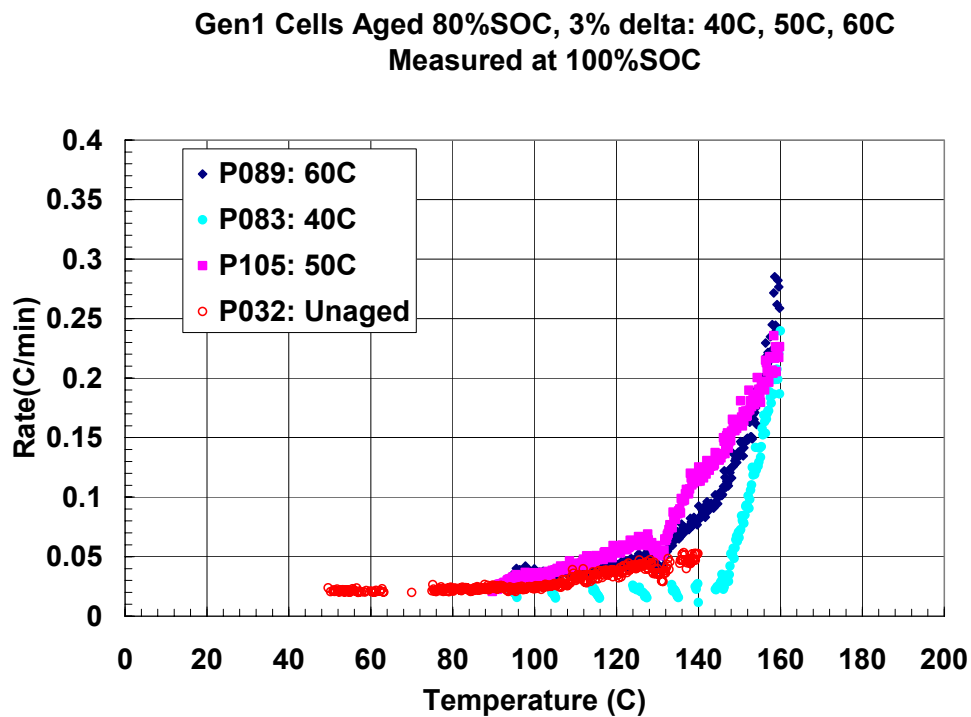
Figure 5-31. ARC runs of Gen1 cells (100% SOC) aged 80% SOC, 3% delta at 40ºC, 50ºC, and 60ºC.

Gen1 Cells Aged 80%SOC, 6% delta: 40C, 50C, 60C
Measured at 100%SOC
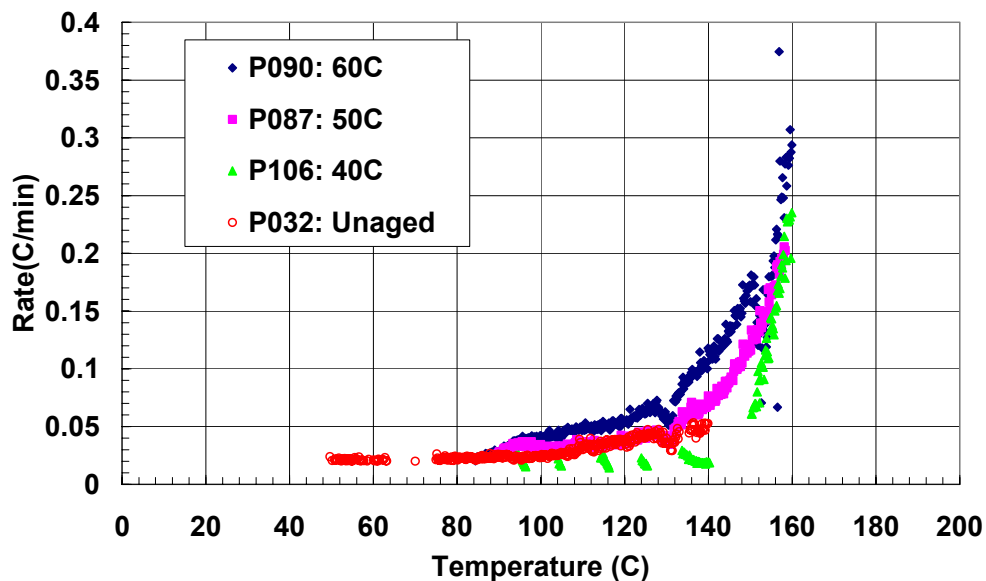
Figure 5-32. ARC runs of Gen1 cells (100% SOC) aged 80% SOC, 6% delta at 40ºC, 50ºC, and 60ºC.

Gen1 Cells Aged 80%SOC, 9% delta: 40C, 50C, 60C
Measured at 100%SOC
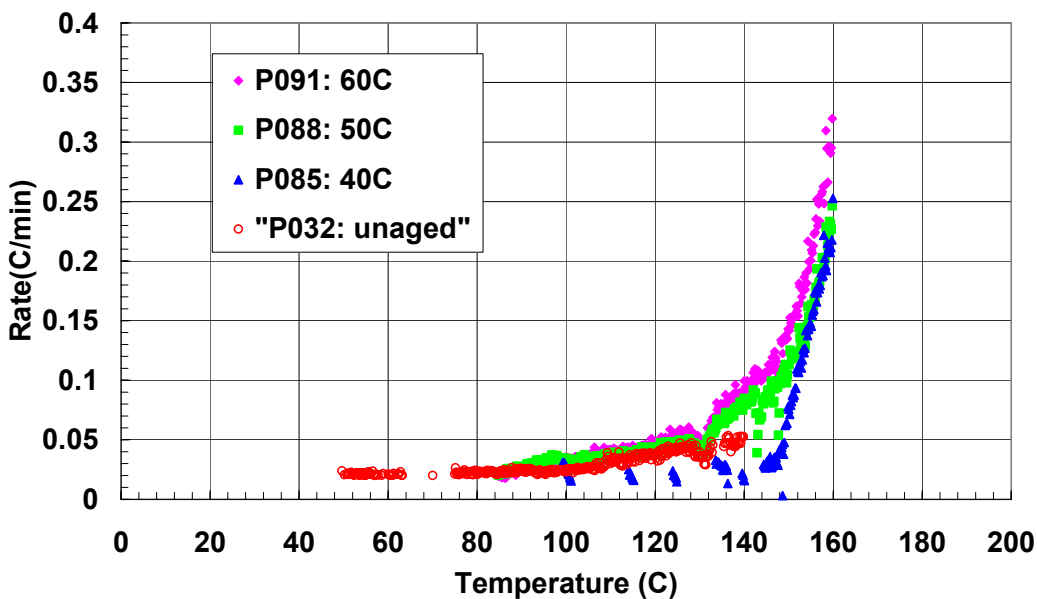
Figure 5-33. ARC runs of Gen1 cells (100% SOC) aged 80% SOC, 9% delta at 40ºC, 50ºC, and 60ºC.

5.2.4 Gen2 Cell Measurements

Measurements of Gen2 cells encompassed characterization of full cells and cell components from disassembled cells as was done for the Gen1 and Sony cells. ARC measurements of full cells were performed on cells in a special cell fixture that was pressure tight up to 400°C and allowed monitoring of cell voltage and measurement of the evolved cell gases. Cells were measured at different SOCs and as a function of aging. Cell components were measured in ARC bombs as well as by DSC. Evolved gases from electrolyte decomposition were measured to determine the relative contribution of the electrolyte components to heat and gas generation. The Gen2 thermal properties are compared with Gen1 and Sony data to determine a mechanistic understanding of general Li-ion cell abuse tolerance.

5.2.4.1 ARC Measurements (Unaged Cells)

Gen2 cells were measured by ARC at 100%SOC and compared with Gen1 and Sony cells at the same SOC. Figure 5-34 shows the thermal runaway profile of these Gen2 cells up to 160°C. The Gen2 cells were much more reactive than the Gen1 cells, exhibiting sustained, accelerating heating rates as low as 50°C. The heating rate increased smoothly up to the maximum run temperature and showed very similar heating rates to the Sony cells above 110°C. However, the Gen2 cells did not show the increased knee in the heating rate above 110°C seen for the Sony cells resulting from SEI decomposition. The Gen2 cells did show the characteristic endotherm resulting from separator melt but then resumed accelerated heating as projected from the previous rate. Many of these initial "fresh" cells did not vent up to the maximum temperature of 160°C while some cells vented around 130°C. Figure 5-35 shows the ARC data for both unvented and vented cells. Venting resulted in significant cell cooling from the escaping gases but the accelerating heating continued until the higher temperature explosive decomposition temperature was reached. Gas evolution resulted from decomposition reactions of the cell electrolyte and call electrodes. This intrinsic gas evolution in the full cell was measured by pre-puncturing the cell vent immediately prior to placing the cell in the ARC cell fixture. The gas and heat evolution was then monitored from room temperature to the final ARC maximum run temperature. Figure 5-36 shows that gas generation began around 125°C, which was just below the vent temperature seen in the non-punctured cells. The punctured cell data revealed that the onset of significant gas generation was quite abrupt. Pressure and heating rate data for vented cells are shown in Figure 5-37. These cells were at 60% SOC but had experienced some additional aging at elevated temperature. This figure shows that venting can occur over a wide range of temperatures depending on cell condition and history. The cells initially showed some cooling but the exothermic reactions continued to increase the cell temperature. Gas generation increased with increasing temperature and showed evidence of discrete reaction events with increasing temperature. ARC bomb measurements of cell components will reveal the source and nature of this decomposition reaction. Analysis of the generated gas species was performed using GC techniques and are reported in a later section of this report.

The effects of cell state of charge are shown in Figure 5-38 for cells at 100% SOC and 60%SOC. The cells showed increased heating rate for cells at higher SOC as was seen for the Sony and Gen1 cells. However, the increase in the heating rate for the higher SOC cell did not become evident until above 110°C, the temperature previously associated with SEI

decomposition. The cell voltages are also shown. The voltages did not decrease until the end of the separator endotherm, at which temperature the separator would have lost integrity and the open porosity necessary for ionic conduction. No discontinuous increase in heating rates was observed which suggests that no hard short circuits occurred after separator melt.

Cell Comparisons: Sony, Gen1, Gen2
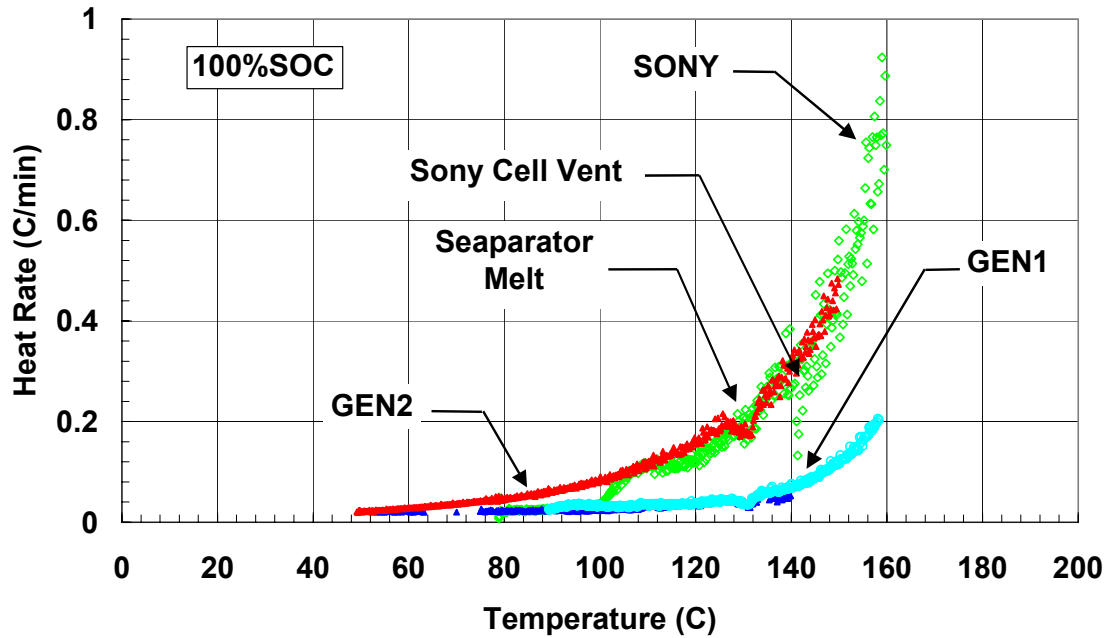
Figure 5-34.   **ARC runs of Sony, Gen1, and Gen2 cells at 100% SOC.**
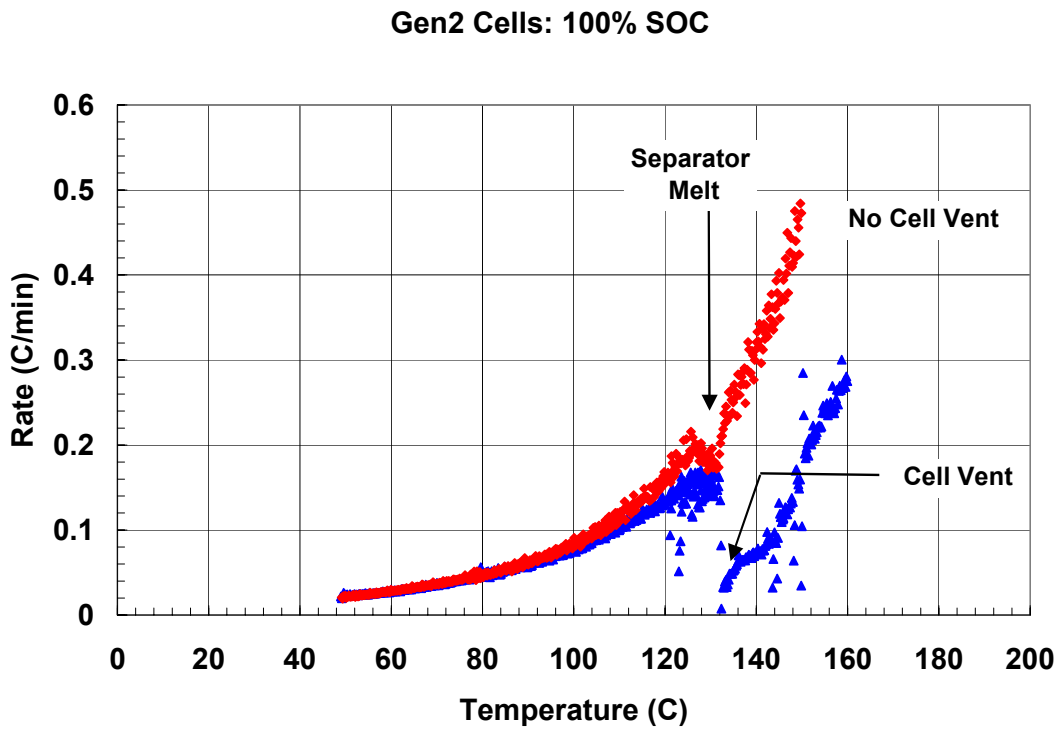
Gen2 Cells: 100% SOC

Figure 5-35.   ARC runs of Gen2 cells at 100% SOC, vented and non-vented.

Gen2 Cell: 100%SOC
Pre-Punctured
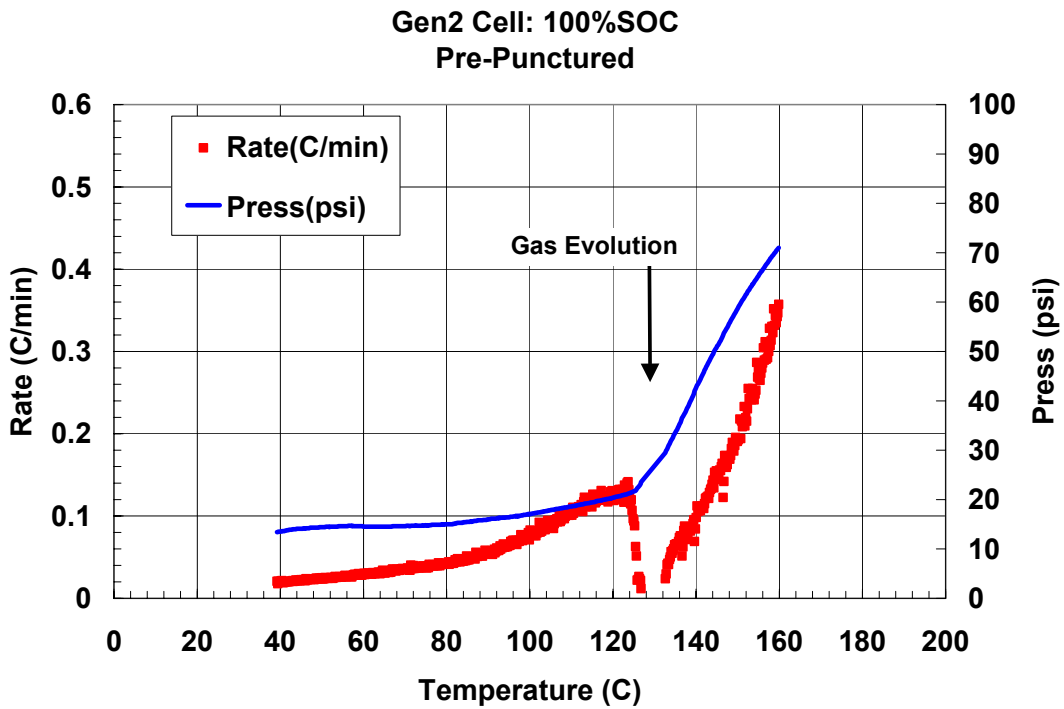
Figure 5-36.   ARC run of Gen2 cell (100% SOC) pre-punctured.

60%SOC Cells Aged
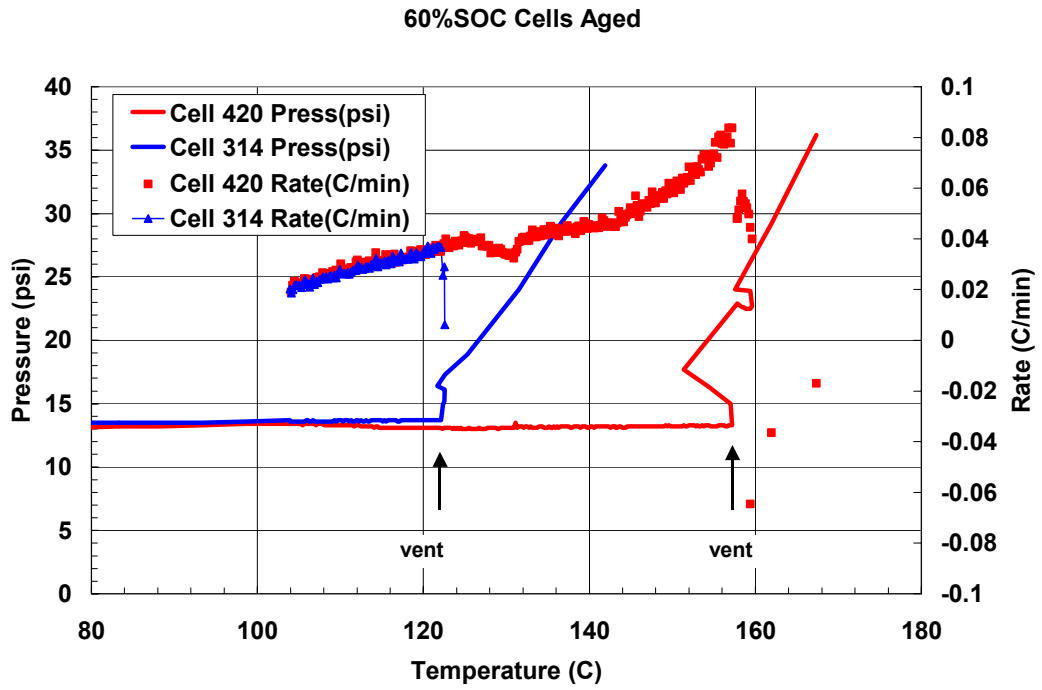
Figure 5-37. ARC runs of Gen2 cells (60% SOC) vented at 125ºC and 155ºC.

GEN2 Cells: 100% SOC; 60% SOC
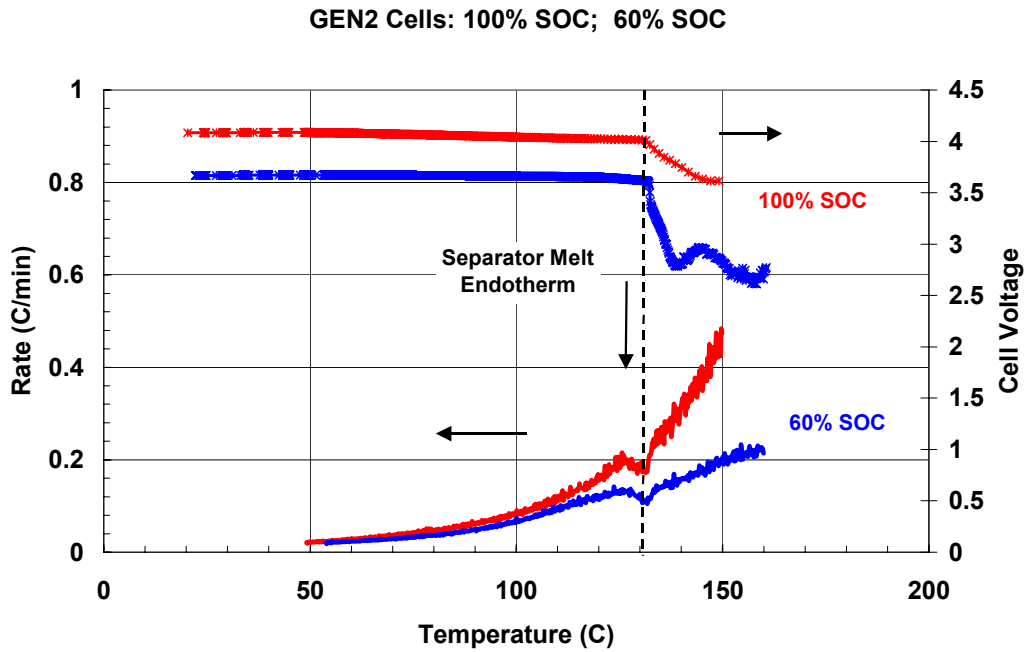
Figure 5-38. ARC runs with cell voltages of Gen2 cells at 60% and 100% SOC.

5.2.4.2 DSC Gen2 Cell Components

Differential scanning calorimetry (DSC) was performed on Gen2 electrode materials up to 400°C both in crimped-sealed Al pans and hermetic steel pans. Materials were obtained from disassembled cells and from fresh Gen2 electrodes that were cycled in a T-cell. The T-cell electrodes were cycled against Li using Gen2 electrolyte and placed in a known state of charge. The thermal signature of these materials were compared to similar measurements of Gen1 materials and used to identify heat generation mechanisms observed by ARC runs of full cells and cell components.

Initial DSC measurements were performed of the Gen2 electrolyte and compared to the thermal response of the Gen1 electrolyte. Samples were run in the steel hermetic sealed pans at a heating rate of 5°C/min. Figure 5-39 shows that the Gen2 EC:EMC/1.2M LiPF$_6$ had very similar decomposition profile compared to the Gen1 EC:DEC/1M LiPF$_6$. Both electrolytes had a peak in the DSC exotherms at 250°C. The Gen2 electrolyte showed a slightly higher exothermic peak and had a more pronounced endotherm just prior to the exothermic region. This behavior has been reported previously for this material [16].
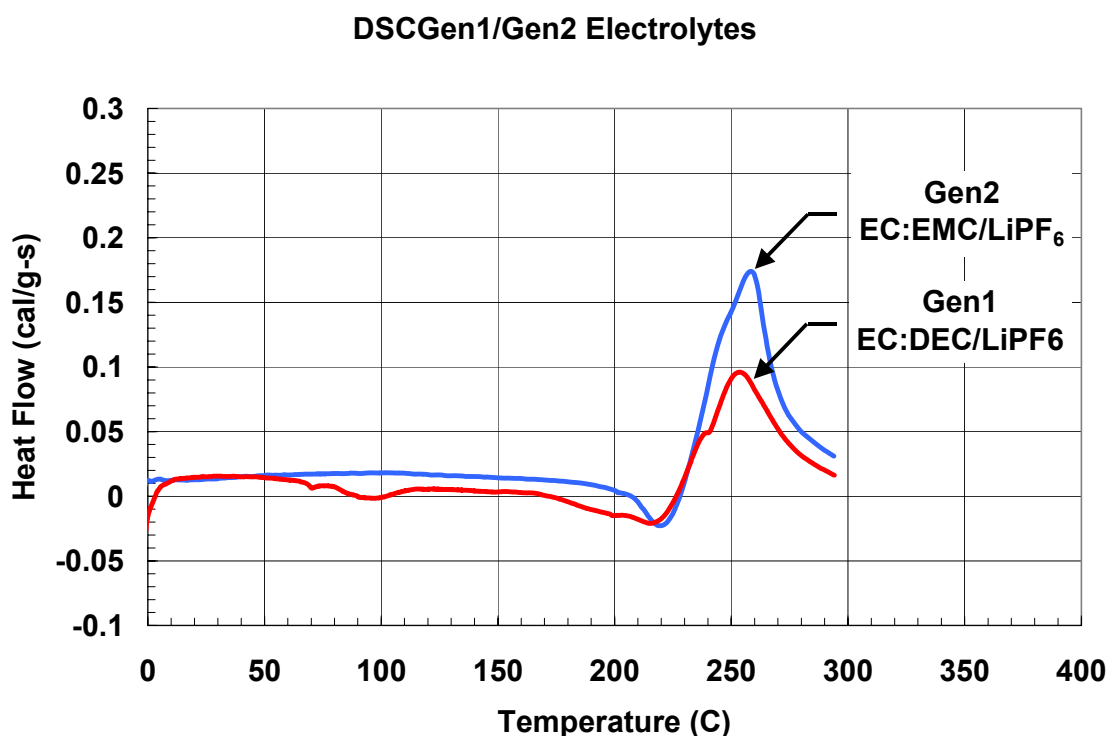
Figure 5-39.   DSC runs of Gen1 and Gen2electrolytes in hermetic sealed pans.

Gen2 anode materials were measured in both the charged and discharged state and the DSC profiles are shown in Figure 5-40. A baseline Gen2 cell that had only been held in the open circuit state at 10°C was used as a source of material. The DSC heat flow was computed using the film weight of the anode material that includes active carbon, conductive carbon, binder and electrolyte. The 100%SOC material showed an onset of exothermic reaction beginning around 120°C and increased with increasing temperature. A peak in the reactivity

was measured at 250°C followed by a sharp drop off in reaction rate above this temperature. The endothermic dip at 275°C resulted from venting of the cell gases. The discharged anode material showed very little exothermic reactivity. A narrow exothermic peak at 100°C is associated with SEI decomposition as seen for the previous materials and was followed by the slight venting endotherm at 275°C.

The Gen2 cathode materials from the same cell source were also measured in the charged and discharged state and the DSC data are shown in Figure 5-41. The cathode materials also showed a very strong dependence on state of charge. The charged Gen2 cathode material (in excess electrolyte) showed a peak in reactivity at 250°C followed by a very abrupt reduction in heat output. The discharged cathode material showed only a small exothermic region between 250°C and 300°C.
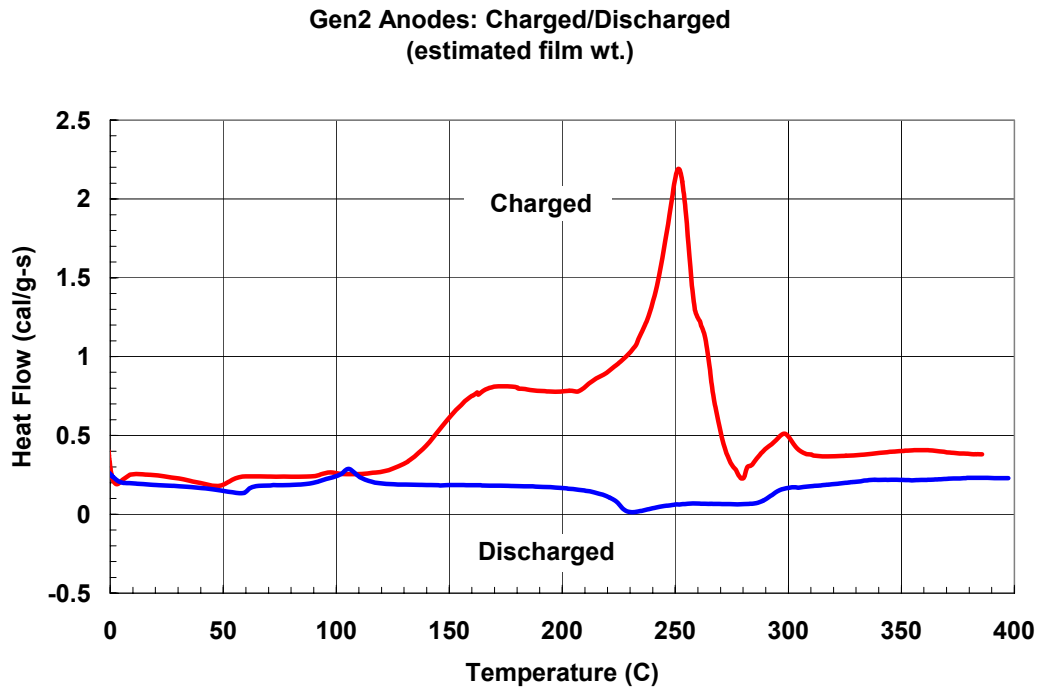
Figure 5-40.   DSC runs of Gen2 anodes, charged and discharged.

Gen 2 Cell (aged 45C/80%SOC/8 wks)
Cathodes with Electrolyte
(estimated film wt.)
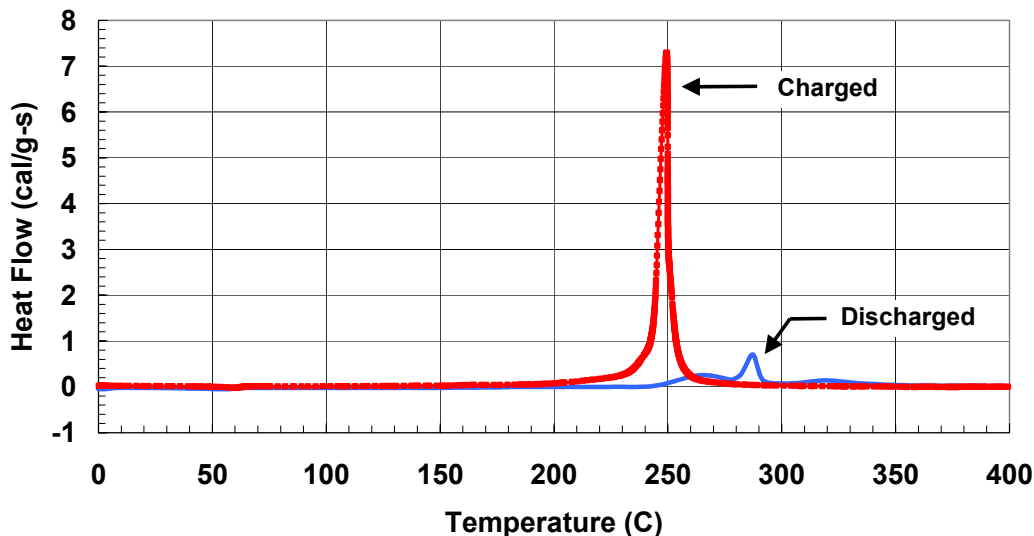
Figure 5-41.   DSC runs of Gen2 cathodes, charged and discharged.

The reactions with the charged cathode were found to be a function of the electrolyte to cathode mass ratio as shown in Figure 5-42. An initial reaction around 230°C to 240°C was observed whose magnitude scaled with the cathode mass and was independent of electrolyte level. This reaction was followed by a reaction peak at 260°C that increased with increasing electrolyte mass. The first reaction can be attributed to exothermic decomposition of the cathode material and reaction with the electrolyte. The second peak increased significantly when the ratio of electrolyte to cathode film exceeded 10wt%-15wt%. This level of electrolyte is consistent with the level of electrolyte absorbed into the pores of the cathode film. Thus, the second peak corresponds to decomposition of the excess electrolyte while in the first peak the absorbed electrolyte was combusted within the porosity of the cathode film.

The Gen2 anode and cathode materials measured in the Al DSC pans are compared in Figure 5-43. The anode and cathode material show peaks in reactivity very close to the same temperature but the anode shows the onset of low-rate reactions at much lower temperatures while the cathode shows a much sharper high-temperature reaction peak. These materials were also measured in the hermetic steel pans to contain all generated gas species during the DSC scan. These scans were performed at 5°C/min as compared to the 10°C/min for the Al pans. Because of the lower scan rate, the heat power measurements for the steel pans need to be multiplied by a factor of two for direct comparison with the Al pan data. Figure 5-44 compares the anode and cathode scans performed with these hermetic pans. The peaks in the heating rates were only slightly higher than was observed for the Al pans and both anode and cathode still showed coincident peak temperatures. The magnitude of the anode reaction was higher in the hermetic pans suggesting that this reaction involved the electrolyte decomposition gas species more so than did the cathode reaction. The low-rate anode

69

reactions beginning around 125°C were still evident. The cathode peak reaction rate was very close to that seen in the Al pans after appropriate scaling.

The Sony, Gen1, and Gen2 anode materials at 100%SOC are compared in Figure 5-45. The Sony anodes showed the most distinct SEI decomposition reaction at 120°C of the three materials. This is consistent with the knee in the heating rate seen in the ARC runs of these cells. The Gen1 and Gen2 anodes showed a continuous reaction starting at 100°C increasing with temperature. The Gen2 anode showed a peak reaction temperature at 250°C, slightly below that for the Gen1 anode material at 275°C, suggesting that the Gen2 anode SEI underwent a more rapid final decomposition and reaction with the electrolyte [11]. Neither Gen1 nor Gen2 anode materials showed the higher temperature exotherm at 350°C as seen for the Sony anodes. The SEI decomposition reaction is most clearly seen for the discharged anode materials where there is no confounding exotherms from electrolyte reduction. Figure 5-46 compares the Gen1 and Gen2 discharged anode DSC scans. This figure shows that the Gen2 anode SEI decomposes at a lower temperature than seen for the Gen1 anode SEI. This data is consistent with the ARC results obtained for the full cells. These results are consistent with the differences in the anode carbon materials. The Gen1 cell used MCMB carbon that has small spherical particles and can be easily passivated with an SEI layer. The Gen2 carbon active material was MAG10, which was non-spherical graphite with flaky edges. SEM micrographs of these anode carbons are shown in Figure 5-47 [19]. Our data (ARC, DSC and microcal) indicate that these MAG10 carbon particles do not form an effective passivating layer and allow continued reaction of the lithiated carbon with the electrolyte. These reactions begin as low as 50°C and constitute the initial source of heat output leading to thermal runaway.

The Sony, Gen1 and Gen2 cathode materials are compared in Figure 5-48. The Sony cathode material ($LiCoO_2$) showed the greatest thermal stability with a peak reaction temperature around 225°C. The nickel containing Gen1 cathode material was less stable than the pure cobalt material while the Gen2 cathode ($LiNi_{0.8}Co_{0.15}Al_{0.05}O_2$) was more stable than the Gen1 material ($LiNi_{0.85}Co_{0.15}O_2$) [13-15]. The aluminum doping achieves a small but measurable increase in thermal stability as determined by DSC. The exothermic reaction of the cathode is believed to result primarily from combustion of the electrolyte by evolved oxygen from the decomposing cathode oxide [13,14]. The exact nature of the reaction is a function of the inherent stability of the cathode material and relative amounts of cathode and electrolyte [14].

70

Gen2 EOL Cell Cathode/Electrolyte
80%SOC (Hermetic Pans)
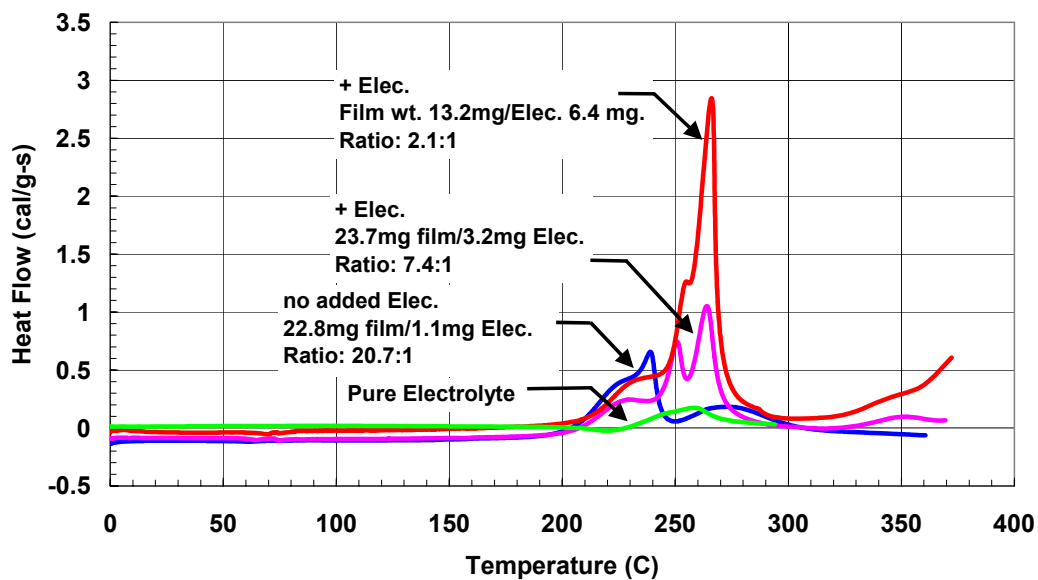
Figure 5-42.   DSC runs of Gen2 cathodes with increasing electrolyte/film ratios.

Gen 2 Anodes/Cathodes with Electrolyte
(estimated film wt.)
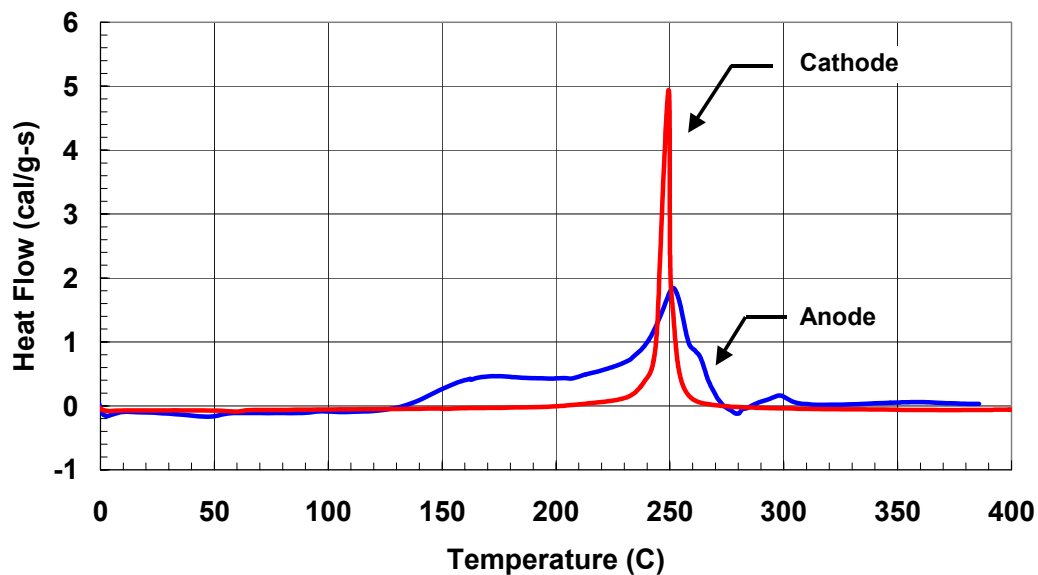
Figure 5-43.   DSC runs of Gen2 anode and cathode (100% SOC) in crimped pans.

Gen2 cell 446 Cathode & Anode (80%SOC) + Elec.
(Hermetic Steel Pans)

Cathode: 587 cal/g

Anode: 386 cal/g
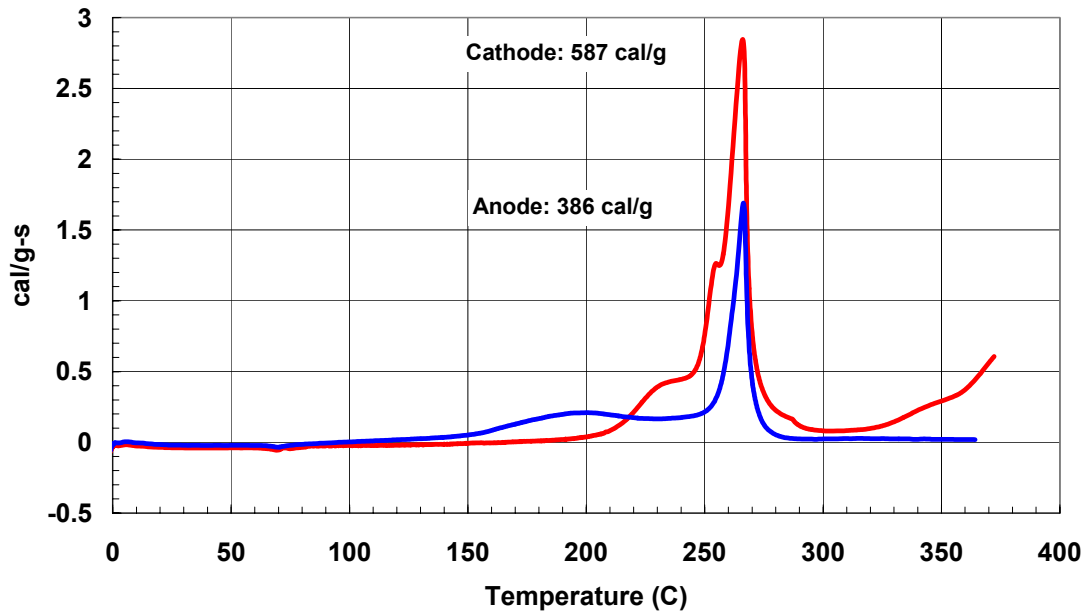
Figure 5-44.   DSC runs of Gen2 anode and cathode in hermetic sealed pans.

Gen2 Gen1 Sony Anodes Charged
(estimated film wt.)
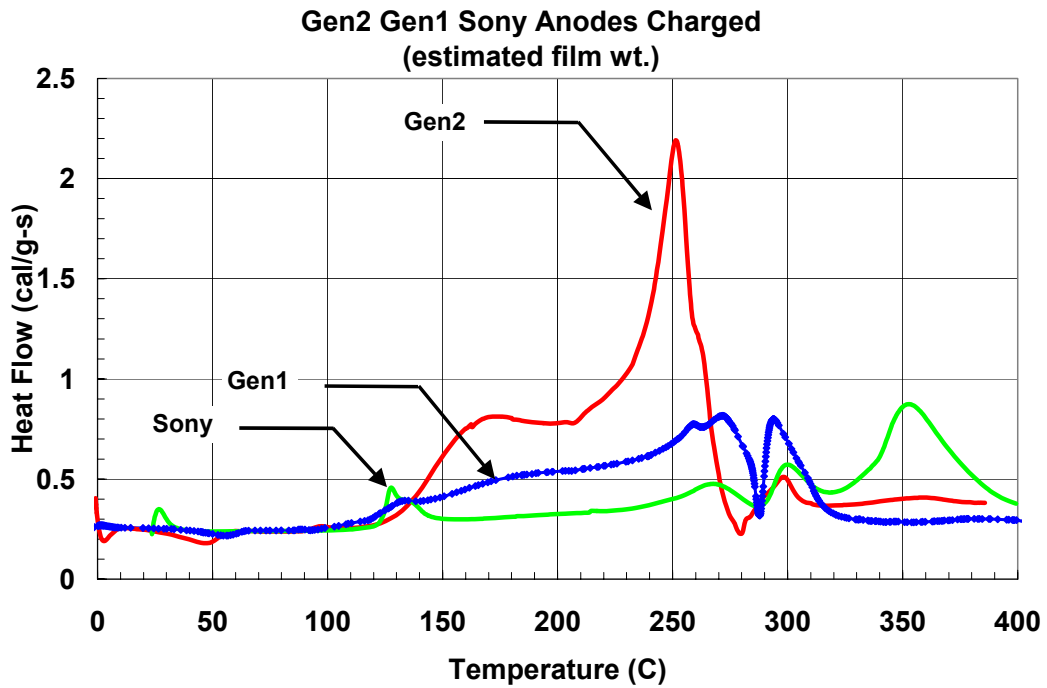
Gen2

Gen1

Sony

Figure 5-45.   DSC runs of SONY, Gen1, and Gen2 anodes (100% SOC) in electrolyte.
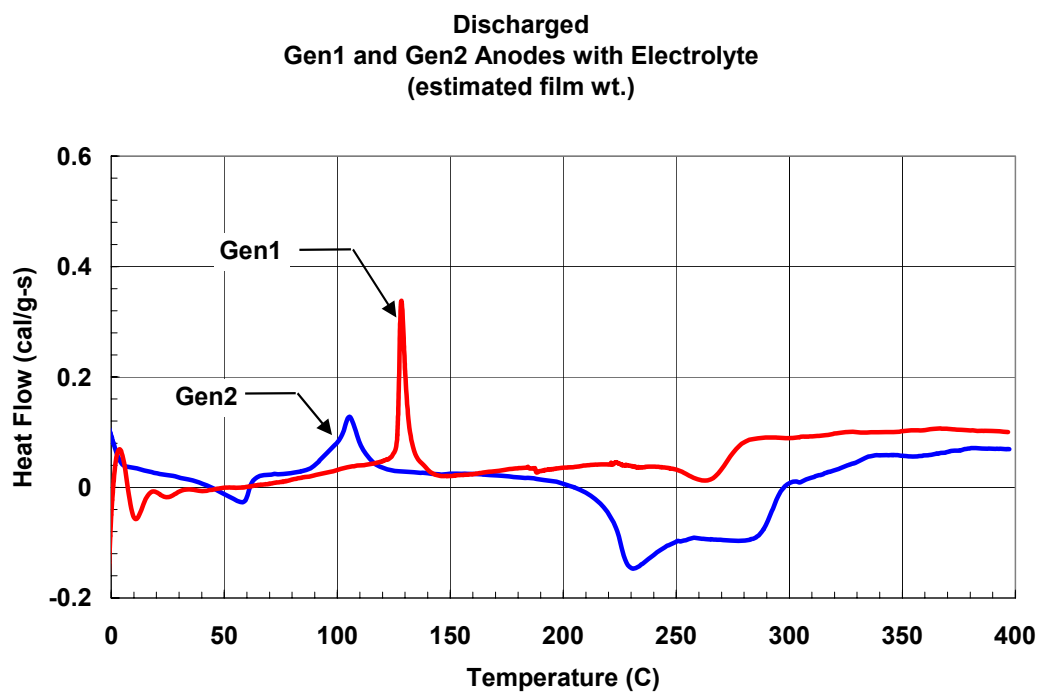
Figure 5-46. DSC runs of discharged Gen1 and Gen2 anodes in electrolyte.

**MCMB-6
(Gen 1anode)**
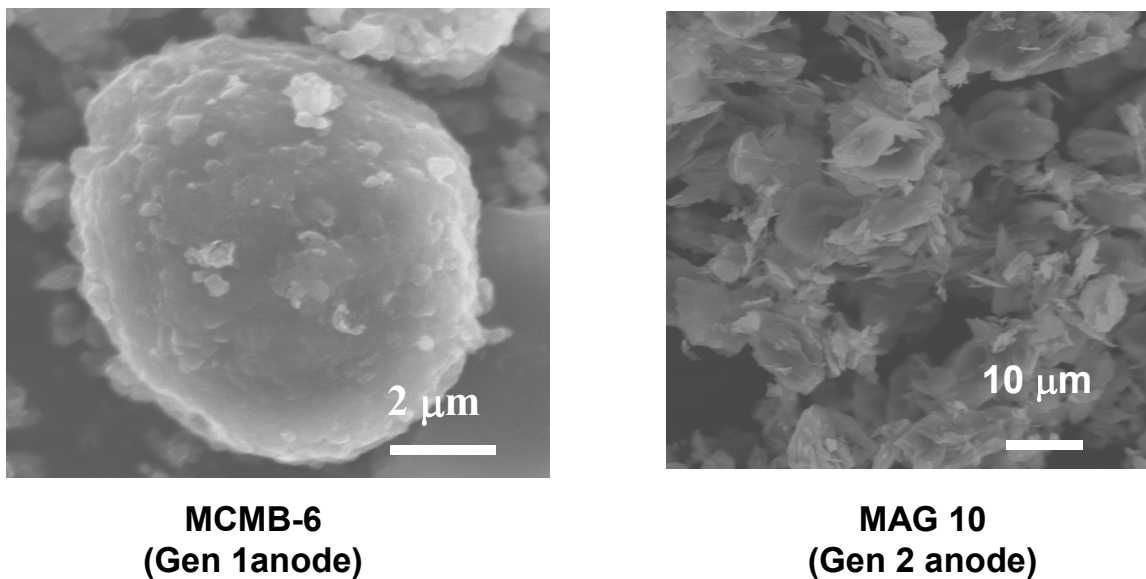
**MAG 10
(Gen 2 anode)**

Figure 5-47. SEM micrographs of Gen1 (MCMB) and Gen2 (MAG10) anodes.

Gen2 Gen1 Sony Charged Cathodes
(est. film wt.)
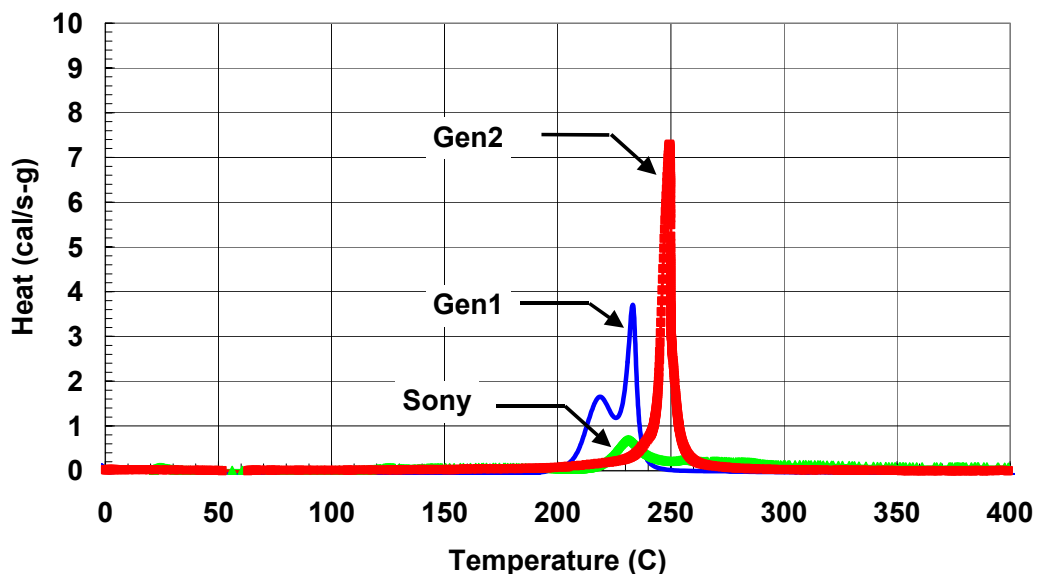
Figure 5-48.   DSC comparison runs of Sony, Gen1, and Gen2 cathodes (100% SOC) in electrolyte.

5.2.4.3 Aged Gen2 Cells – DSC Measurements

The effects of aging at elevated temperatures were measured by performing DSC and ARC runs of thermally aged Gen2 cells. A total of 12 cells were aged at 45°C/80%SOC for 8 weeks. Reference Performance Tests (RPTs) were performed at 4 weeks and 8 weeks to measure power fade [18]. The aging test was terminated when 15% capacity fade was reached, which is about half the allowed PNGV power fade limit. DSC scans of materials from the disassembled cells were performed in Al pans and compared to scans of the unaged materials. Figure 5-49 shows the data for the anode materials measured at 100%SOC. This figure shows that aging resulted in a decrease in the reactivity of the anode material over the entire temperature range. Similarly, the aged and unaged cathode materials are compared in Figure 5-50 along with fresh cathode material from a T-cell. The fresh T-cell cathode showed a reaction peak at 275°C while the cycled, full-cell cathode materials showed a reaction peak that moved to lower temperature with increased aging. Aging can possibly result in continued development of a passivation layer that impedes the reaction of the cathode decomposition products with the electrolyte. The 20-week aged cathode also showed a second exotherm around 265°C which may result from further reaction of the cathode with residual electrolyte. Since the initial lower-temperature reactions were impeded, not all of the electrolyte was consumed and further reactions could take place. These reactions have been postulated to result from reduction of the metal oxide (CoO, Ni_xCo_yO, etc.) to the pure metals [14] but the exact reaction products are not known. The aged cathode materials also showed a small exotherm around 120°C which was very similar to that seen in the discharged anode material.

74

Aging Effect in Gen2 Anodes
(estimated film wt.)
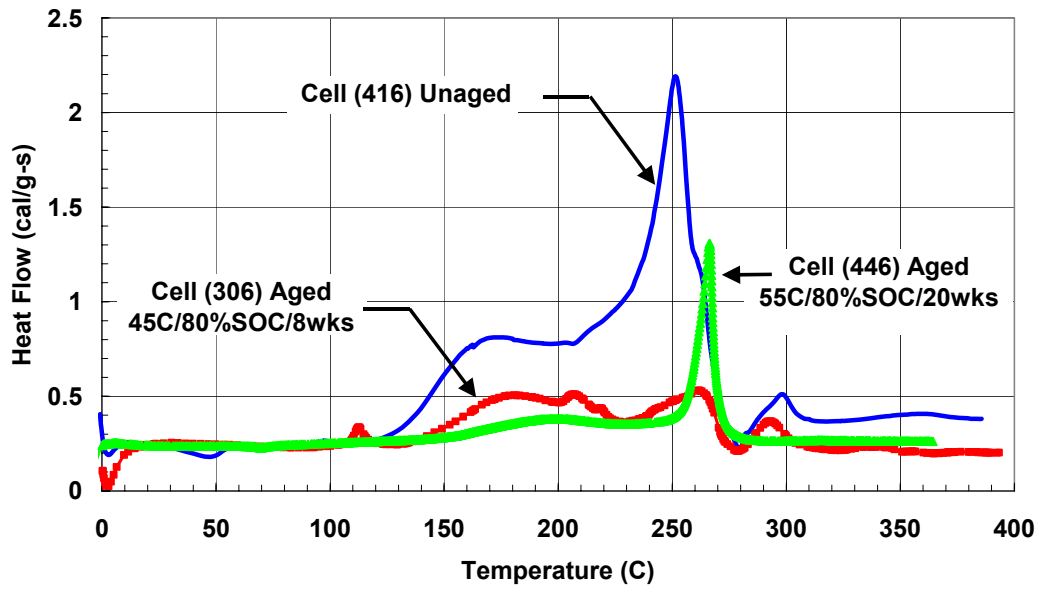
Figure 5-49.   DSC runs of Gen2 anodes unaged and aged 45ºC, 80% SOC, 8 weeks.

Effect of Aging
Gen2 Cathodes in Electrolyte
(estimated film wt.)
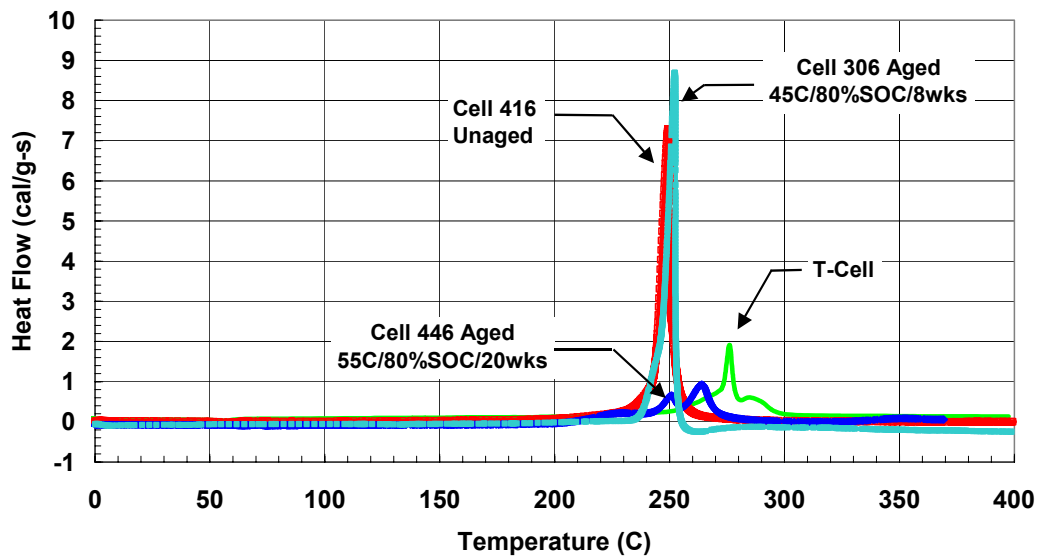
Figure 5-50.   DSC runs Gen2 cathode material, effect of aging.

5.2.4.4 Aged Gen2 Cells – ARC Measurements

Initial ARC runs were performed on the aged cells at 100% SOC and compared to unaged cells. Figure 5-51 shows that the aged cells have lower heat rate than the unaged cells as was seen for the aged Gen1 and Sony cells. Passivation of the anode by the SEI diminishes the electrolyte reduction by the lithiated carbon. The aged cells all vented during the ARC runs, even at low SOCs, which indicates that gas continued to develop in the cell headspace during aging. Aged and unaged cells at 60%SOC are compared in Figure 5-52. Aging again reduced the heating rate but the effect at low SOC was greatly reduced compared to the higher SOC cells. The reduced Li level in the low SOC cells would naturally result in a reduced exothermic reaction rate with the electrolyte even as the SEI layer breaks down. The effect of aging on the Gen2 cells was less noticeable than was observed for the Gen1 cells and especially as was observed for the Sony cells. This aging difference can again be attributed to the nature of the Gen2 anode carbon particles that are less effective in forming a protective SEI layer. The full cell ARC behavior was consistent with the shift in the material properties seen by DSC.
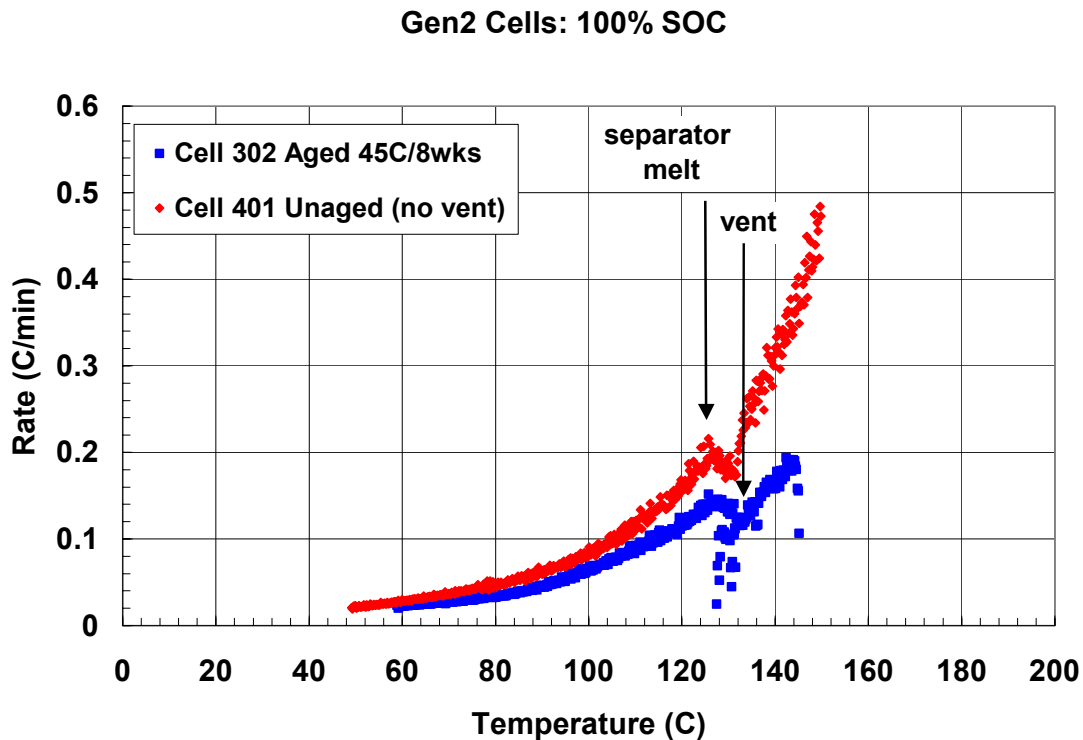
Gen2 Cells: 100% SOC

Figure 5-51.   ARC runs of Gen2 cells (100% SOC), effect of aging.

Gen2 Cells: 60%SOC aged/unaged
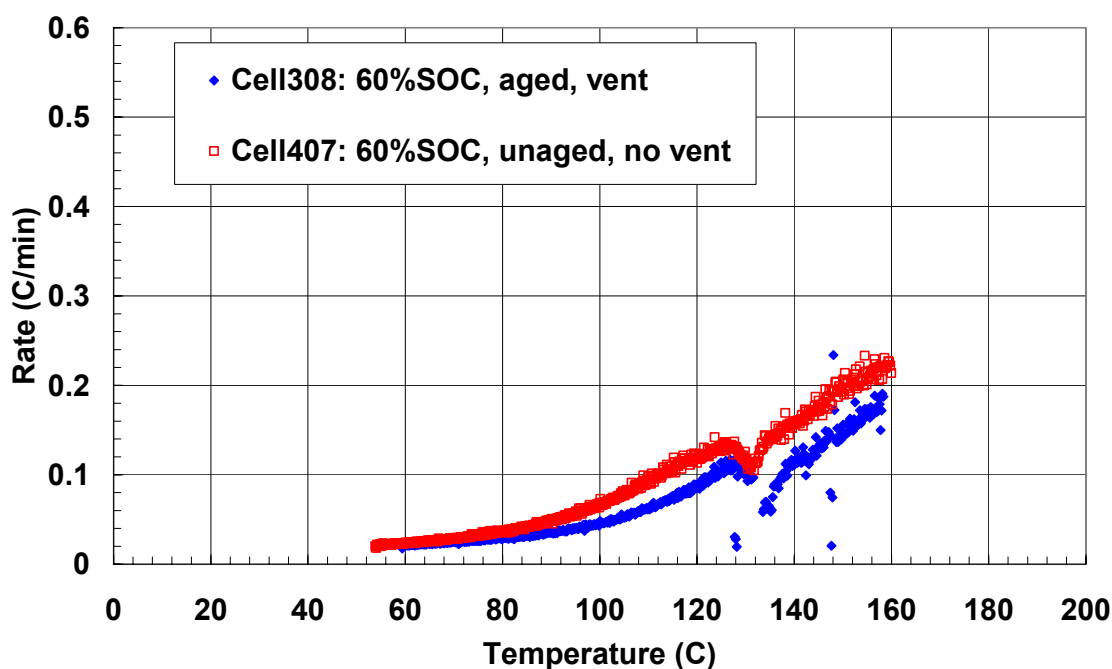
Figure 5-52.   ARC run of Gen2 cells (60% SOC), effect of aging.

5.2.4.5 Cell Materials – ARC Bomb Runs Gen2 Electrolyte and Electrode Reactions

The Gen2 material components were measured using the ARC bomb technique as described earlier. These measurements give a more representative measure of cell material performance under conditions similar to actual cell thermal runaway. Measurements were performed of Gen2 electrolyte and of anode and cathode material removed from disassembled cells. The cell chosen for these runs was an end of life cell which had been aged at 55°C/80%SOC for 20 weeks and had experienced a 57% power fade.

The Gen2 electrolyte (EC:EMC (3:7) /1.2M LiPF$_6$) decomposition reaction is shown in Figure 5-53. The exothermic reaction abruptly increased above the ARC threshold at 180°C with a peak in the reaction rate at 190°C followed by a rapid decrease in rate by 210°C. This narrow peak in exothermic decomposition of the electrolyte occurred in the same temperature region as the peaks in cathode and anode reactions. All three of these reactions contribute to the explosive decomposition of the cell seen in the heating block runs starting at 180°C. The pressure associated with gas generation during the electrolyte decomposition is also shown in the figure. Gas generation started to increase rapidly at 150°C and was complete by the end of the exotherm at 210°C. Gas generation was not directly linked to heat generation during the decomposition of the electrolyte. Pressure increase at higher temperatures resulted from continued heating of the gas species during the ARC run. No further reactions were observed up to the maximum temperature of 300°C. Gas samples were taken for later GC analysis.

The anode materials from the disassembled Gen2 cell were measured in the ARC bomb with a similar amount of Gen2 electrolyte. Figure 5-54 shows that low-level reactions were observed as low as 140°C but were not self-sustaining. The quantity of anode material was not sufficient to allow accurate measurements of low-rate reactions above the threshold limit of the ARC. A sharp peak in reaction rate was observed at 225°C. The peak reaction temperature measured in the ARC bomb was lower than that measured in the DSC runs due to the near equilibrium reactions measured in the ARC. ARC runs typically run for 24 hours or longer (rate < 0.2°C /min) while the DSC scans at a fixed rate of 5-10°C /min. DSC scans will force kinetically limited reactions to occur at higher temperatures during the scan.

Gas generation by the anode material occurred at higher temperatures than observed for just pure electrolyte even though similar amounts of electrolyte were present. The anode materials have a porous structure such that the anode films absorb 60%-100% electrolyte by weight. Thus, the reaction of the electrolyte occurs in intimate contact with the anode particle surfaces. The gas generation during the anode decomposition occurred during the exothermic peak temperature region at 225°C. This is opposed to the electrolyte gas generation that initiated at much lower temperature and was not associated with the exothermic reactions. Pressure increase prior to and following this event resulted primarily from heating of the headspace gases.

The ratio of electrolyte to anode film can affect the overall decomposition reaction. ARC bomb runs were performed using both "as removed" anode material and anode material with added electrolyte. The "as removed" anode films were estimated to have about 40% by weight of electrolyte. Two runs were performed with electrolyte/film ratios of 0.4:1 and 1.07:1. The ARC data are compared in Figure 5-55. The lower electrolyte/film ratio sample showed a reaction temperature peak 25°C lower than seen for the high ratio sample. These low-ratio reactions may more closely represent the anode reactions in a vented cell that has lost much of the electrolyte.

The Gen2 cathode film material was measured in the ARC bombs in a similar manner as the anode material. The cathode films typically only absorb 5%-10% electrolyte by weight. Initial ARC bomb runs were performed on "as removed" cathode material with this low electrolyte content. Figure 5-56 shows that the onset of exothermic reactions occurred as low as 130°C followed by a rapid increase in heating rate up to a peak temperature of 190°C. The reaction rate dropped rapidly following the peak indicating exhaustion of the reactants. The gas generation associated with this decomposition began at the same initial temperature but increased steadily throughout the temperature range, even after the peak in the exotherm had dropped below threshold.

The effect of electrolyte/cathode film ratio was measured by performing ARC runs of "as removed" cathode film and cathode film with added electrolyte. The "as removed" film weighed 1g while the cathode/electrolyte sample consisted of 0.75g film with 1g of added electrolyte. Figure 5-57 shows the heating rate and pressure data for these two runs. The "as removed" sample is the same sample shown previously in Figure 5-56. The effect of added electrolyte was to decrease the overall reaction rate of the cathode material while increasing the gas generation. Gas generation from the excess electrolyte began above 150°C as was seen for the pure electrolyte runs. This gas generation could result in cooling of the overall

sample and thus shifted the onset of the exotherm to higher temperatures. However, the peak in the reaction rate occurred at 190°C as was seen for the "as removed" sample. These measurements show that added electrolyte did not affect the intrinsic reactions occurring at the cathode at these temperatures.

The Gen2 anode and cathode materials are compared in Figure 5-58. The cathode reaction peak occurred prior to the anode peak and both peaks occurred in the region where explosive decomposition of the cell has been observed. The magnitude of the heating rate was dependent on the mass of material used in the ARC bomb and thus a comparison of the relative contribution of each electrode material to overall cell thermal runaway performance needs to include the balance of each material in the cell. A more accurate comparison of the anode and cathode materials was performed by normalizing the heat rate by the electrochemical state of each material. Thus, the ARC heat rates were divided by the estimated charge capacity (mAh) of each material that then approximated the relative heat contribution that would occur in a balanced cell. Figure 5-59 shows these normalized data along with the exotherm peak for the electrolyte. The electrolyte peak is included only to compare peak reaction temperatures and has not been normalized for its relative contribution to the whole cell. The cathode film is for the "as removed" low-electrolyte film while the anode is for the high-electrolyte film. These reaction profiles suggest that the cathode was contributing significantly to the magnitude of cell heat generation above 140°C while all three cell components contributed to the peak reactions during the explosive decomposition of the cell above 190°C. The full cell thermal response depends on the quantities of each electrode material in the cell and the relative amounts of electrolyte either incorporated in the electrode pores or remaining as free electrolyte. The consumption of electrolyte at the electrodes for a given thermal abuse profile will also determine the high-temperature response of the cell.

Gen2 EC:EMC/1.2M LiPF$_6$
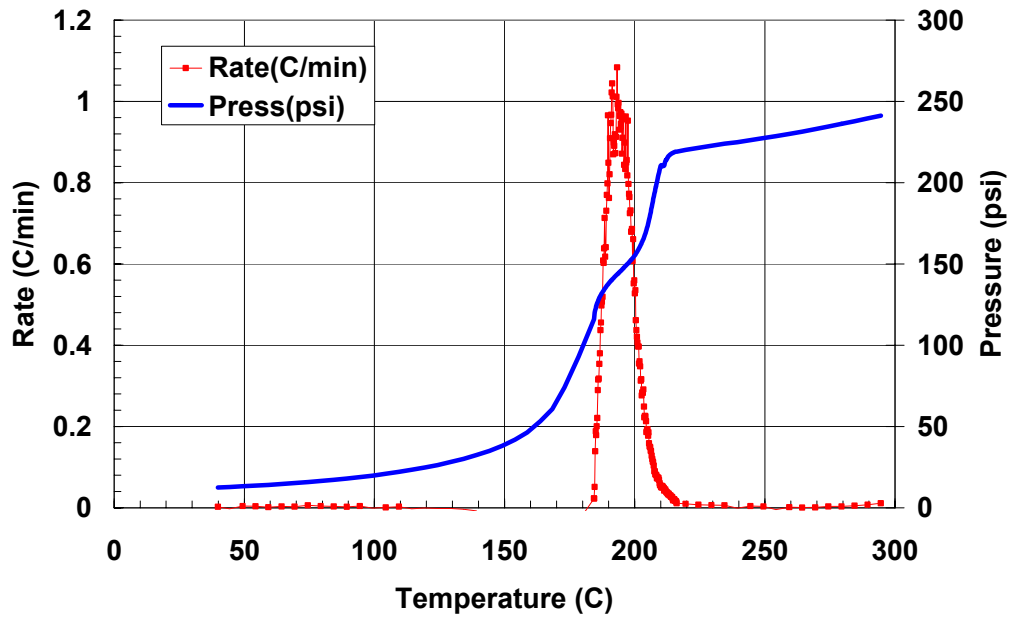
Figure 5-53. ARC bomb runs of Gen2 electrolyte: heat rate and pressure.

**Gen2 Anode Cell 446 (303mg dry film)
with Electrolyte (est. 325mg)**
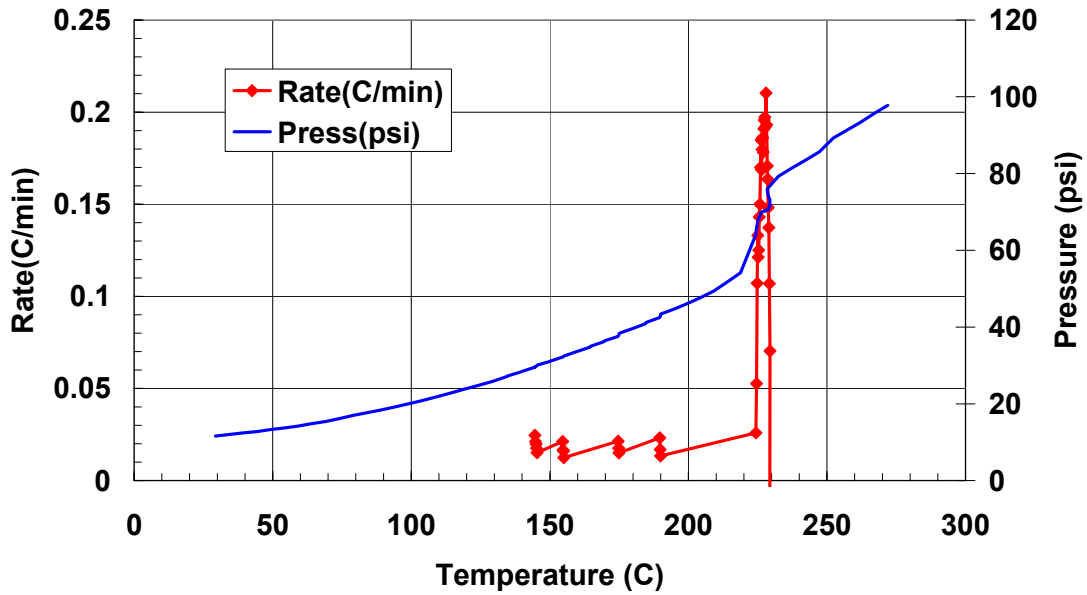
Figure 5-54. ARC bomb run of Gen2 anode (80% SOC) in Gen2 electrolyte: heat rate and pressure

Gen2 Anodes Cell 446
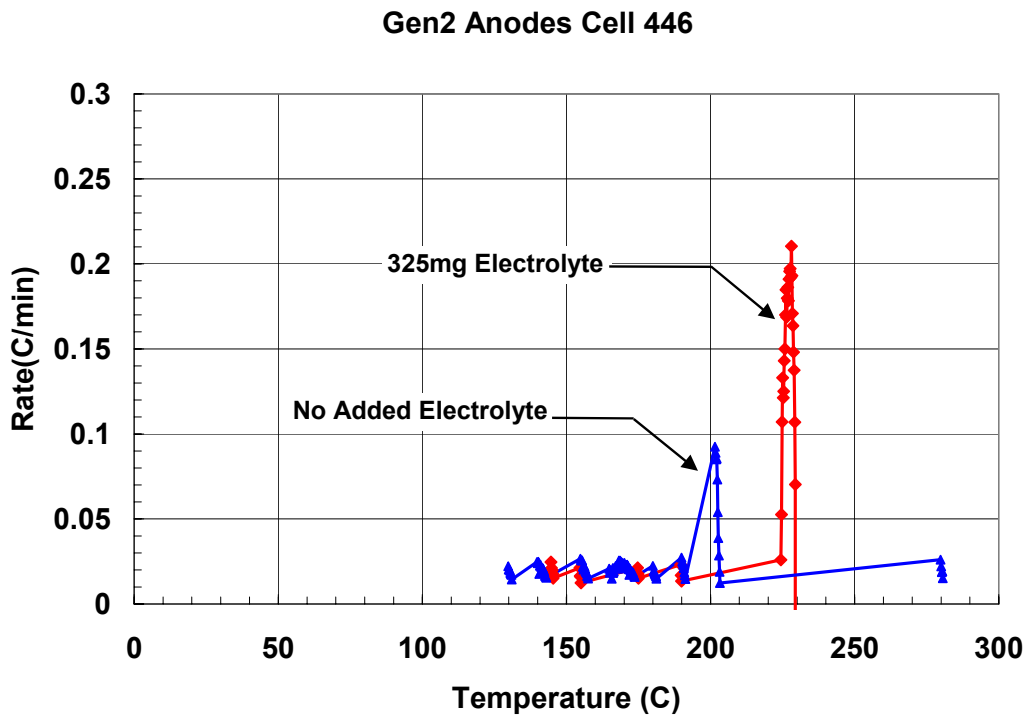
Figure 5-55. ARC runs of Gen2 anodes with and without added electrolyte.

Gen2 Cathode (EOL Cell 446) (no added electrolyte) 80%SOC
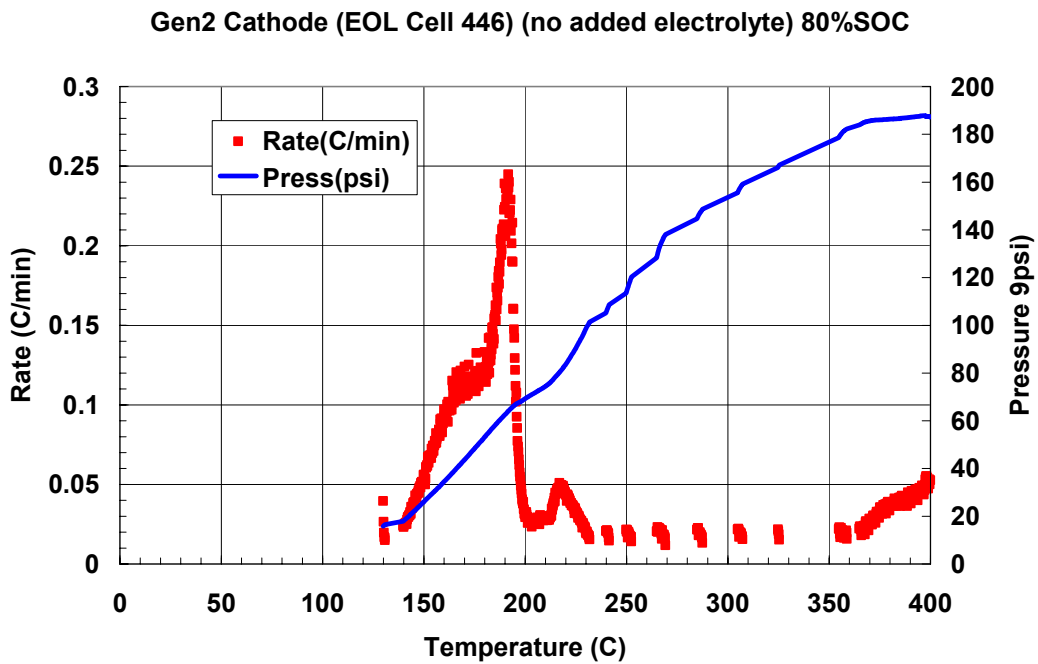
Figure 5-56. ARC runs of Gen2 cathode (80% SOC) with no added electrolyte: heat rate and pressure.

Gen2 Cathodes/Electrolyte
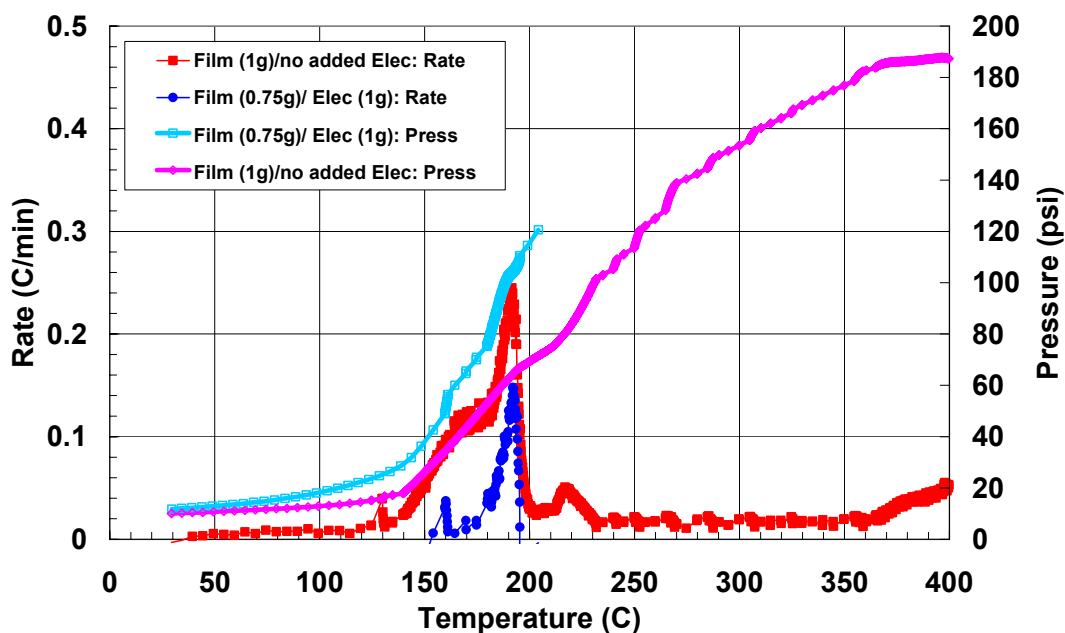
Figure 5-57. ARC run comparisons of Gen2 cathodes (80% SOC) with and without added electrolyte: heat rate and pressure.

ARC Bomb Runs
Gen2 Anode /Cathode with Electrolyte
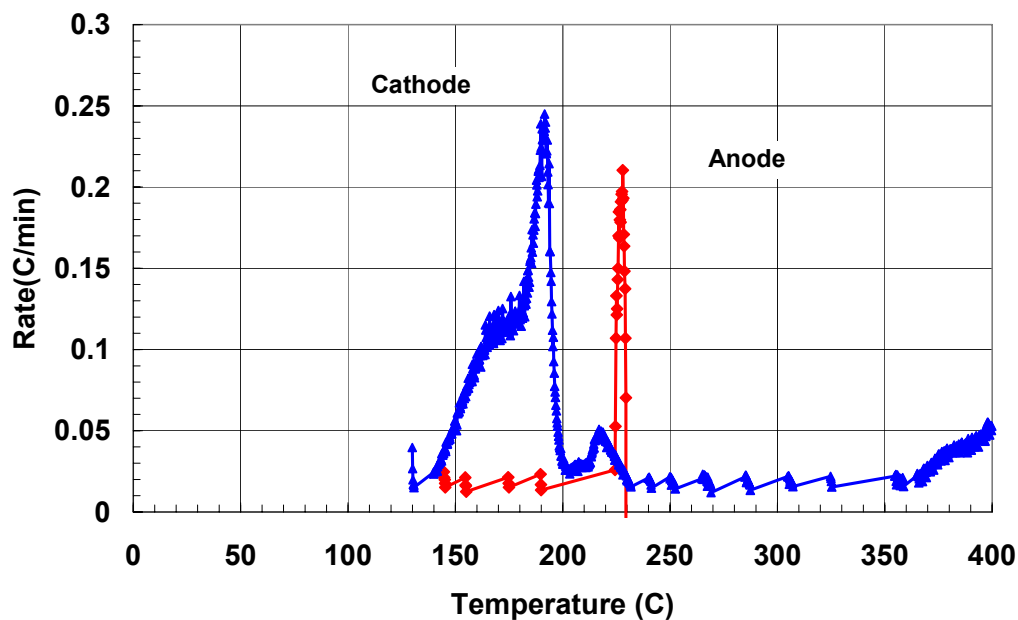
Figure 5-58. ARC bomb run comparisons of Gen2 anode and cathode (80% SOC) with added electrolyte.
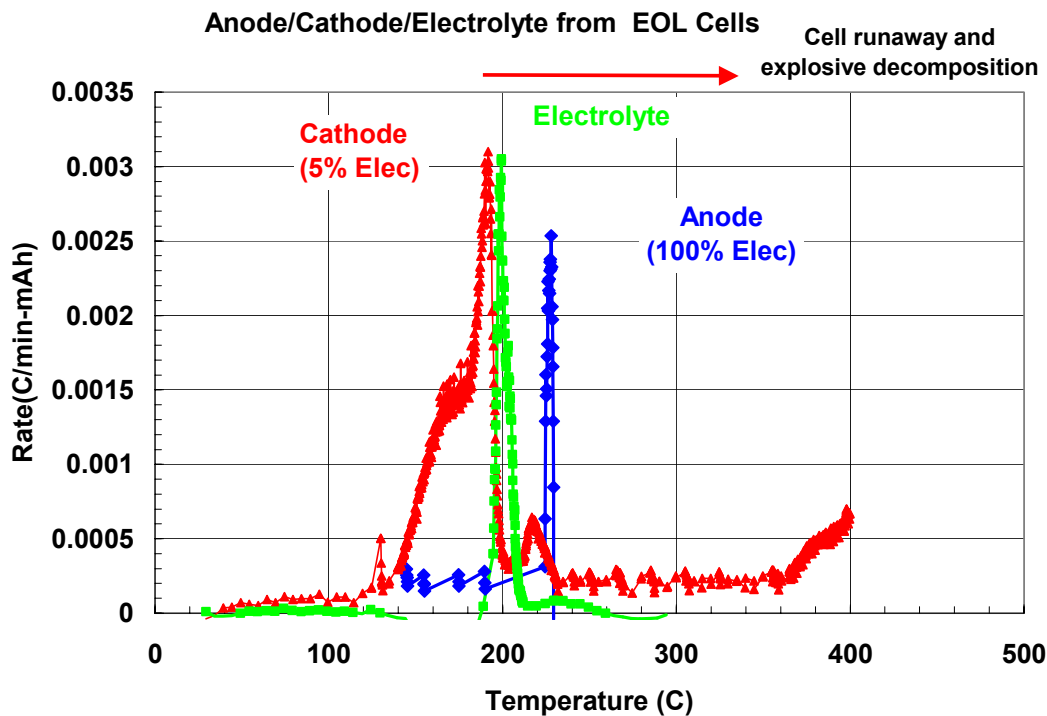
Figure 5-59.　　ARC bomb run comparison of Gen2 electrolyte and anode/cathode material normalized by charge state capacity.

5.2.4.6 Gen1 and Gen2 ARC Bomb Comparisons

The Gen1 and Gen2 electrode materials are more accurately compared by normalizing the ARC bomb heat rate data by the mass of the electrode films. This representation accounts for the mass effect but, however, does not account for differences of electrolyte contained in each material. Figure 5-60 shows the comparison of the Gen1 and Gen2 anode materials. This figure shows that both Gen1 and Gen2 anode materials underwent low-rate reactions beginning as low as 125°C and had peak reaction rates at 225°C. Neither material showed the electrolyte decomposition peak at 190°C. The magnitude of the Gen1 reaction peak at 225°C was significantly greater than that of the Gen2 material. The mechanism of this difference in reaction rates is not clearly understood at this time but may relate to the differences in anode particle morphology shown earlier or may be due to different levels of gas generation which can affect the apparent heat generation rate.

The Gen1 and Gen2 cathode materials are compared in Figure 5-61 and the heat rates are normalized by film weight. The Gen1 and Gen2 cathodes both showed reaction peaks near 190°C that may result from the reaction of the excess electrolyte but the Gen1 cathode showed greater overall heat generation. A similar output was observed by DSC scans which also showed greater overall heat output by the Gen1 cathode. This response is consistent with the effect of the Al doping on stabilizing the Gen2 cathode.

83

Gen1/Gen2 Anodes (80%SOC) in Electrolyte
Normalized by film weight
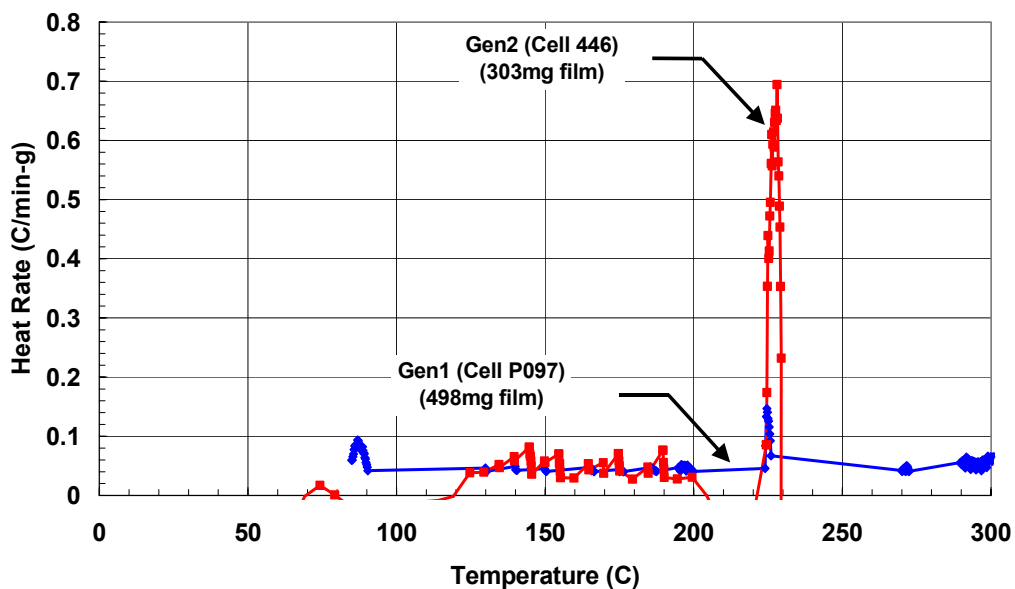
Figure 5-60.   **ARC bomb run comparison of Gen1 and Gen2 anodes in electrolyte normalized by film weight.**

Gen1/Gen2 Cathodes in Electrolyte
Normalized by film wt.
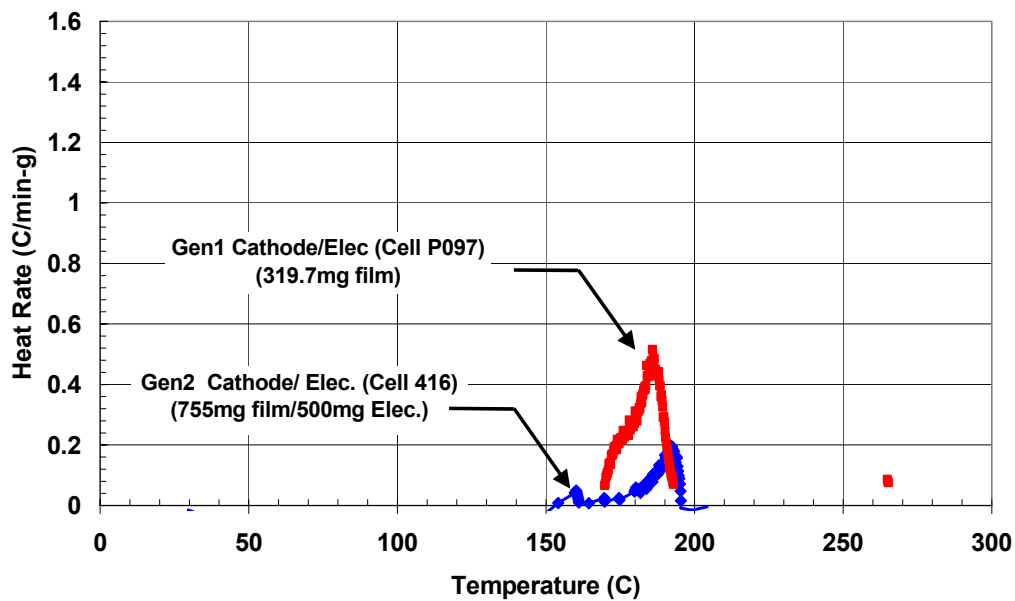
Figure 5-61.   **ARC bomb run comparison of Gen1 and Gen2 cathodes in electrolyte normalized by film weight.**

5.2.4.7 Gen2 Electrolyte Decomposition Study

The thermal runaway response of the Gen2 cells, from initiation of heat generation through venting and explosive decomposition, is greatly affected by the thermal and gas generation behavior of the Gen2 electrolyte. We have previously shown that heat and gas generation are not directly linked during decomposition of this electrolyte. The effect of each individual component in the electrolyte on the overall electrolyte response was investigated by performing ARC bomb runs of the components in various combinations. ARC bomb runs were performed first using only the EMC, then with EMC/1.2M $LiPF_6$ and finally the full EC:EMC (3:7)/1.2M $LiPF_6$. The heat rate data are shown in Figure 5-62 and the gas generation data in Figure 5-63.

The EMC component showed no exothermic behavior over the entire temperature range up to 300°C. The gas generation only showed the effect of boiling at 150°C during which the pressure remained constant. Addition of $LiPF_6$ salt to the EMC resulted in an endothermic dip between 160°C and 175°C with an associated sharp increase in gas generation. Some of the endotherm may result from this gas generation but endothermic reactions between $LiPF_6$ and the EMC have been reported in the literature [16]. However, no exothermic reactions were observed up to 200°C. The response of the full Gen2 electrolyte (EC:EMC/$LiPF_6$) shows the exothermic peak around 190°C as shown previously. Gas generation increased steadily starting at 150°C and did not show any increase during the exotherm. These measurements indicate that the source of gas generation during electrolyte decomposition is the EMC/$LiPF_6$ reaction while the exotherm seen in the full electrolyte results from reaction involving the EC component. The $LiPF_6$ salt plays a necessary and critical role in the decomposition reactions in the electrolyte.

The role of the $LiPF_6$ was investigated by preparing a series of electrolyte solutions of EC:EMC (3:7) with different salt molarities. Solutions were prepared with 0.0M, 0.2M, 0.6M, 1.2M, and 1.8M of $LiPF_6$. The ARC heat rate data are shown in Figure 5-64 and the pressure data in Figure 5-65.

No exothermic reactions were observed for molarities less than 0.6M while only a small exotherm at 210°C was observed for the 0.6M solution. Strong exotherms were observed for the 1.2M and 1.8M solutions at 195°C and 185°C, respectively. Gas generation increased with increasing salt molarity with a divergence in gas generation rate between the different molarities occurring only above 160°C.

The pressure and temperature data from the ARC runs were used to calculate the number of moles of evolved gas for each of these electrolyte solutions. The ARC gas system was first calibrated to determine the overall system volume. The volumes of the hot and cold regions were determined and used with the ARC temperature data to determine the total number of moles of gas in the whole system using the ideal gas law. Corrections to the pressure data were made for the temperature dependent pressure of the N_2 cover gas. The number of moles of generated gas was divided by the number of moles of EMC that was postulated to be the source of the generated gas species. Figure 5-66 compares the calculated molar ratios for each of these electrolyte solutions up to 300°C. The pure EC:EMC solution showed only a steady increase in generated gas starting about 120°C. The amount of evolved gas was still increasing at the maximum temperature indicating that the solution had not completely

decomposed. The 0.2M salt electrolyte showed a similar response to that of the pure EC:EMC. However, the gas generation appeared to occur in two steps starting at 175°C and 225°C. Above 275°C the quantity of gas generated remained constant at 0.8 Moles gas/Mole EMC. The 0.6M electrolyte showed increased gas generation beginning at 200°C and reached a plateau by 250°C. No further gas species were generated above this temperature. The 1.2M and 1.8M electrolytes showed very similar behaviors. These electrolytes showed a sharp increase in gas generation beginning at 160°C and reached a plateau in the evolved gas at 210°C. The final ratio in the plateau region was 1.8 moles of generated gas per mole of EMC solvent. The plateaus in the gas generation indicate that the $LiPF_6$ was consumed in the decomposition reaction. Increased salt molarity increased the ratio of evolved gas up to a limit of 1.2M $LiPF_6$. Increasing salt molarity did not increase the gas evolution indicating that the maximum decomposition limit of the solvent had been achieved.

Our previous measurements showed the important role of EMC in gas generation. We continued the investigation of the role of the EMC component by preparing solutions of the EMC solvent with increasing molarities of $LiPF_6$ salt as was done for the full electrolyte. Solutions were prepared at 0.2M, 0.6M, 1.2M, and 1.8M $LiPF_6$ and run in the ARC bombs. No heat generation was observed with less 1.2M salt and only transient, unsustained heat output was seen for the 1.2M and 1.8M solutions as seen in Figure 5-67. However, the gas generation was comparable to that of the full electrolyte. Figure 5-68 shows the results of the calculations of the molar ratios of evolved gas to EMC. The 0.2M salt solution showed a plateau in gas generation similar to the first plateau seen in the 0.2M full electrolyte solution but gas generation did not resume at the higher temperatures. The 0.6M and 1.2M solutions showed increased gas generation beginning at 190°C but with about half of the total evolved gas of the equivalent molarity solutions of the full electrolyte. The 1.8M solution showed a significant increase in gas generation comparable to that of the 1.8M electrolyte solution. The two 1.8M solutions with the EMC and EC:EMC are compared in Figure 5-69 which shows that the evolved gas ratios of the two electrolytes are equivalent. These results definitively show that the EMC is indeed the source of gas evolution in the full EC:EMC electrolyte. However, the decomposition of the EMC is greatly increased at a given temperature by the action of the $LiPF_6$ salt and also by the action of the EC solvent component.
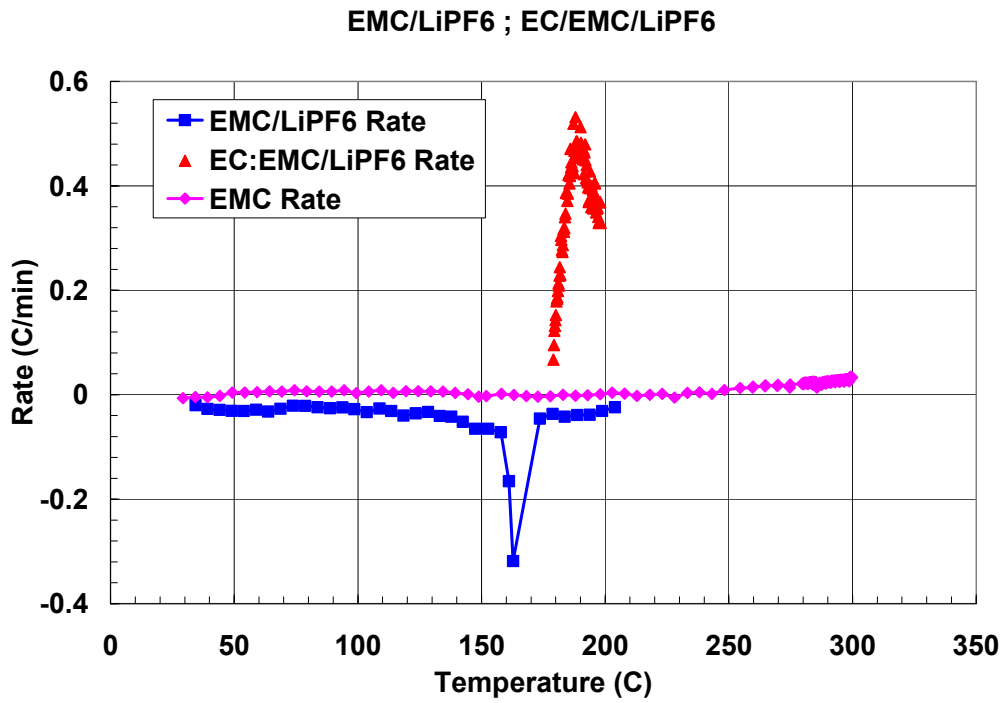
Figure 5-62. ARC bomb run heat rate data for Gen2 electrolyte components, EMC and EC:EMC with and without $LiPF_6$.
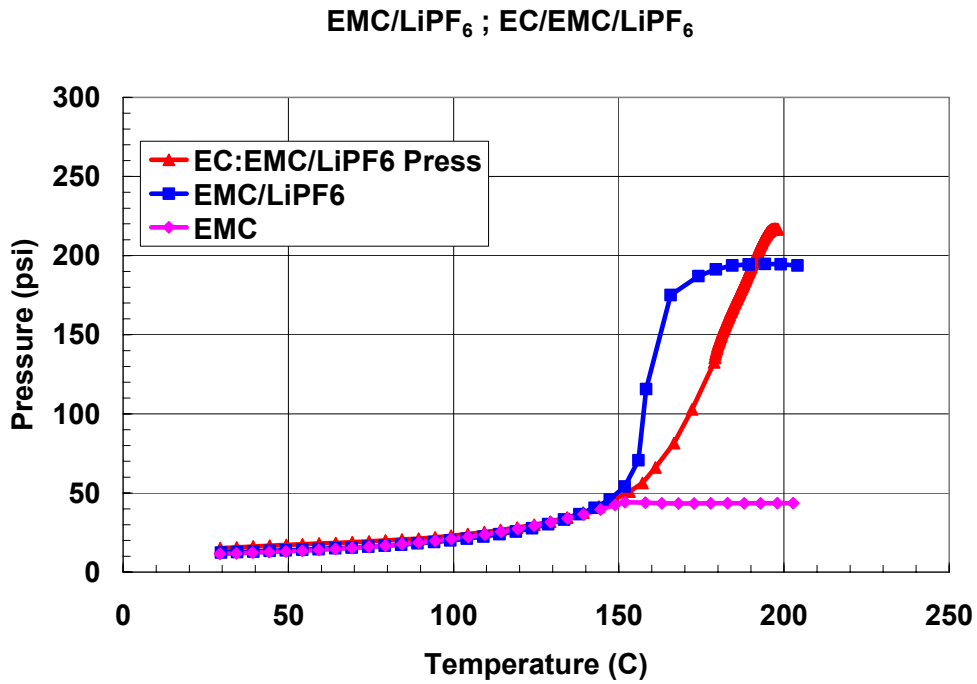
Figure 5-63. ARC bomb pressure data for Gen2 electrolyte components, EMC and EC:EMC with and without $LiPF_6$.

LiPF6/EC:EMC
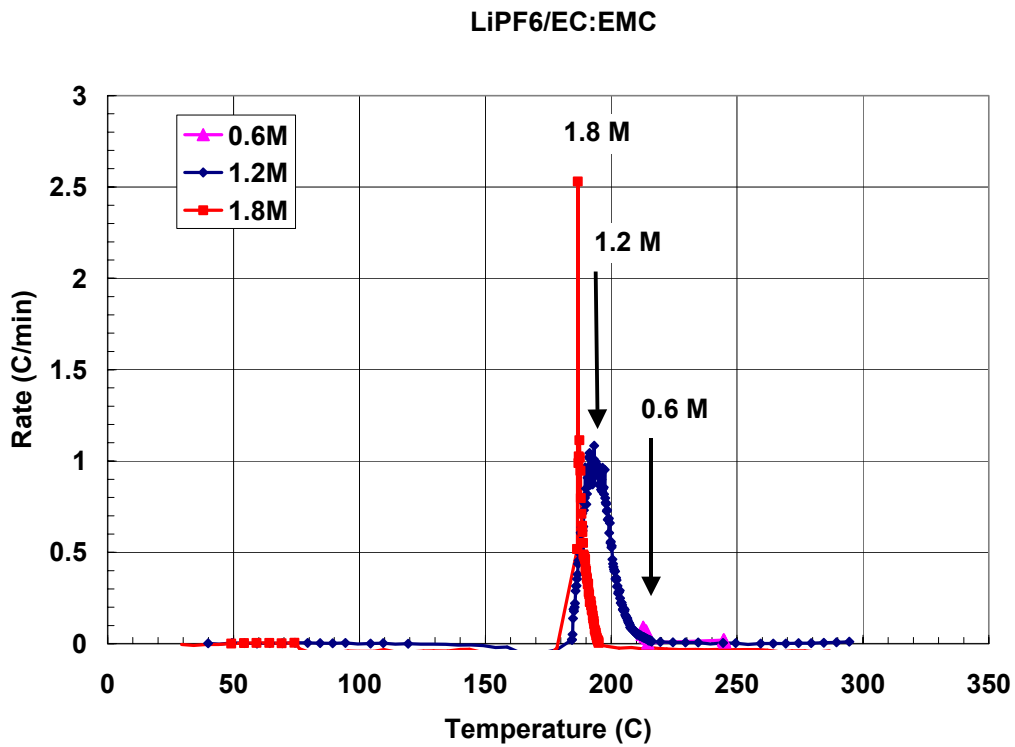
Figure 5-64. ARC bomb run heat rate data for EMC with increasing LiPF$_6$.

LiPF$_6$/EC:EMC
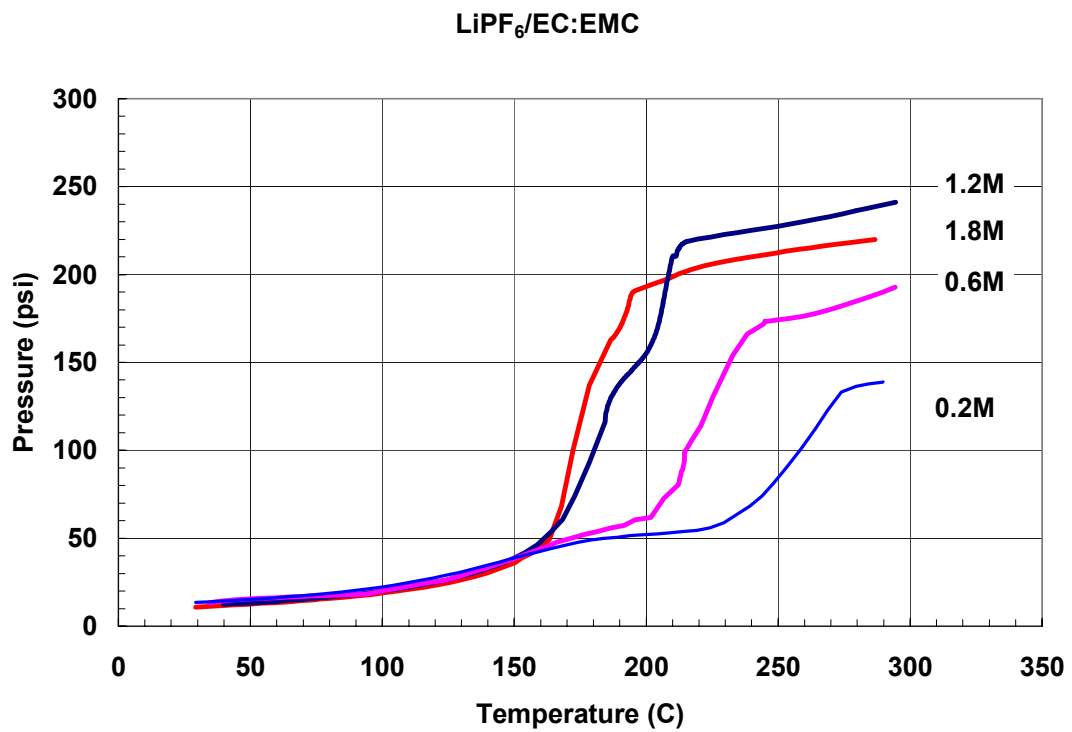
Figure 5-65. ARC bomb pressure data for EC:EMC with increasing LiPF$_6$.

LiPF$_6$/EC:EMC
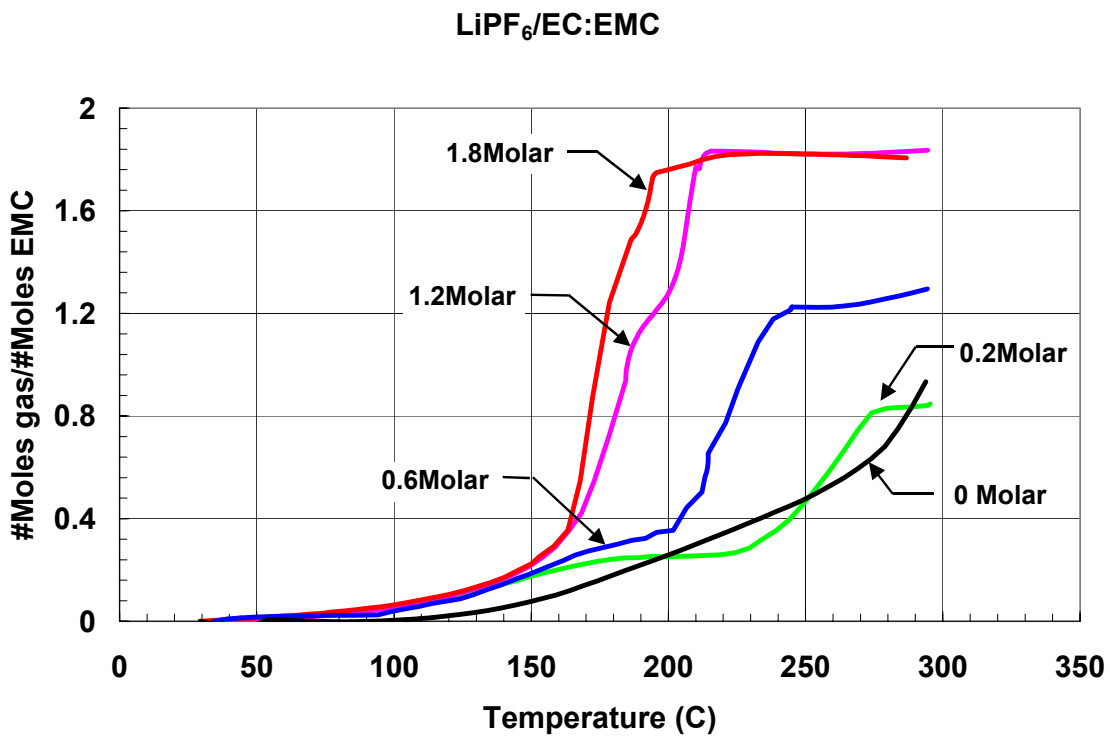
Figure 5-66.   Calculated ratio of moles of evolved gas to moles of EMC for solutions of EC:EMC with increasing LiPF$_6$.

EMC/LiPF$_6$
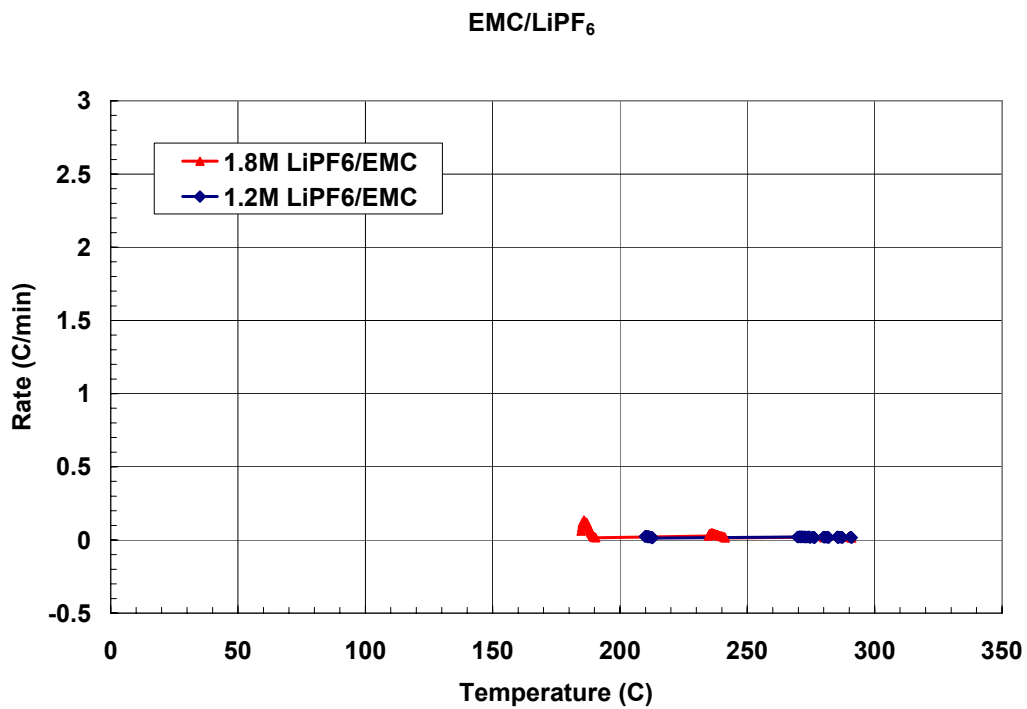
Figure 5-67.   ARC bomb heat rate data for EMC with increasing LiPF$_6$.

EMC/ LiPF$_6$
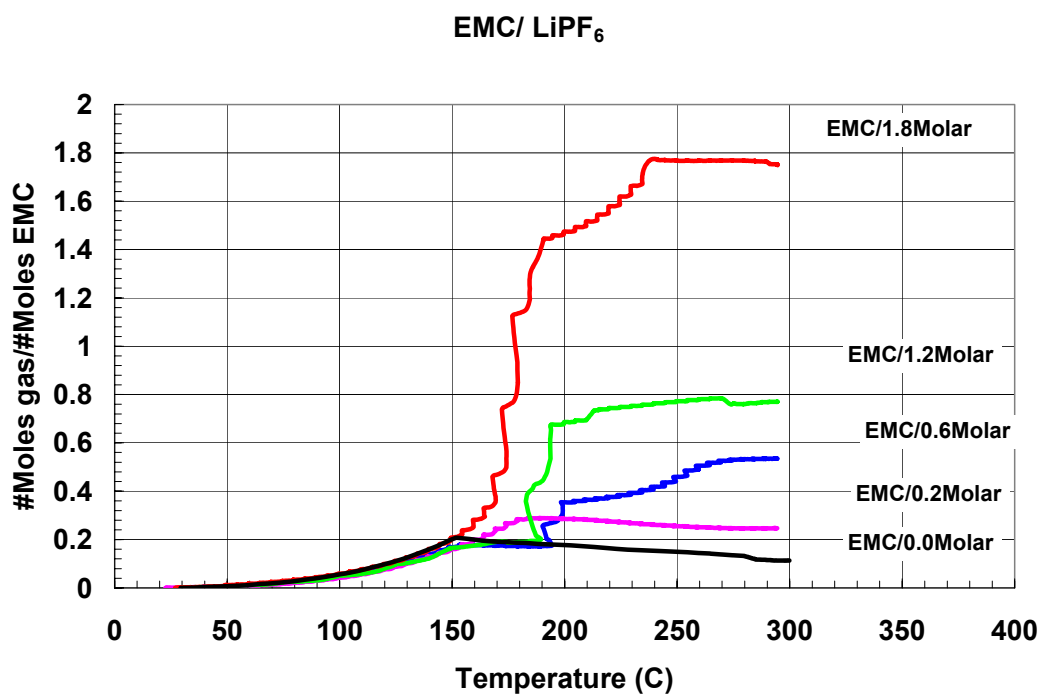
Figure 5-68. Calculated ratio of moles of evolved gas to moles of EMC for solutions of EMC with increasing LiPF$_6$.

1.8M LiPF$_6$/EC:EMC
1.8M LiPF$_6$/EMC
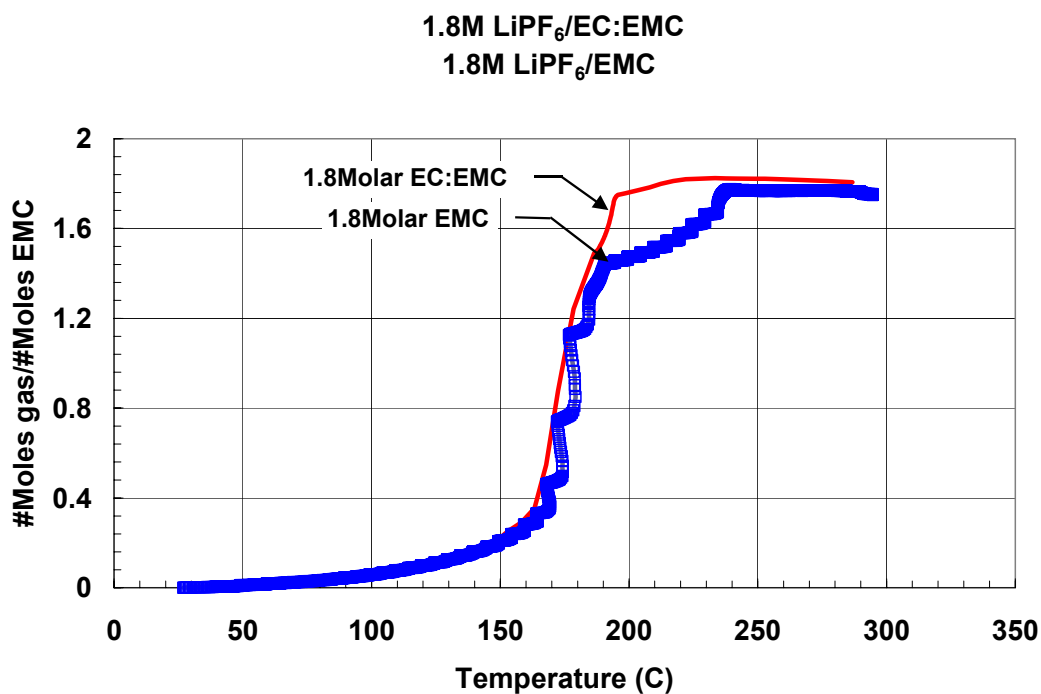
Figure 5-69. Comparison of calculated ratio of moles of evolved gas to moles of EMC for solutions of EC:EMC and EMC with 1.8M LiPF$_6$.

5.2.5 Gas Generation from Gen2 Electrode/Electrolyte Reactions in ARC Runs

5.2.5.1 Effect of Salt Molarity on Gas Generation

Gas generation by the Gen2 electrodes in the presence of Gen2 electrolyte was also measured using materials from the disassembled cells. The anode films have been seen to absorb 60%-100% electrolyte by weight, so equal ratios of 1.2M electrolyte to anode film were used in the ARC bombs. The mole ratios of evolved gas to EMC solvent were computed throughout the run as was done for the electrolyte solutions. Figure 5-70 shows that anode/electrolyte gas generation began almost immediately at a higher rate than the pure electrolyte but did not show the sharp increase in generation at 160°C as was seen for the 1.2M electrolyte. The anode film showed a sharp increase in gas generation around 220°C and had a gas generation profile similar to the 0.6M electrolyte. The anode had not reached the limit for maximum gas generation by the maximum run temperature of 275°C.

The suppression of gas generation from the anode/electrolyte porous film was further investigated by performing measurements of cycled MAG10 anode carbons as well as of uncycled MAG10 carbon powder. Anode pellets were prepared using the Gen2 MAG10 carbon powder and PVDF. The pellets were cycled in a button cell, removed at 100%SOC and measured with the Gen2 electrolyte. In addition, uncycled MAG10 carbon powder was measured with the same amount of Gen2 electrolyte. Figure 5-71 compares these ARC runs with those of anode films from disassembled cells and with pure Gen2 electrolyte. The figure shows that the cycled anode films from both the button cell and the full cell showed similar suppression of the evolved gas beyond the normal decomposition temperature of the pure electrolyte. However, the uncycled carbon showed increased gas generation beginning as low as 125°C. The uncycled carbon surface can serve as an active site for enhanced electrolyte decomposition and gas generation. These measurements indicate that the cycled, lithiated carbon surface interacts with the electrolyte through some mechanism that reduces the generation of gas or removes the evolved gas species. One possible mechanism is the reduction in the molarity of the electrolyte by reaction of the salt with the cycled, lithiated carbon. This would account for the similar response to that of the low-molarity pure electrolytes.

The cathode/electrolyte gas generation is shown in Figure 5-72. Equal weights of 1.2M electrolyte and cathode film were measured as for the anodes. Gas generation remained essentially identical to that of the pure electrolyte until 170°C. The gas generation continued to increase with increasing temperature but did not plateau at the higher temperatures as was seen for the electrolytes. Gas generation continued up to the maximum run temperature of 350°C and reached a ratio of 2.8 moles of gas to moles of EMC. This gas generation profile is very similar to that measured for the "as removed" cathode material shown in Figure 5-57. These measurements indicate that the cathode material itself is a source of decomposition gases in addition to the decomposition gases from the electrolyte.

Anodes in EC:EMC/ 1.2M LiPF$_6$
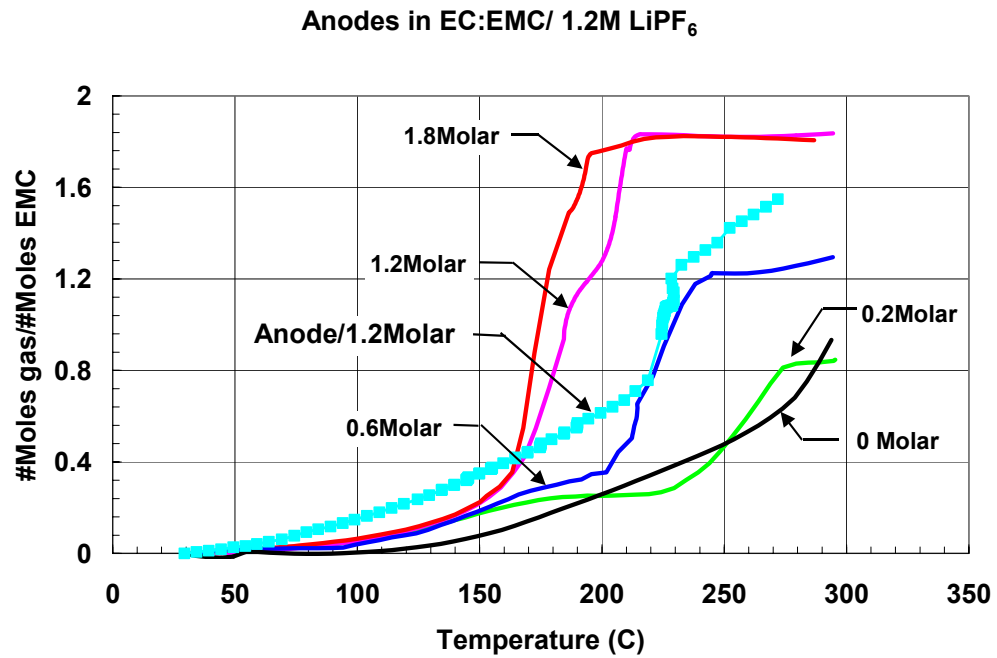
Figure 5-70. Comparison of calculated ratio of moles of evolved gas to moles of EMC for Gen2 anode in 1.2M LiPF$_6$ with solutions of EC:EMC with increasing LiPF$_6$.

MAG10 Anode Material + Gen2 Electrolyte
Uncycled/Cycled (100%SOC)
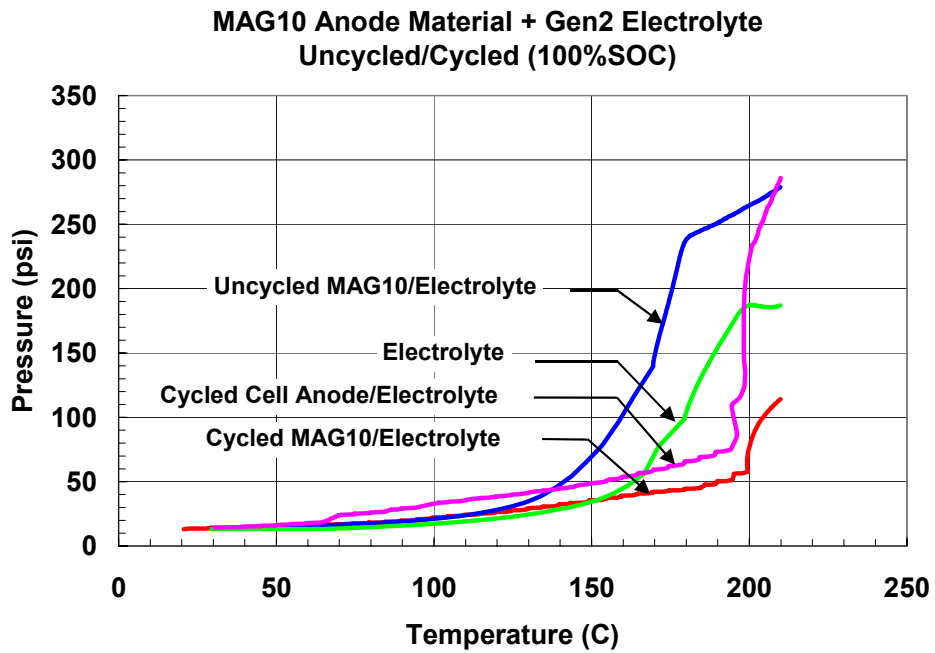
Figure 5-71. ARC bomb pressure data for cycled and uncycled MAG10 anode material from button cells compared to MAG10 anode material removed from a Gen2 cell. All measurements with Gen2 electrolyte.

LiPF$_6$/EC:EMC
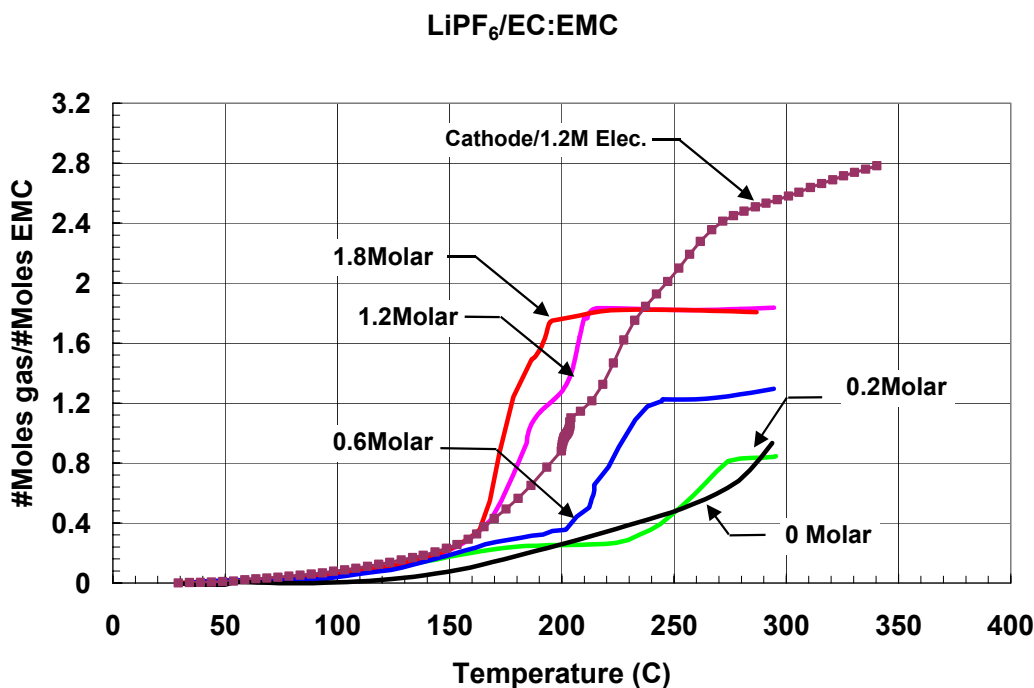
Figure 5-72. Comparison of calculated ratio of moles of evolved gas to moles of EMC for Gen2 cathode in 1.2M LiPF$_6$ with solutions of EC:EMC with increasing LiPF$_6$.

5.2.5.2 Gas Decomposition Products of Gen2 Cell Components

In the previous sections we have shown that gas evolution results from reactions of the cell electrodes and the cell electrolyte. The gas evolution attributable to electrolyte breakdown was determined by performing ARC bomb capsule runs of the Gen2 solvent and electrolytes. The ARC system was modified to allow not only measurement of the total pressure increase during the ARC run but also to allow gas collection. Grab samples were taken either during or at the end of the ARC bomb runs and submitted for GC analysis. The quantities of the identified species were normalized to the total quantity of evolved gas since the majority of the gas sampled consists of the N$_2$ cover gas. The initial ARC runs to determine quantities of evolved gas were performed up to 300°C as shown if Figure 5-66 and Figure 5-68. A separate series of ARC runs were performed to determine gas composition species up to a maximum temperature of 400°C. Gas samples were also taken from the ARC bomb runs of the electrode/electrolyte measurements shown previously Figure 5-70 and Figure 5-72.

5.2.5.2.1   Electrolyte Gas Decomposition Species

Initial gas measurements were made of the EC:EMC/1.2M LiPF$_6$ decomposition reaction as a function of increasing temperature. Figure 5-73 shows the normalized gas results of three grab samples taken from separate ARC bomb runs to 200°C, 300°C and 400°C. The low temperature (200°C) gases consisted almost solely of CO$_2$ and ethylene (ethyl fluoride was not analyzed). At higher temperatures where complete decomposition of the electrolyte was observed, the dominant gas species were still CO$_2$ and ethylene with much increased levels of H$_2$, CH$_4$, C$_2$H$_6$ and C$_2$H$_5$F (ethyl fluoride). The presence of the ethyl fluoride indicates that

$LiPF_6$ plays a role in the decomposition of the EMC. These figures represent the distribution of generated gases but do not indicate the increasing volume of gas generated with increasing temperature.

Figure 5-74 shows a comparison of the gas products from decomposition of electrolyte without the presence of EC (EMC/1.2M LiP_6) at 210°C and 400°C. CO_2 was again the main decomposition gas with significant amounts of ethylene and ethyl fluoride even at the low temperature. Increasing temperature resulted in a broader spectrum of simple gas molecule species. The full Gen2 electrolyte showed similar gas composition to the EMC/$LiPF_6$ except for reduced levels of ethyl fluoride. The ratio of $LiPF_6$ to EMC is lower in the full EC:EMC electrolyte than in the EMC only electrolyte, which can result in reduced reaction of $LiPF_6$ with the EMC and lowered ethyl fluoride levels. The effect of the EC in the electrolyte decomposition is shown in Figure 5-75 for the low-temperature decompositions and in Figure 5-76 for the higher temperature. No significant difference was observed in the gas decomposition species at the low temperature as a result of the EC in the electrolyte. However, we have seen that the EC increases the amount of gas evolution at the lower temperatures as was shown in Figure 5-66 and Figure 5-68. At the higher temperature the EC resulted in an increase in CO_2 and H_2 with a corresponding decrease in CO.

The effect of LiP_6 salt (1.2M) on the gas species generated by the EC:EMC solvents is shown in Figure 5-77. These two ARC runs at 200°C and 300°C showed that the salt did not result in any change in the spectrum of the evolved gas species. As indicated previously in Figure 5-66, the salt did increase the volume of the generated gases. The combined effect of the LiP_6 and the EC is to increase the decomposition reactions of the EMC linear carbonate without generating new gas species.
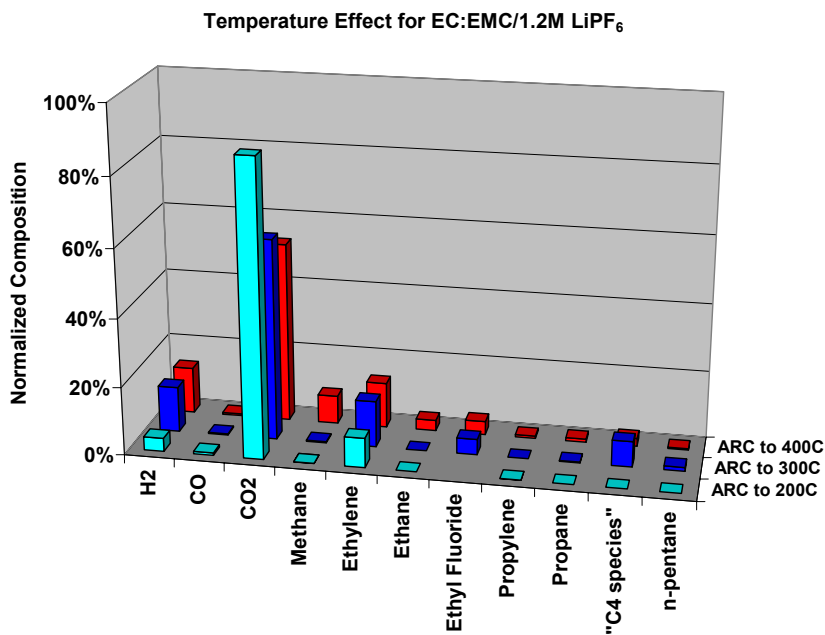
Figure 5-73.   Gas decomposition products of EC:EMC/1.2M LiPF6 from ARC bomb runs to 200ºC, 300ºC and 400ºC.

Temperature Effect for EMC /1.2M LiPF$_6$
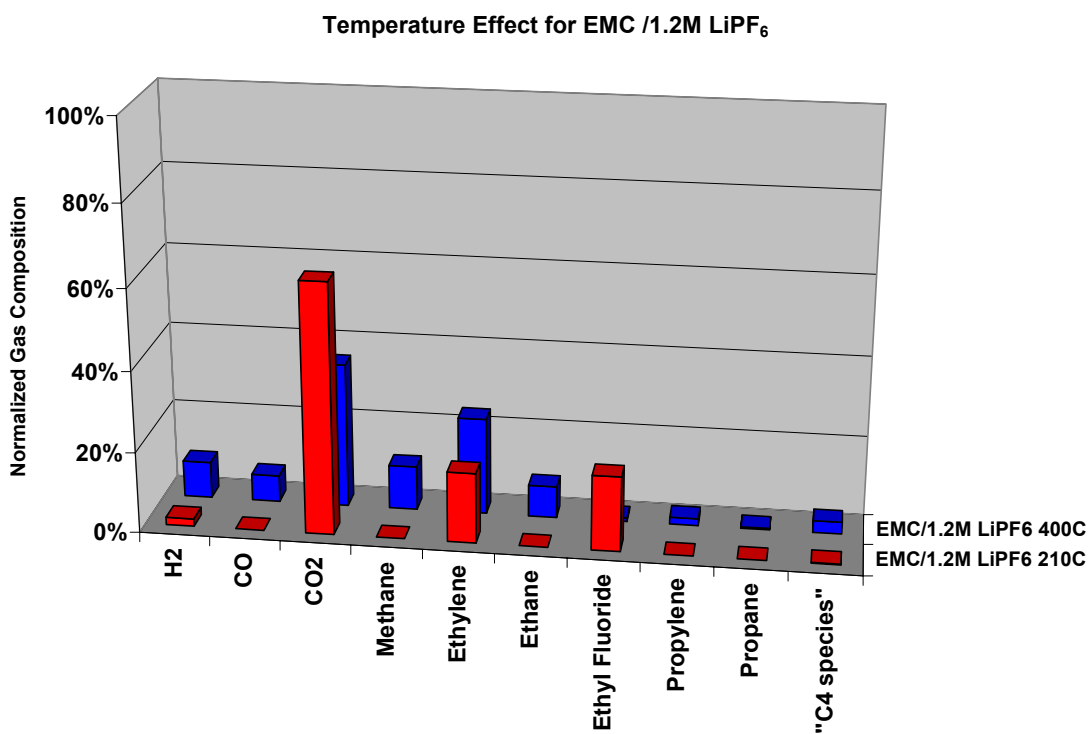
Figure 5-74.   Effect of temperature on gas decomposition of EMC/LiPF$_6$..

Effect of EC in EMC/1.2M LiPF$_6$ (200C)
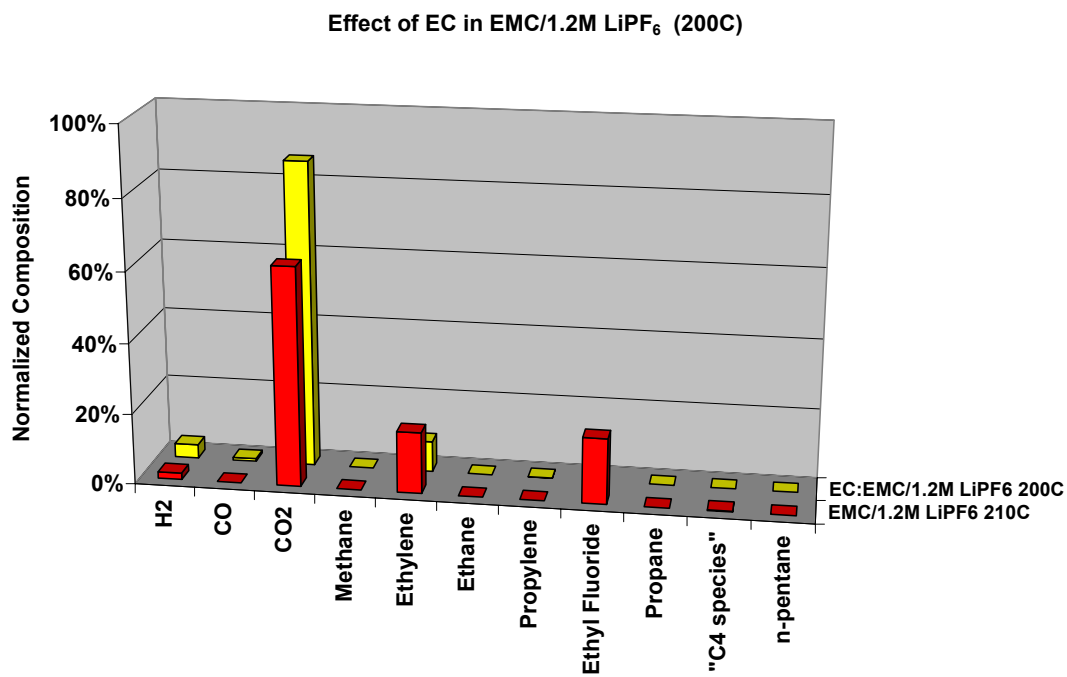
Figure 5-75.   Effect of EC on gas decomposition of EMC/1.2M LiPF$_6$ electrolyte up to 200ºC.

Effect of EC in EMC/1.2M LiPF$_6$ (400C)
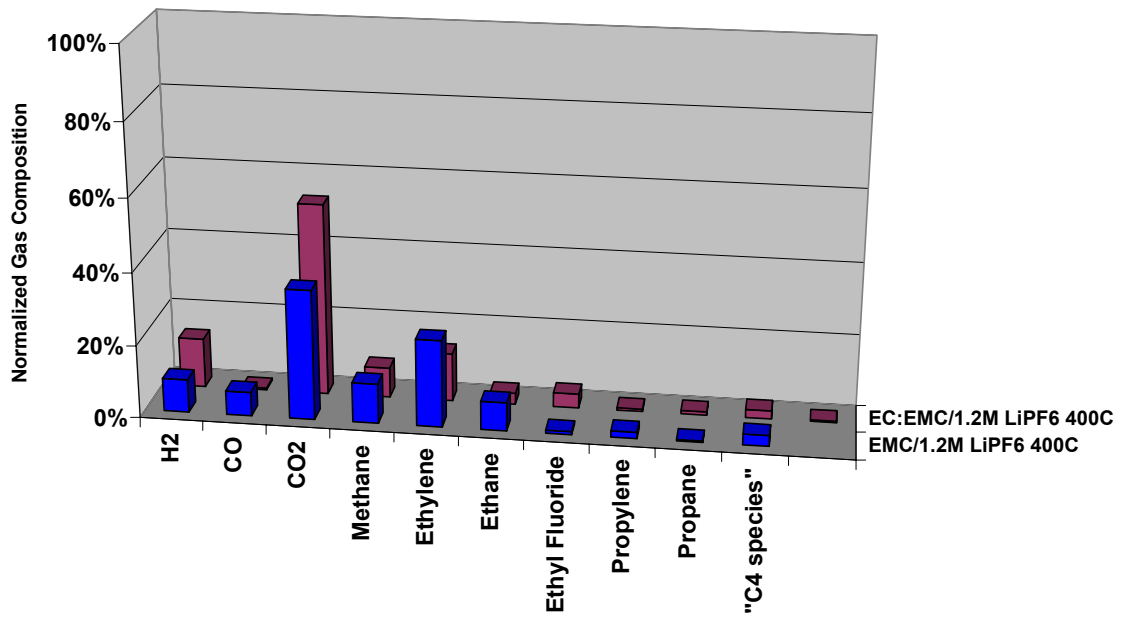
Figure 5-76. Effect of EC on gas decomposition of EMC/1.2M LiPF$_6$ electrolyte up to 400ºC.

Solvent/ Electrolyte Normalized Decomposition Products
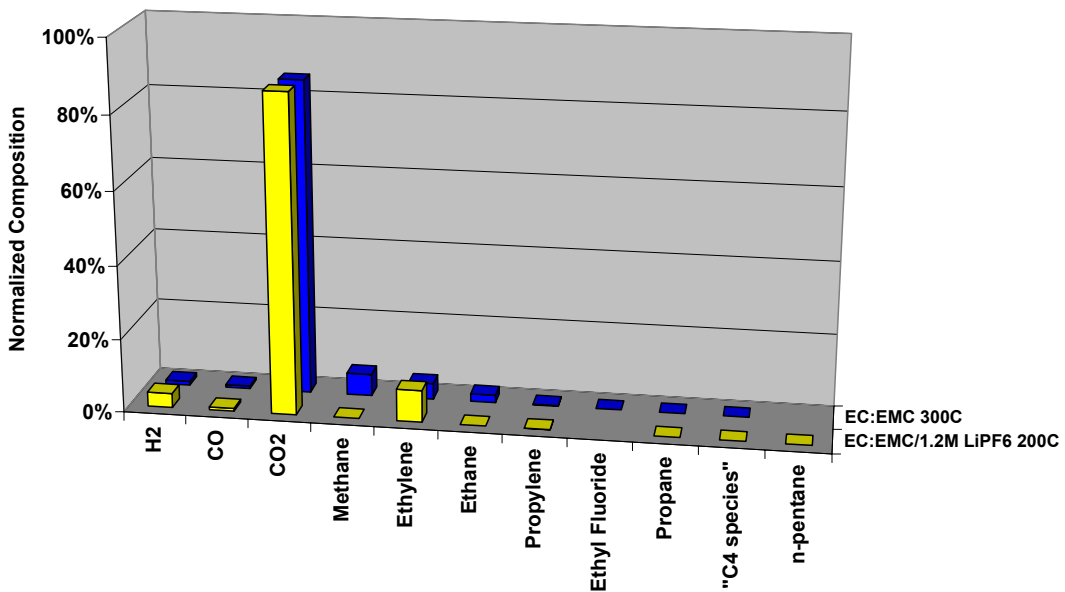
Figure 5-77. Effect of LiPF$_6$ on gas decomposition of EC:EMC electrolyte.

The effect increasing salt molarity on gas composition was also determined for the EC:EMC/LiPF$_6$ and EMC/LiPF$_6$ electrolytes from 0.2M LiPF$_6$ to 1.8M LiPF$_6$. GC analysis was performed on grab samples taken at the end of each 400ºC ARC run. Figure 5-78 shows the normalized gas composition of the evolved gases for the EC:EMC/LiPF$_6$ electrolytes. The composition was quite stable across the full range of salt molarities. We previously showed in Figure 5-66 that the molar ratio of total evolved gas to the moles of EMC reached a plateau at 1.2M LiPF$_6$. The actual max ratio of total evolved gas per mole of EMC varied from 1.8 to 2.4 for different configurations of the gas manifold system. Uncertainties in the system volumes account for some of the variation in the calculated values while different system volumes and the resulting differences in peak system pressures can also result in different equilibrium constants for the gas products. Figure 5-79 shows the molar ratios of each evolved gas species to moles of EMC for each of the salt molarities. The ratio of CO$_2$ evolved reached a plateau of 1.29 moles per mole of EMC for this system configuration while other runs showed a ratio 0.97. Since the structure of EMC should result in no more than one CO$_2$ per EMC molecule, the EC component or EC decomposition products may also be contributing to the amount of CO$_2$ evolved.

The effectiveness of the LiPF$_6$ on the decomposition of the EMC is shown more clearly by plotting the molar ratio of each gas species to EMC as a function of the molar ratio of LiPF$_6$ to EMC. Figure 5-80 shows that the molar ratio of CO$_2$ to EMC was always much greater (5-10 times) than the salt/EMC ratio for all salt molarities. This high CO$_2$ ratio indicates that the LiPF$_6$ was acting as a catalyst for EMC decomposition. The dashed line shows the ratio that would result from a 1:1 generation of each gas species by the LiPF$_6$. The ethylene and H$_2$ ratios lie above this line indicating that they may also arise from catalytic reaction involving the LiPF$_6$. However, the gas species can also arise from reactions involving the EC as well as from purely thermal decomposition, thus the role of the salt in generating these gases is not unambiguous in the EC:EMC system.

EC:EMC/LiPF$_6$: Normalized Gas Composition with increasing LiPF$_6$ (400C)
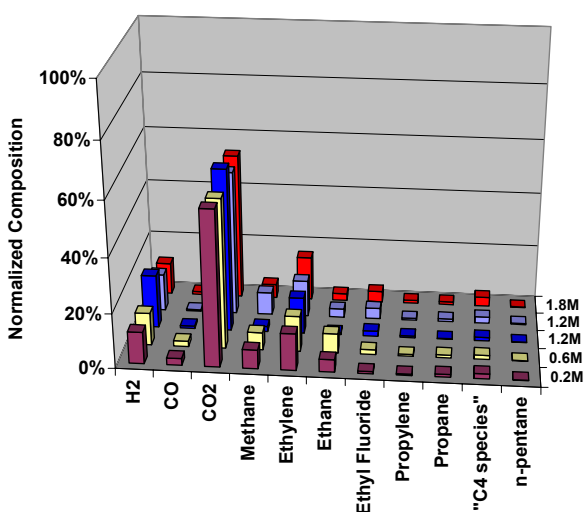
Figure 5-78. **Normalized gas composition of EC:EMC/LiPF$_6$ electrolyte with increasing LiPF$_6$ molarity from ARC bomb run to 400ºC.**
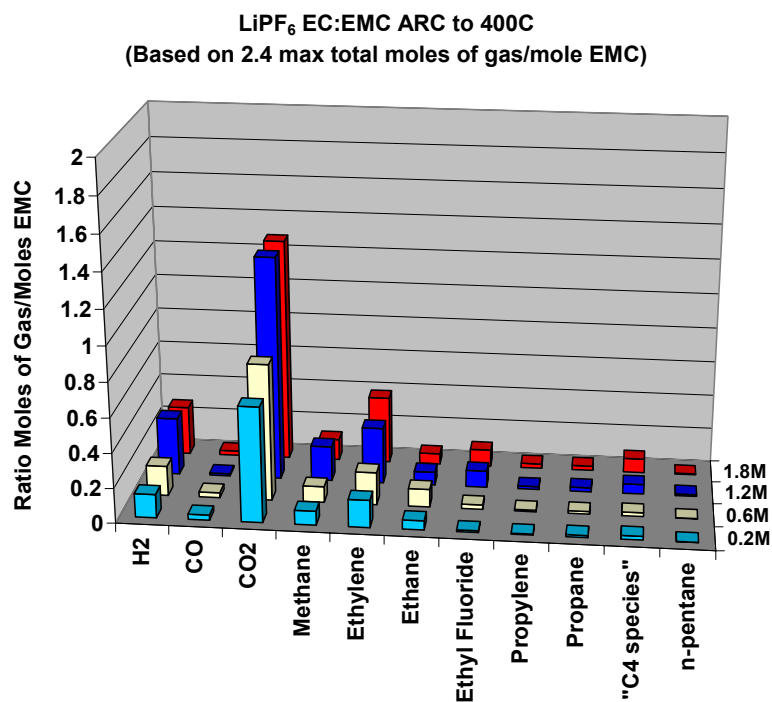
Figure 5-79. Ratio of moles of gas to moles of EMC for EC:EMC/LiPF$_6$ electrolyte with increasing LiPF$_6$ molarity from ARC bomb run to 400ºC.
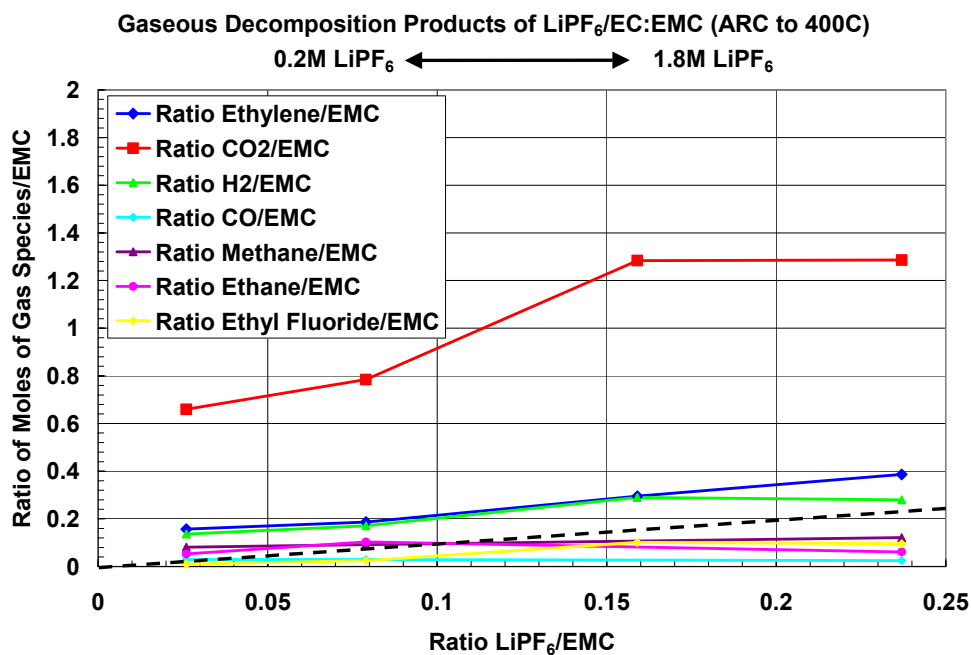
Figure 5-80. Ratio of moles of each evolved gas species to moles of EMC with increasing ratio of LiPF$_6$ to EMC for the EC:EMC/LiPF$_6$ electrolyte from ARC bomb run to 400ºC.

The effect of EC on the decomposition of EMC was investigated by performing a salt molarity study of just an EMC based electrolyte with the $LiPF_6$. Molar solutions of the $LiPF_6$ in EMC were made with values of 0.6M, 1.2M and 1.8M. ARC bomb runs to 400ºC were performed as for the EC:EMC electrolyte and gas composition determined at the end of each ARC run. Figure 5-81 shows the normalized gas compositions for the three molarities. These EMC based electrolytes showed a broader spectrum of gas species than was seen for the EC:EMC electrolytes with the same salt molarities (Figure 5-78). The addition of the EC resulted in an increase in the relative amount of CO_2 and H_2 while reducing the amount of CO as shown earlier in Figure 5-76. The molar ratios of each gas species to EMC are shown in Figure 5-82. The final increase in total gas generation is seen to occur only at the 1.8M $LiPF_6$ level as compared to the max gas generation limit at 1.2M $LiPF_6$ for the full EC:EMC electrolyte. The ratio of moles of each evolved gas species to moles of EMC as a function of increasing ratio of $LiPF_6$ to EMC is shown in Figure 5-83. Comparing this figure with Figure 5-77 or the EC:EMC electrolyte shows that much less CO_2 gas generation results at each salt/EMC ratio. The catalytic behavior of the $LiPF_6$ is much reduced without the presence of the EC.
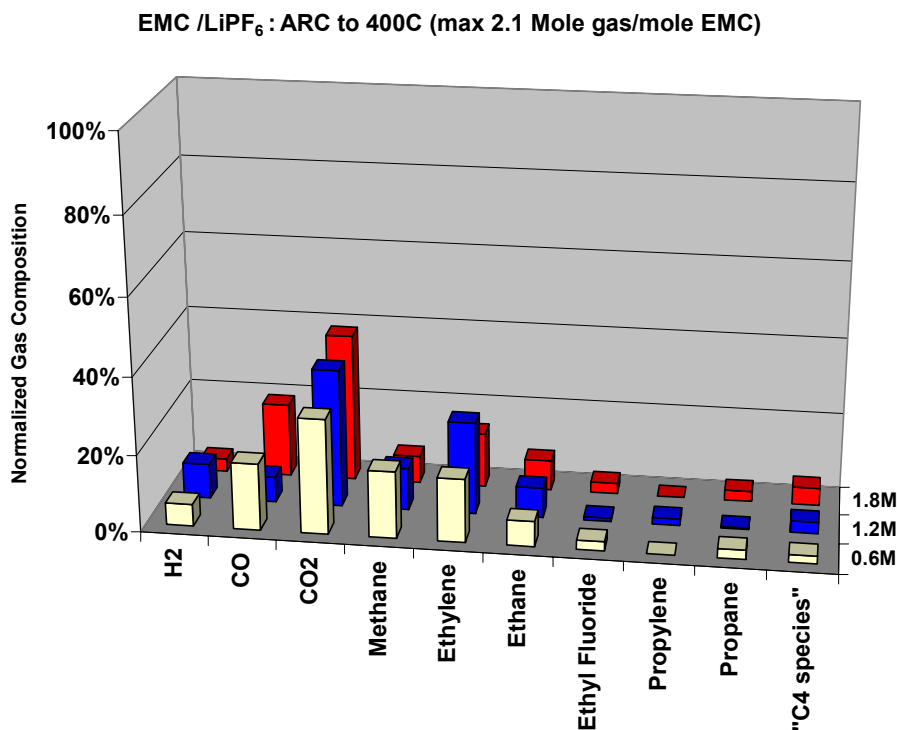
Figure 5-81. **Normalized gas composition of EMC/LiPF$_6$ electrolyte with increasing LiPF$_6$ molarity from ARC bomb run to 400ºC.**

EMC /LiPF$_6$ ARC to 400C
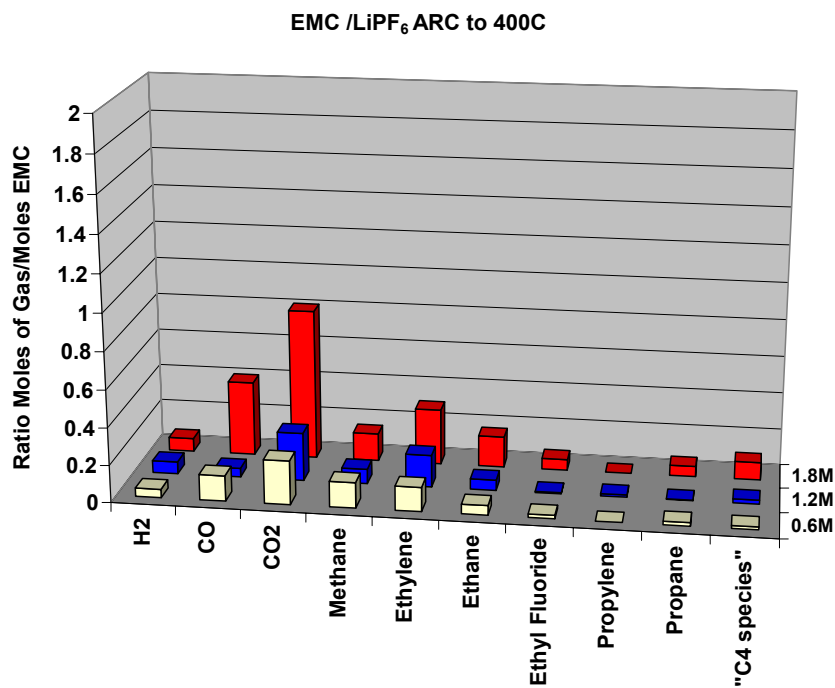
Figure 5-82. Ratio of moles of gas to moles of EMC for EMC/LiPF$_6$ electrolyte with increasing LiPF$_6$ molarity from ARC bomb run to 400ºC.

Gaseous Decomposition Products of LiPF$_6$/EMC (ARC to 400C)
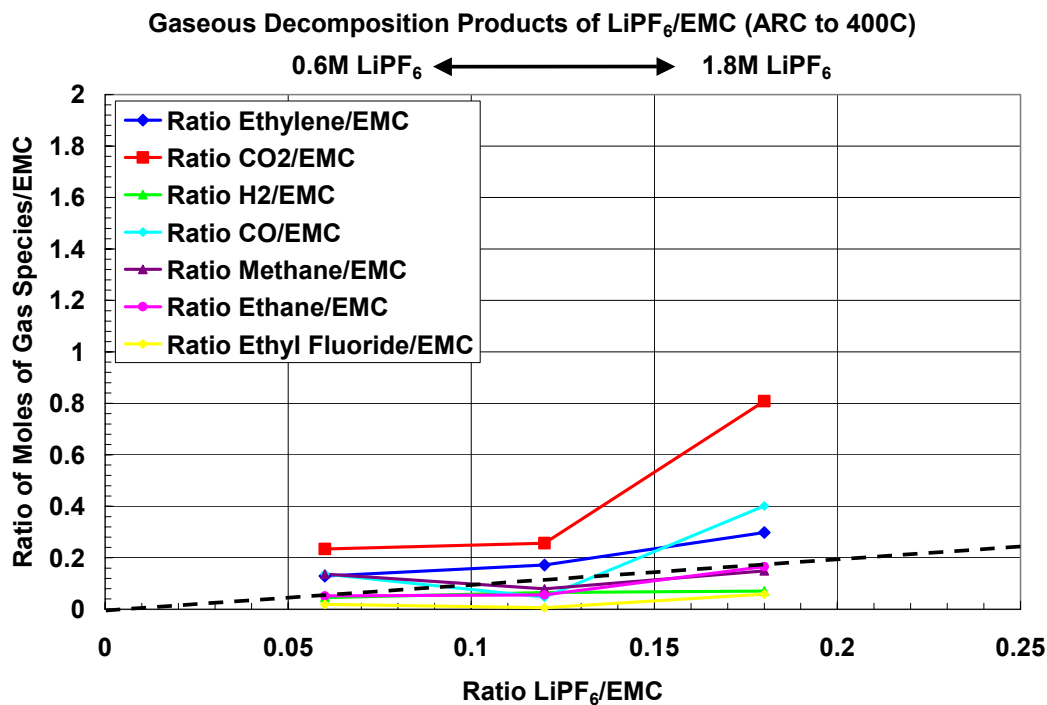
Figure 5-83. Ratio of moles of each evolved gas species to moles of EMC with increasing ratio of LiPF$_6$ to EMC for the EMC/LiPF$_6$ electrolyte from ARC bomb run to 400ºC.

5.2.5.2.2 Electrolyte/Electrode Gas Decomposition

The gas generation from the cell electrode materials in Gen2 electrolyte was shown in Figure 5-71 and Figure 5-72. The electrodes reduced the amount of gas generated at any given temperature compared to the same amount of pure electrolyte indicating that the salt may be consumed at the electrode interfaces. The GC analyses of the anode/electrolyte and cathode/electrolyte gas species from the ARC bomb runs are shown in Figure 5-84 along with the analysis of the full electrolyte. The cathode/electrolyte gases were very similar to the gases from the pure electrolyte but with reduced ethyl fluoride levels. The anode gases showed new H_2 and CO species, which had not been observed at any appreciable level in the other gas analyses at this temperature. Reduced ethylene and ethyl fluoride levels suggest that the salt ionic species may be reacting with the electrodes as suggested by the previously observed reduction in gas generation level.
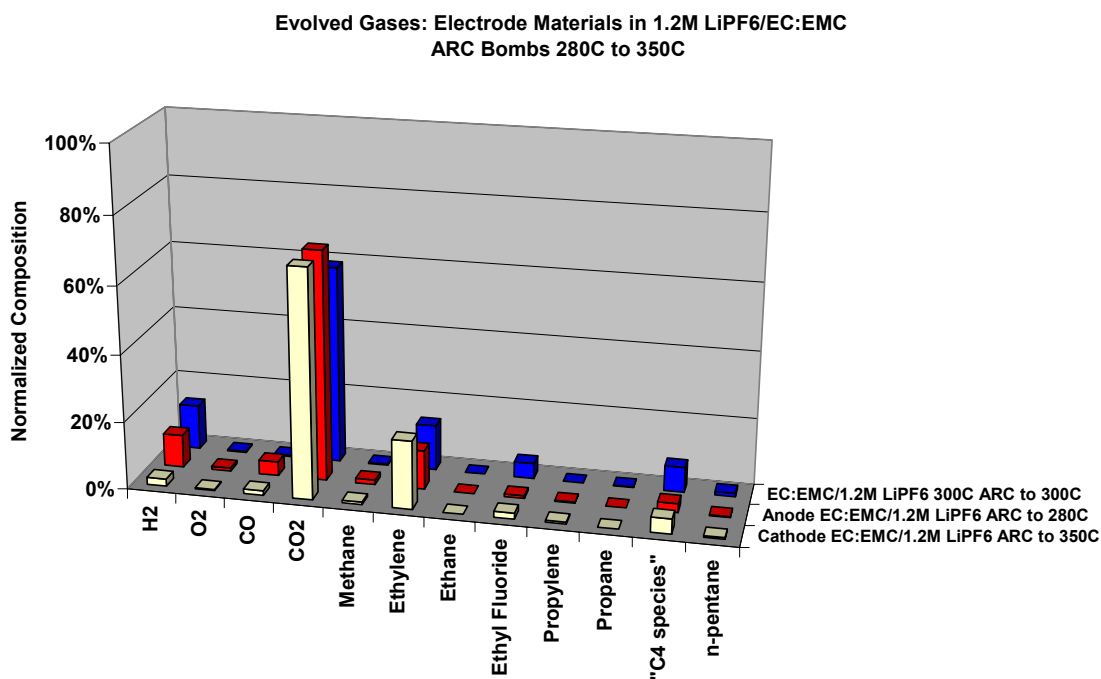
Figure 5-84. Gas decomposition product comparison of Gen2 electrolyte, cathode/electrolyte and anode/electrolyte from ARC bomb runs over the temperature range of 280ºC to 350ºC.

5.2.5.3 Electrolyte Decomposition - TGA/FTIR Analysis of Gases

The gas decomposition products of the Gen2 and Gen1 electrolytes were also measured using simultaneous TGA/FTIR analysis. Electrolyte was sealed in Al DSC pans in the Ar glove box but with only a partially crimped seal. This partial seal minimized loss of the volatile solvent components but also allowed escape of the evolved gas during the temperature scan. Scans were performed in the TGA apparatus at 10°C/min while the evolved gases were analyzed in real time with an attached FTIR system. The Gen2 gases evolved between 65°C and 305°C are shown in Figure 5-85. The first observable gas species was the volatile EMC component. The EC component did not vaporize until 160°C. At 110°C a POF_3 gas species was observed which was present up to 260°C. PF_5 was only observed at the higher temperatures. The Gen1 gas analysis was similar to Gen2 and is shown in Figure 5-86. Initial gas released was the volatile DEC followed by EC at 165°C. POF_3 was observed at the first analyzed temperature of 140°C and was continuously present up to 305°C. This gas analysis gives further information in determining decomposition reactions.
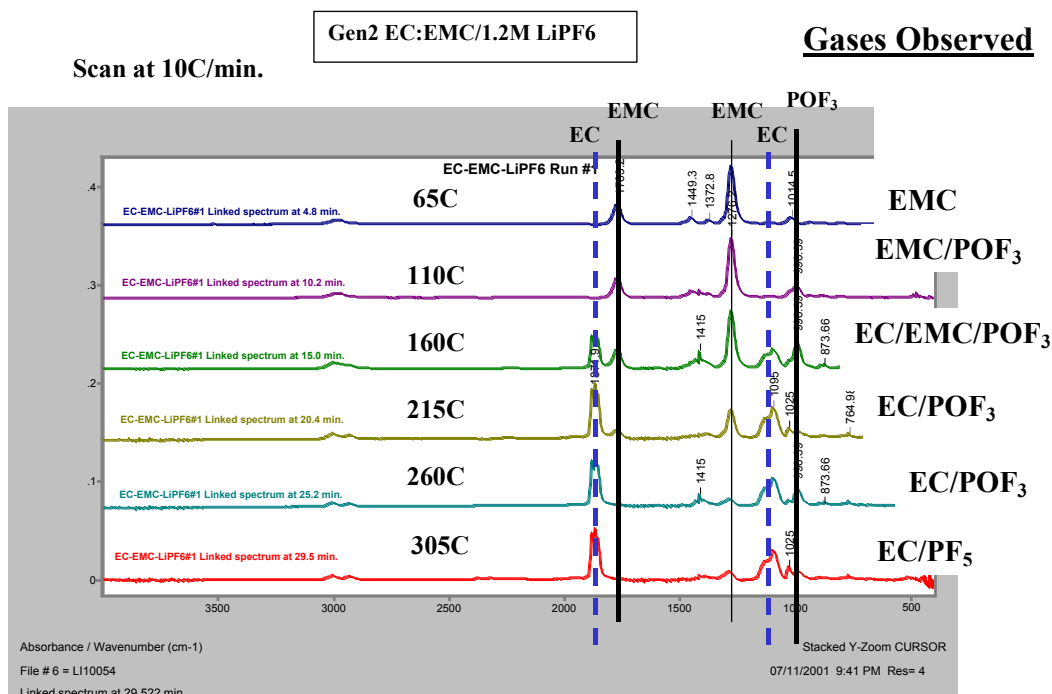
Figure 5-85. FTIR spectra from decomposition of Gen2 electrolyte (EC:EMC/LiPF$_6$) during thermal ramp to 305ºC at 10ºC/min

Figure 5-86. FTIR spectra from decomposition of Gen1 electrolyte (EC:DEC/LiPF$_6$) during thermal ramp to 305°C at 10°C/min.

5.2.5.4 Electrolyte Decomposition – Liquid Chromatography/Mass Spectrometry (LC/MS) Analysis

The EMC, unsymmetrical chain alkyl carbonate solvent has been shown to be inherently unstable and forms an equilibrium balance with the symmetrical linear alkyl carbonates through an alkyl exchange reaction (sometimes call a "transesterification" reaction) as shown below [20].

$$2EMC \leftrightarrow DMC + DEC \qquad (1)$$

We performed LC/MS analysis of the Gen2 electrolyte for baseline material and for electrolytes that had been spun out of Gen2 cells. Electrolyte was taken from cells that had been both aged and electrically abused. Significant changes were seen in the LC/MS spectrum for the cells. The baseline electrolyte showed mainly EC and EMC peaks as expected but we also observed the presence of PF$_5$ and the trimer of the poly(ether/carbonate) even in this EC:EMC/LiPF$_6$ electrolyte standard. In the full cell electrolyte the LC/MS spectrum revealed the presence of several phosphorus compounds including PF$_5$, PF$_3$, POF$_3$, and LiPF$_6$. Polymerization of solvent molecules was also observed. We measured the presence of poly(ether/carbonates) in the form of monomers, dimers, and trimers. The n-mer

of the poly(ether/carbonate) is shown in Figure 5-87 below. This polymer can result from "chain opened" EC reacting with the linear carbonates [21].

Dimerization products were seen resulting from reaction of two linear carbonate molecules (or the EC with the linear carbonates) resulting in DMDOHC, EMDOHC, and DEDOHC. These products result from reaction of the EC with the various linear carbonate species that are present in the cell, as shown in Eq. 1. These species were observed to increase with aging and abuse. However, "transesterification" products were also seen to develop even during cold storage at 10°C. Figure 5-88 below shows the total ionization count for some of the cells measured indicating the decomposition products that developed under aging/abuse.
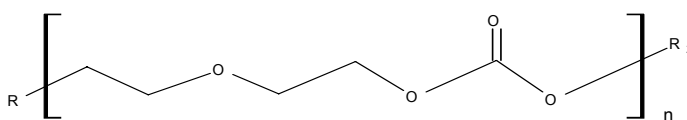
Figure 5-87.   **Polymer chain of the poly(ether/carbonate) formed in the Gen2 electrolyte.**
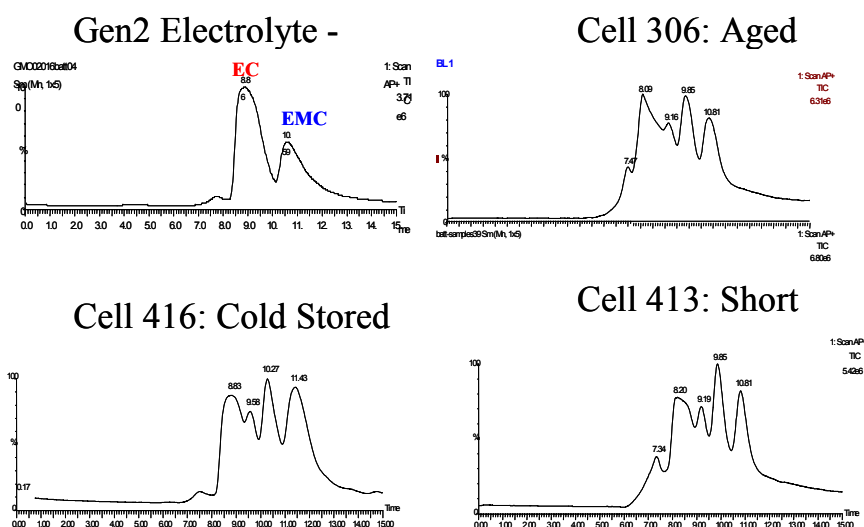
Figure 5-88.   **Electrolyte products measured by LC/MS for the Gen2 electrolyte and some of the aged/abused Gen2 cells indicating electrolyte decomposition even during cold storage.**

5.2.5.5 Gas Decomposition Products of Full Cells

The ARC system was modified to allow capture of vented gases from full cells during the ARC runs. A closed 18650 cell fixture was installed that allowed measurement of cell temperature, cell voltage and total system pressure in a leak tight assembly. Gases were collected at the end of the ARC run and analyzed by gas chromatography (GC). Cells that did not vent were punctured in a special fixture that allowed direct injection of the cell gases into the GC instrument and also allowed determination of the total volume of the cell gases released.

Baseline, unabused cells at 100%SOC were initially punctured for direct GC analysis of the headspace formation gases as shown in Figure 5-89. An unaged baseline cell maintained at 10°C storage had 4.5ml (STP) of formation gases. Argon was the largest constituent and resulted from the original cell assembly in a He/Ar atmosphere. Measurable quantities of air (N_2/O_2) were also detected which likely remained from absorbed gas in the starting materials. Evolved gases were H_2, CO, CO_2, methane and ethylene. No ethyl fluoride was detected. An aged cell was also measured which had been held at 45°C, 80%SOC for 8 weeks. The headspace gas volume had increased to 7.1ml but showed the same volume of Ar, as expected for a non-leaking cell. The most significant change in the gas species volumes was an increase in CO and CO_2 and a decrease in H_2. These gas species will also be present in the abused cells and thus represent a baseline of comparison for the evolved gases.

The cells run in the ARC to high temperatures (150°C -160°C) showed new generation of H_2 and increased levels of CO, CO_2 and ethylene as shown in Figure 5-90. CO generation in the unvented cells occurred primarily in the 130°C to 160°C region based on comparison to the gases seen for the 130°C vented cells (shown later) which showed little CO generation even up to 160°C. Calculations made from the pressure increase in the calibrated gas collection system showed generation of 8ml of gas above baseline by 150°C and 26ml by 160°C. This sharp increase in gas generation agrees with the observations made on ARC bomb runs of the electrolyte/cathode reaction (Figure 5-57) where gas generation increased significantly above 140°C. A summary of the gas compositions and the calculated gas species volumes are listed in Table 6 and Table 7 for several baseline and ARC cells. The gas volume data is shown in Figure 5-91. Duplicate cell runs at 160°C showed significant variation in amount of CO_2 generation that may have resulted from cell to cell variations in this sensitive temperature regime. A marked increase in ethylene generation was measured between 150°C and 160°C but not with an accompanying increase in ethyl fluoride. A comparison of the normalized evolved gases is shown in Figure 5-92 as a function of increasing temperature. The gas compositions were normalized by the total amount of evolved gases and did not include the baseline headspace gases of Ar, N_2 and O_2. Gas samples taken at 120°C, 150°C and 160°C showed very similar relative gas compositions. The CO and CO_2 remained in relative equal ratios but there was an increase in the ethylene and decrease in methane with increasing temperature.

Table 6. Gas Composition of Punctured Cells Including Baseline and ARC Cells

Cell	Punctured Cells	Max Sample Temp	H$_2$	Ar	N2	O2	CO	CO2	CH4	C2H4	C2H6	Ethyl Fluoride	Propylene	Propane	solvent	Internal Cell Press (psi)	vol (STP) (ml)
													Gas Composition				
Q306	100%SOC Aged 45C, 80%SOC,8 wks	45C	0.3%	27.8%	9.6%	1.7%	11.3%	26.3%	11.5%			not measured		0.06%	11.5%	59.6	7.1
Q416	100%SOC Unaged Baseline	25C	8.2%	44.0%	6.2%	0.1%	4.2%	12.6%	13.5%	3.1%		not measured			11.2%	38.1	4.5
Q401	100% SOC ARC to 150C no vent	150C	9.8%	20.4%	1.6%	0.0%	25.4%	22.5%	10.2%	3.0%	2.6%	not measured	1.2%	0.1%	3.2%	105.1	12.5
Q407	60% SOC ARC to 160C no vent	160C	5.1%	10.7%	0.6%	0.0%	22.5%	32.1%	6.1%	11.0%	2.1%	not measured	0.2%		9.6%	257.2	30.6
Q405	60%SOC ARC to 160C no vent	160C	5.5%	19.1%	1.5%	0.0%	35.6%	18.0%	10.2%	6.3%	2.8%	not measured		1.0%	0.0%	138.5	16.5

Table 7. Gas Volumes of Punctured Cells Including Baseline and ARC Cells

Cell	Punctured Cells	Max Sample Temp	H$_2$	Ar	N2	O2	CO	CO2	CH4	C2H4	C2H6	Ethyl Fluoride	Propylene	Propane	solvent	Total (ml)
								Volume (ml)								
Q306	100%SOC Aged 45C, 80%SOC,8wks	45C	0.0	2.0	0.7	0.1	0.8	1.9	0.8	0.0	0.0	0.0	0.0	0.0	0.8	7.1
Q416	100%SOC Unaged Baseline	25C	0.4	2.0	0.3	0.0	0.2	0.6	0.6	0.1	0.0	0.0	0.0	0.0	0.5	4.5
Q401	100% SOC ARC to 150C	150C	1.2	2.6	0.2	0.0	3.2	2.8	1.3	0.4	0.3	0.0	0.2	0.0	0.4	12.5
Q407	60% SOC ARC to 160C	160C	1.6	3.3	0.2	0.0	6.9	9.8	1.9	3.4	0.6	0.0	0.1	0.0	2.9	30.6
Q405	60%SOC ARC to 160C	160C	0.9	3.1	0.2	0.0	5.9	3.0	1.7	1.0	0.5	0.0	0.0	0.2	0.0	16.5

Cells that vented during the ARC run usually vented between 120°C and 130°C. Gas volumes were not able to be determined since the cell measurements were not performed in a calibrated volume system at that time, thus gas compositions were all normalized to the amount of evolved gas. Gas sampling was usually performed at the end of the ARC run, allowing continued collection of gas from the vented cells between the vent temperature and the final temperature. However, some sampling was done at the vent temperature and at the final temperature.

Figure 5-93 shows a comparison of the normalized gas composition of a 130°C vented cell and a non-vented punctured cell. Both samples were collected after 160°C. The gas composition from vented cells always showed a much higher ratio of CO_2 to CO than seen in the non-vented cells. The gas compositions of the vented cells were all very similar,

independent of SOC or aging. Figure 5-94 shows a summary of gas compositions for several cells at each of these conditions. The dominant gas is always CO_2 followed by lower but comparable levels of H_2, CO and ethylene. Lesser amounts of the alkane gases were also present. The normalized gas compositions are listed in Table 8.

The difference in gas composition of the vented versus the non-vented cells was primarily in the ratio of CO_2 to CO. We have shown that CO_2 primarily arises from decomposition of the EMC. The source of CO can either be decomposition of other compounds such as the SEI layer, reduction of the CO_2 at the lithiated carbon or a pressure dependent decomposition of the solvents that generates more CO at higher CO_2 pressure.

Table 8. Normalized Composition of Evolved Gases in Vented ARC Cells

Vented Cells		H₂	CO	CO2	Methane	Ethylene	Ethane	Ethyl Fluoride	Propylene	Propane
Normalized without N2,O2,Ar										
100%SOC Unaged [313]	ARC to 160C vented 130C/ sampled 130C	5.1%	15.1%	61.4%	7.4%	8.7%	1.9%	Not measured	0.3%	0.0%
100%SOC Unaged [313]	ARC to 160C vented 130C/ sampled 160C	5.9%	6.4%	75.8%	1.9%	8.8%	1.1%	Not measured	0.1%	0.0%
100%SOC Aged [301]	ARC to 160C pre-punctured/ sampled 160C	6.5%	8.4%	68.0%	1.2%	15.5%	0.3%	Not measured	0.0%	0.0%
60%SOC Aged [308]	ARC to 160C vented 130C/ sampled 160C	5.0%	6.5%	66.0%	2.0%	19.0%	1.5%	Not measured	0.0%	0.0%
60%SOC Aged [309]	ARC to 160C vented 130C/ sampled 160C	7.3%	9.1%	58.4%	2.4%	15.7%	1.4%	5.6%	0.0%	0.0%

Baseline Cells: 100%SOC
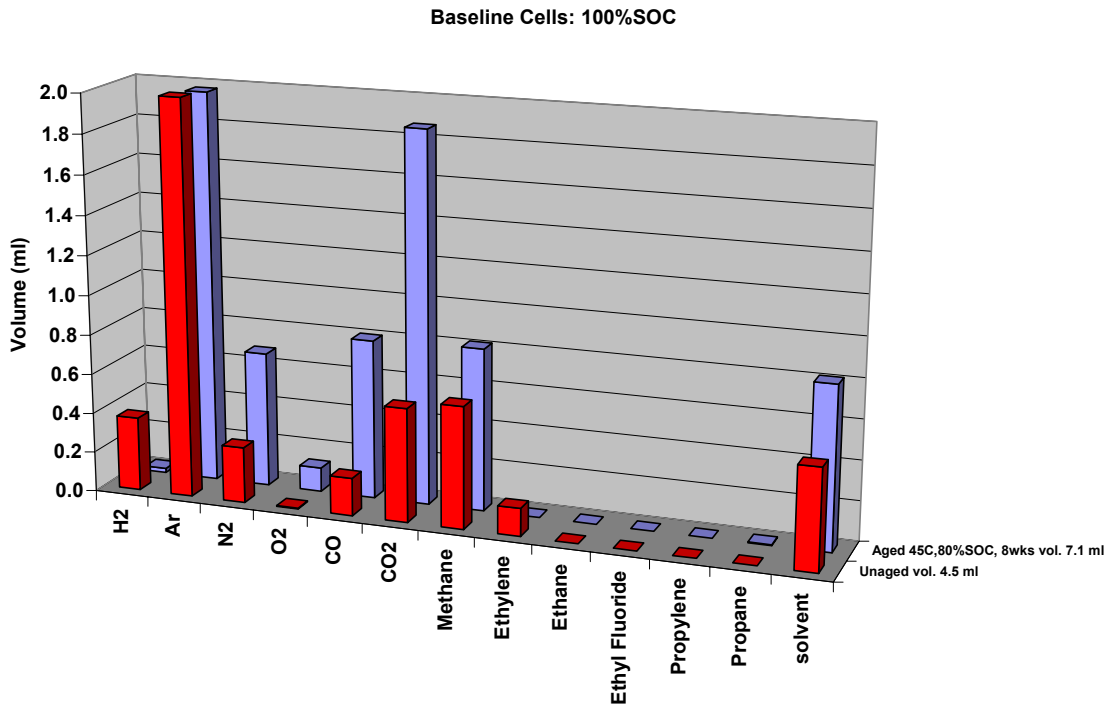
Figure 5-89. Gas volume composition of punctured Gen2 baseline cells, unaged and aged at 45ºC/80% SOC/8 wks.

Non-vented, Punctured Cells
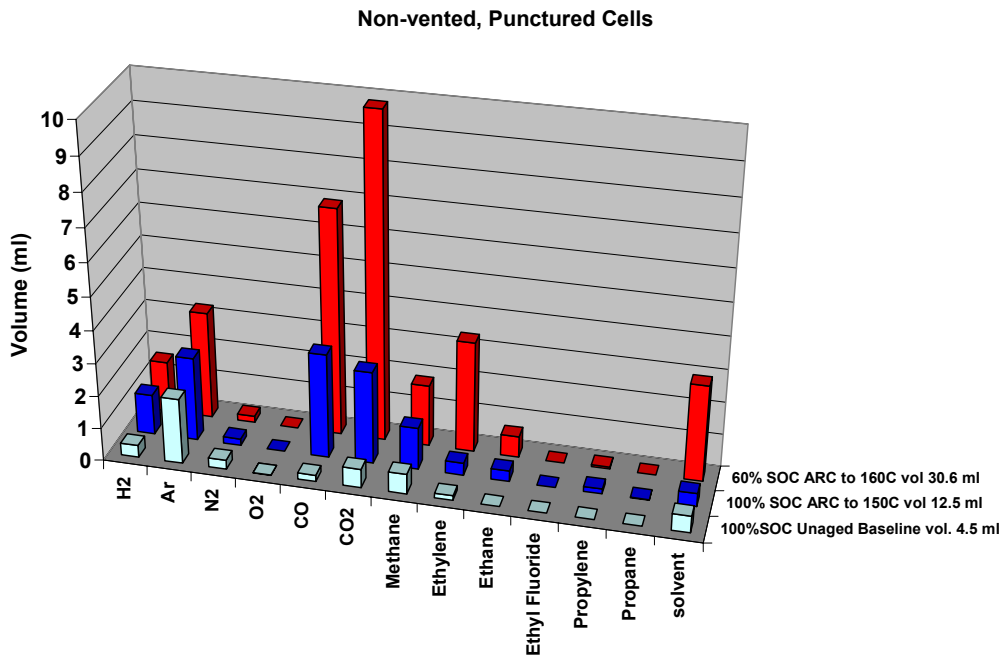
Figure 5-90. Gas volume composition of punctured Gen2 cells at 60% SOC and 100% SOC after ARC run to 160ºC.
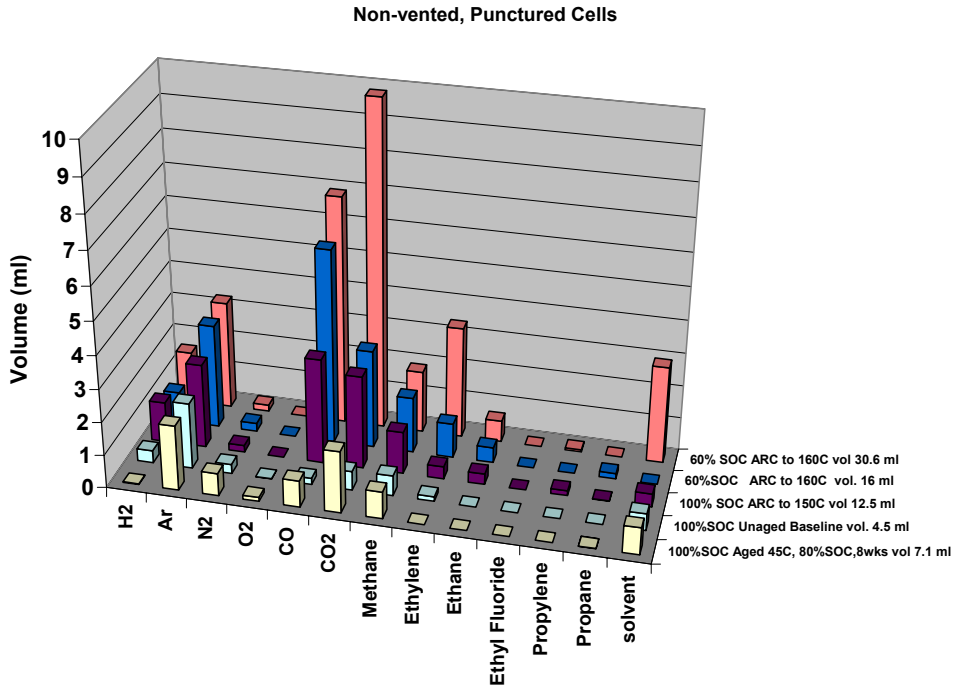
Figure 5-91. Summary of gas volume composition of punctured Gen2 cells at 60% SOC and 100% SOC, aged and unaged after ARC run to 160ºC.
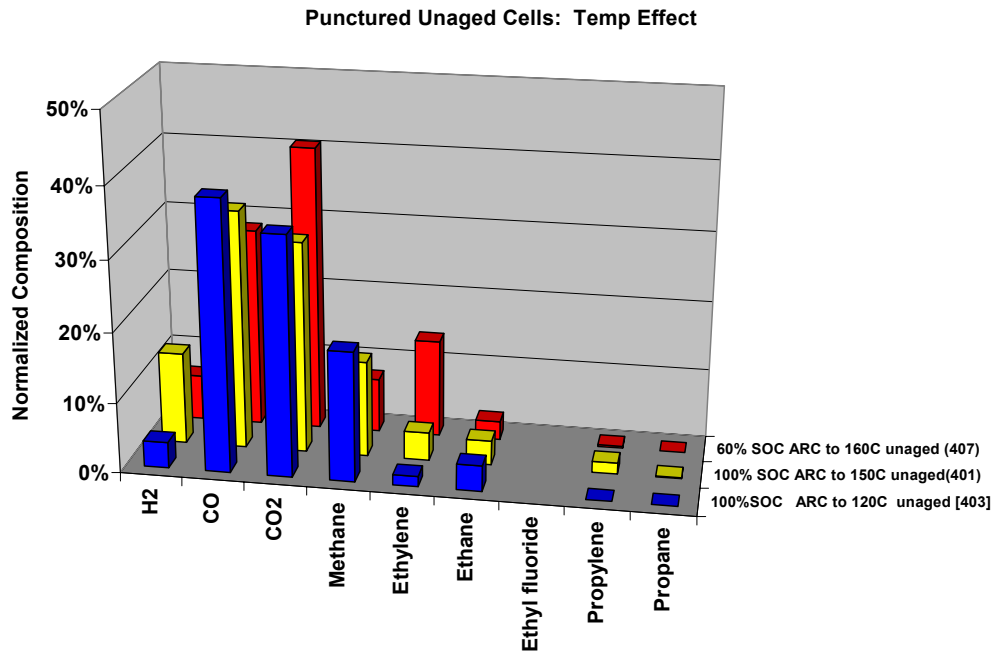
Figure 5-92. Temperature effect on normalized gas composition of punctured 60% SOC and 100% SOC Gen2 cells after ARC runs to 120ºC, 150ºC, and 160ºC.
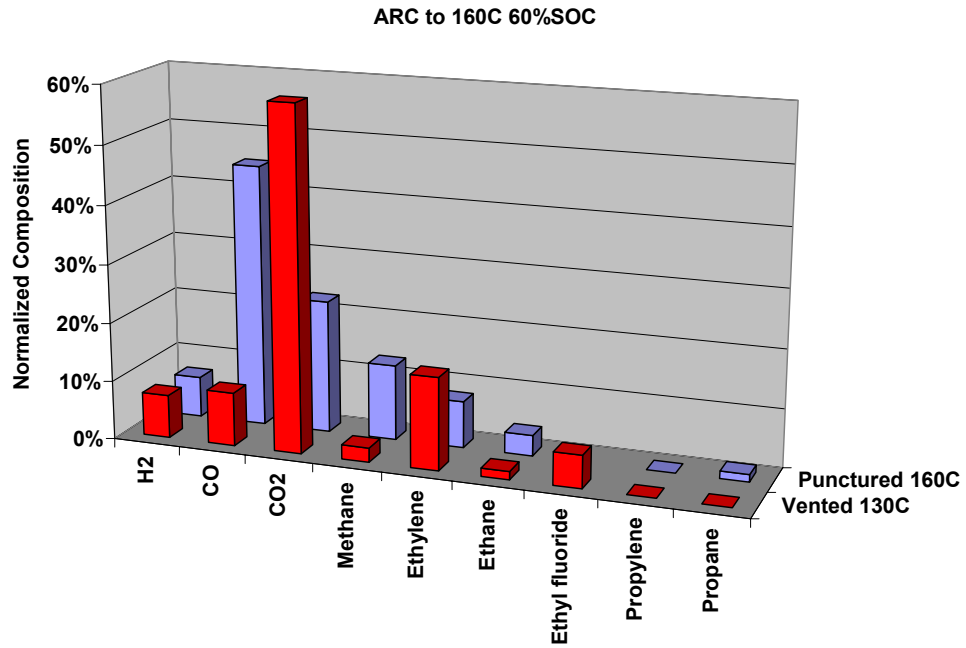
Figure 5-93. Comparison of normalized gas composition of Gen2 cells vented at 130ºC and non-vented. Gas sampled after ARC run to 160ºC.
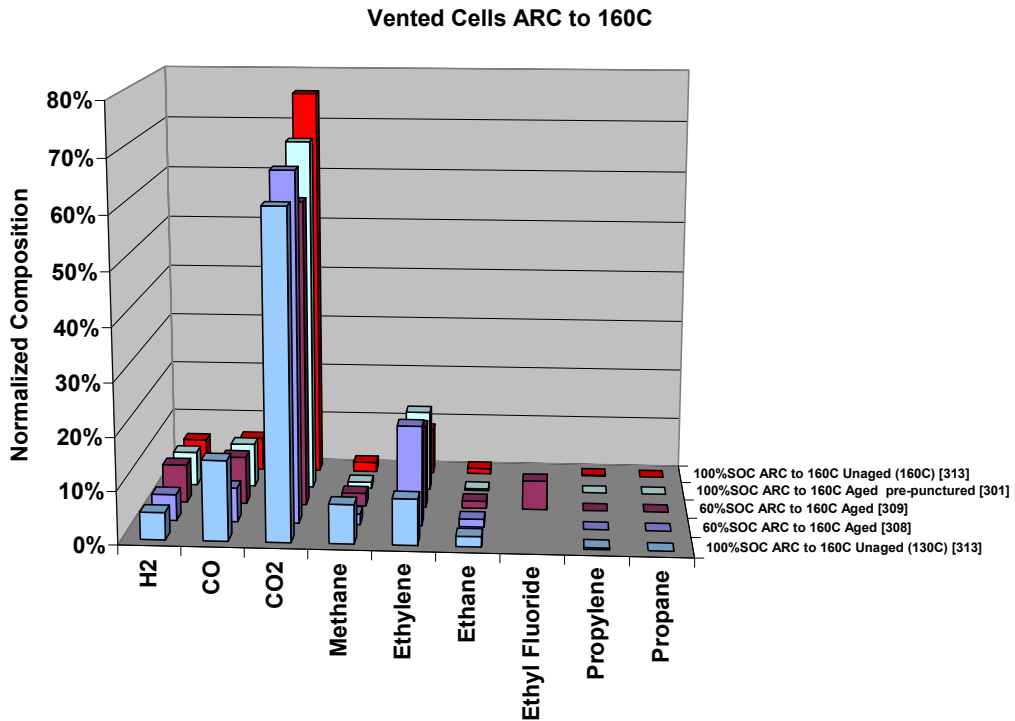
Figure 5-94. Summary of normalized gas composition of Gen2 cells at 60% SOC and 100% SOC that vented at 130ºC during ARC run at 160ºC.

5.2.6 Microcalorimetry

5.2.6.1 Sony and Gen1 Cells

Isothermal microcalorimetry was performed on the Sony and Gen1cells to determine the self-discharge and aging effects as a function of SOC and temperature. Figure 5-95 shows the open-circuit heat output for the Sony cells at 25°C from 0%-100%SOC. All cells showed decaying heat output as a function of time with the minimum heat output occurring for 50%SOC. The decay rate of the heat output was not exponential but followed a power law function as shown in Figure 5-96. The power of the function was SOC dependent varying from –0.25 at 50%SOC up to –1.17 at 0%SOC. The heat output as a function of SOC is more clearly seen in Figure 5-97. This figure shows the heat output at two different times (100h and 350h) after the beginning of the microcal measurement. These data show that the heat output decreased most rapidly at high and low SOCs when the magnitude of the heat output was greatest. Extrapolation of this data indicates that after a sufficiently long period of time the heat output would be relatively constant as a function of SOC below 50%SOC but would then increase with increasing SOC.

The Gen1 cells were likewise measured as a function of SOC. Figure 5-98 shows the heat output for a cell that was monitored up to 800 hours during which the cell was removed and placed at different SOCs and then put back into the microcal for continued monitoring. The cell was initially monitored at 90%SOC and showed a power law decay function as was seen for the Sony cells. The power of the function (-0.69) was very similar to that of the Sony cells at the same SOC. After over 250 hours, the cell was removed and placed at 50%SOC. The adjustment of the SOC was always performed after charging the cell to 100%SOC. The 50%SOC heat output was significantly reduced as was also observed for the Sony cells. The cell was then placed back at 90%SOC and the heat output measurement resumed. The figure shows that the heat output resumed at the same level as when the cell was previously at 90%SOC. The decay rate also was not affected by the cycling of the cell. The cell was then removed and placed at 100%SOC for a period of 200 hours. The heat output increased at this higher SOC as expected and decayed at a higher rate than at 90%SOC. The cell was then placed back at 90%SOC and the measurement resumed. The heat output resumed at a level projected in time from the 90%SOC level by the time spent at 100%SOC. In other words, cycling had no affect on the heat output and the heat output decreased in an irreversible manner, dependent only on SOC, temperature and time. These measurements suggest that a passivation reaction is taking place that results in stable reaction products that greatly reduce the self-heat generation in the cell. This heat output most likely results from low-rate decomposition and reformation of the SEI layer that has been previously measured by DSC and ARC. Heat output will also result from oxidation and reduction reactions of the electrolyte, which can impact the cell lifetime and capacity. Thus, aging is an irreversible process that leads to reduced cell reactivity and increased thermal stability.

Comparison of the Sony and the Gen1 cells at 25°C and 60°C is shown in Figure 5-99 for 90% SOC. Both cell types show significant dependence on temperature, however the GEN 1 cells had greater heat output under the same conditions of SOC and temperature. The differences in reactivity between the Sony and Gen1 cells may result from the different solvents, differences in the morphology of the intercalating carbons and different reactivity of the different metal oxide cathodes. It has been shown that the Gen1 $LiNi_{0.8}Co_{0.2}O_2$

cathodes are more thermally active than the Sony $LiCo_{1.0}O_2$ cathodes, especially at higher SOC. Another factor that is unknown is the total age of the Sony cells. These were commercial cells that had been stored under unknown conditions for an unknown period of time while the Gen1 cells were only a few months old. Passivation reactions in the Sony cells may have already reduced the heat output.
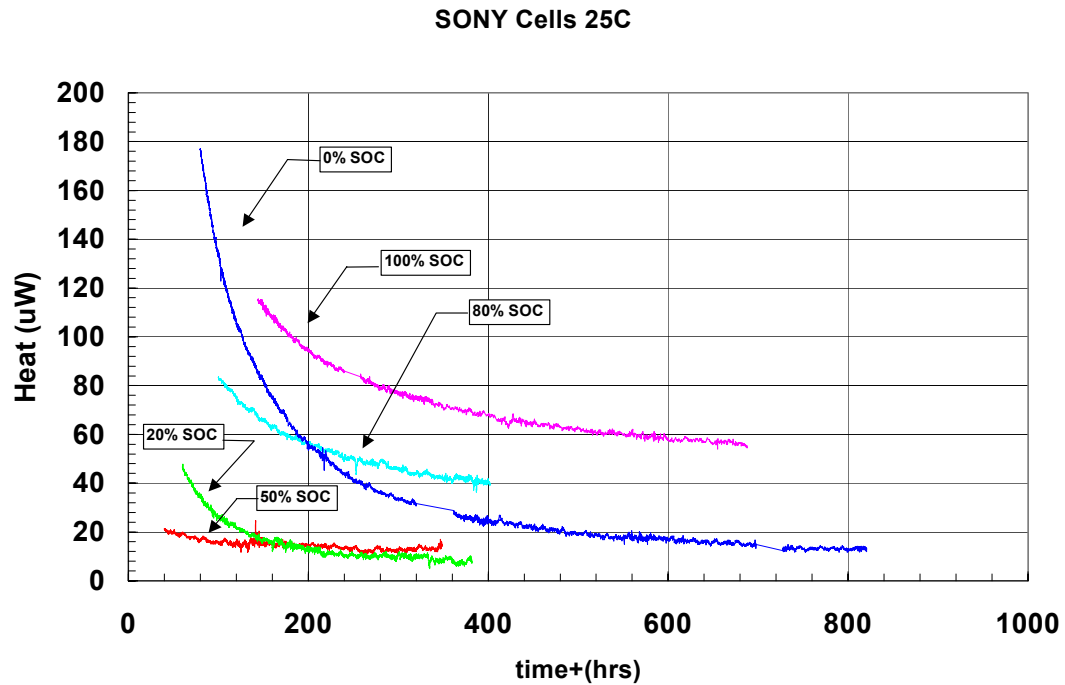
SONY Cells 25C

Figure 5-95.   Microcalorimetry of Sony cells at 25°C from 0% SOC to 100% SOC.
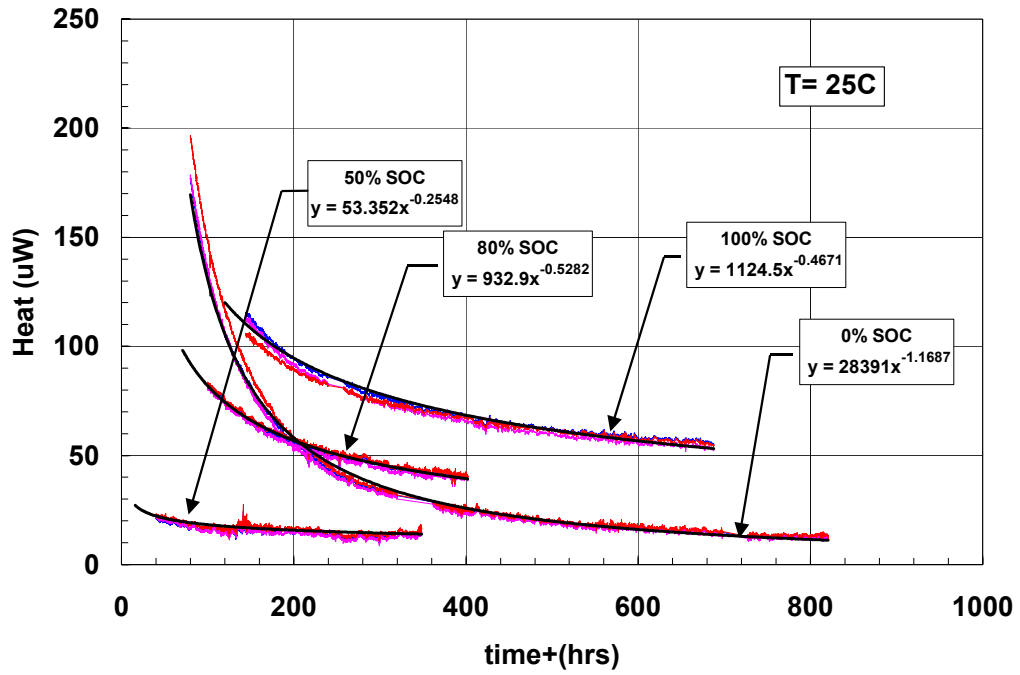
Figure 5-96. Power law fits to microcalorimetry heat output of Sony cells at 25ºC from 0% SOC to 100% SOC.
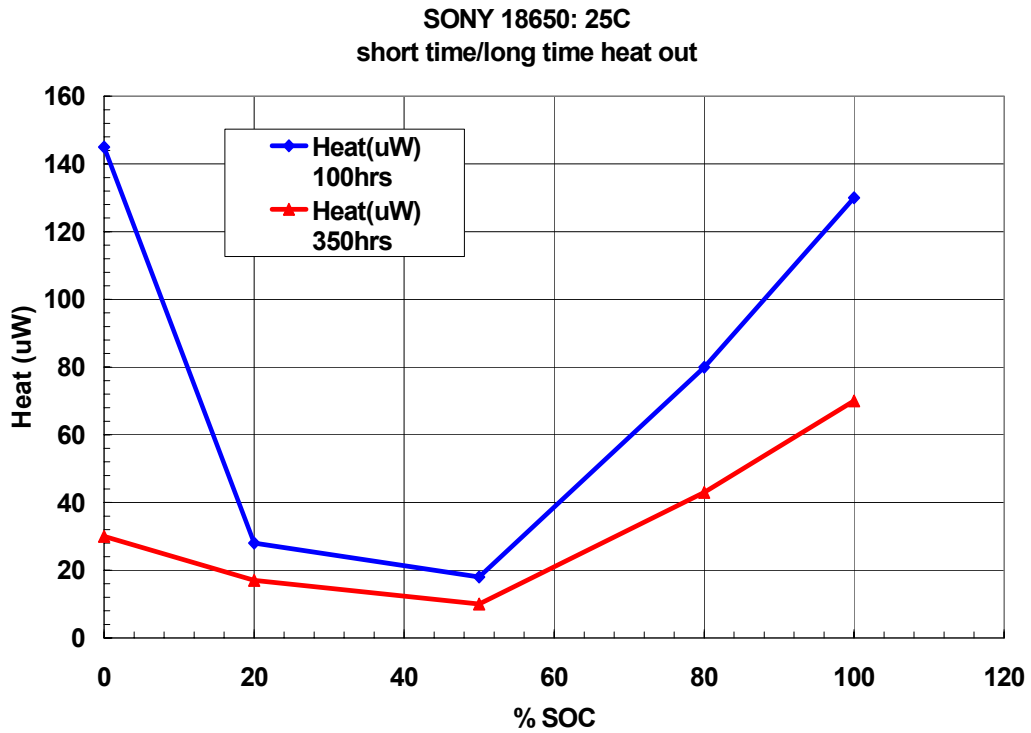
Figure 5-97. Heat output of Sony cells at 100 hours and 350 hours in microcalorimeter at increasing SOC.

ATD Gen1 Cells: $LiNi_{0.8}Co_{0.2}O_2$ Cathodes

$y = 29627x^{-0.6903}$

60C

Charge Cycle

Charge Cycle

Charge Cycle

90%SOC

100%SOC

90%SOC

50%SOC
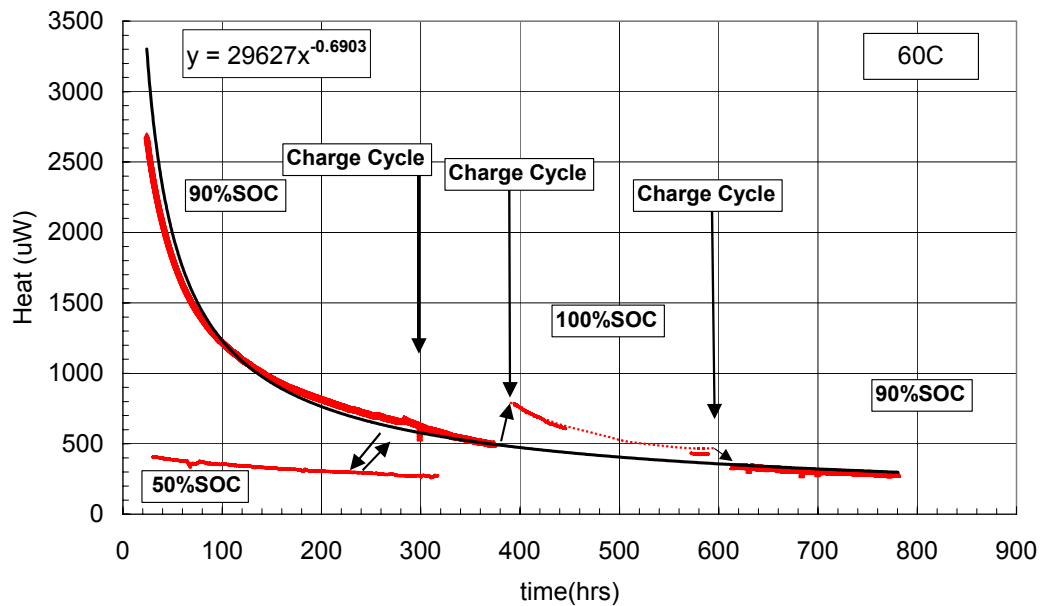
Figure 5-98. Microcal heat output of Gen1 cells at 60ºC and different SOC.

90%SOC

GEN1 60C

Sony 60C

Sony 25C

GEN1 25C
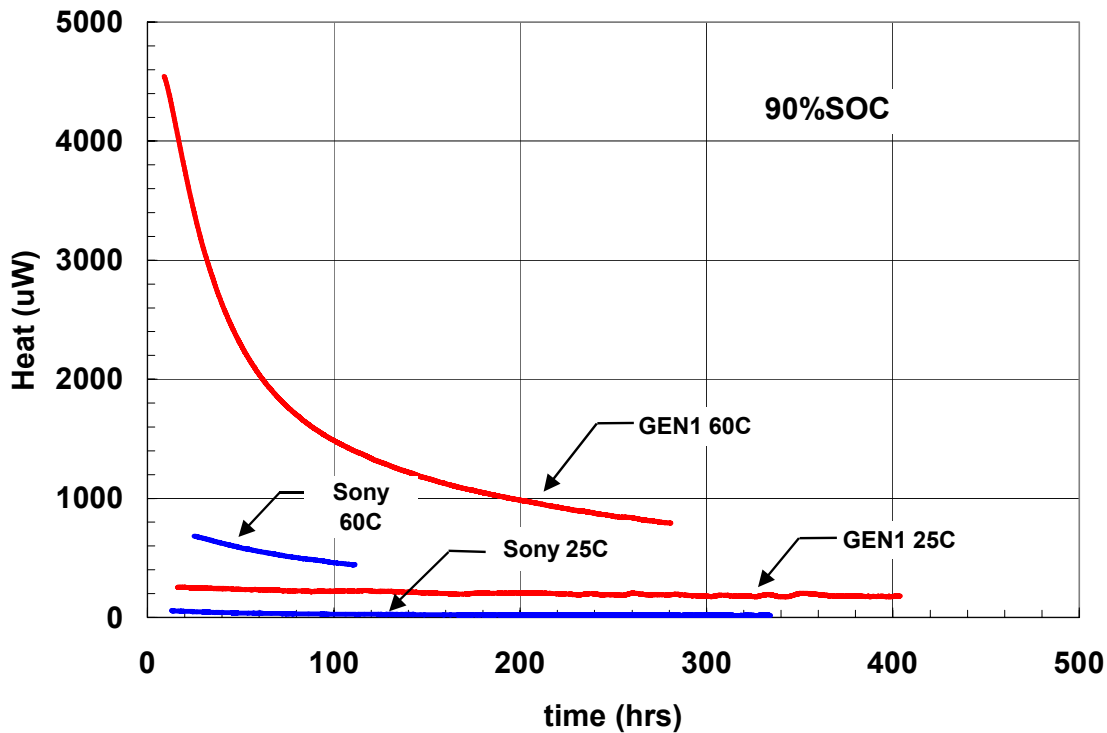
Figure 5-99. Comparison of microcal heat output for Sony and Gen1 cells at 25ºC and 60ºC/90% SOC.

5.2.6.2 Microcal of Gen2 Cells

Microcalorimetry measurements were performed on two Gen2 cells at several states of charge to determine the self-discharge heating rate and activation energy. The cells were held at temperature for only a little over 24 hours to minimize any aging effects in the cells. The heat output and the heat rate of decay after equilibration were determined for each temperature. The cells were all measured at 80%SOC. Figure 5-100 shows this data for the Gen2 cells as well as a comparison to a Gen1 cell measured at 60°C /90%SOC. The Gen2 cells showed comparable heat output to the Gen1 cells but the rate of decrease of the generated heat was much lower indicating that the Gen2 cells were not passivating as well as the Gen1 cells. An Arrhenius plot of the heat output is shown in Figure 5-101. The cells clearly showed thermally activated heat output with average activation energy of 13.2 kcal/mole. Between 55°C and 65°C the magnitude of the heat decay rate increased abruptly suggesting changes in the kinetics of the passivating reactions. The electrical performance of the cells has also shown abrupt changes in this temperature range.
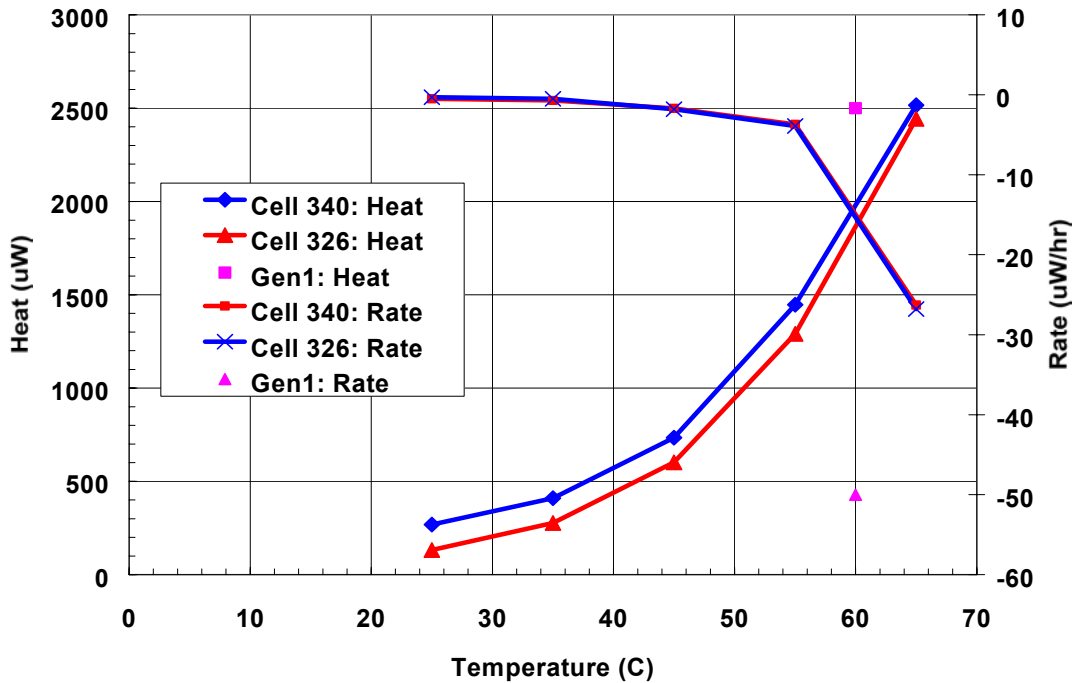
Figure 5-100.   Microcalorimetry of Gen2 cells as a function of SOC showing heat output and heat decay rate.

Average Activation Energy 13.2 kcal/mole

Figure with axes labeled In(heat (uw)) (y-axis, 0 to 9) and 1000/T(K) (x-axis, 2.9 to 3.4). Data points labeled 65C, 55C, 45C, 35C, 25C.

Cell 340: 11.46 kcal/mole
$y = -5.7692x + 24.833$
$R^2 = 0.9895$

Cell 326: 14.8 kcal/mole
$y = -7.4369x + 29.796$
$R^2 = 0.9994$
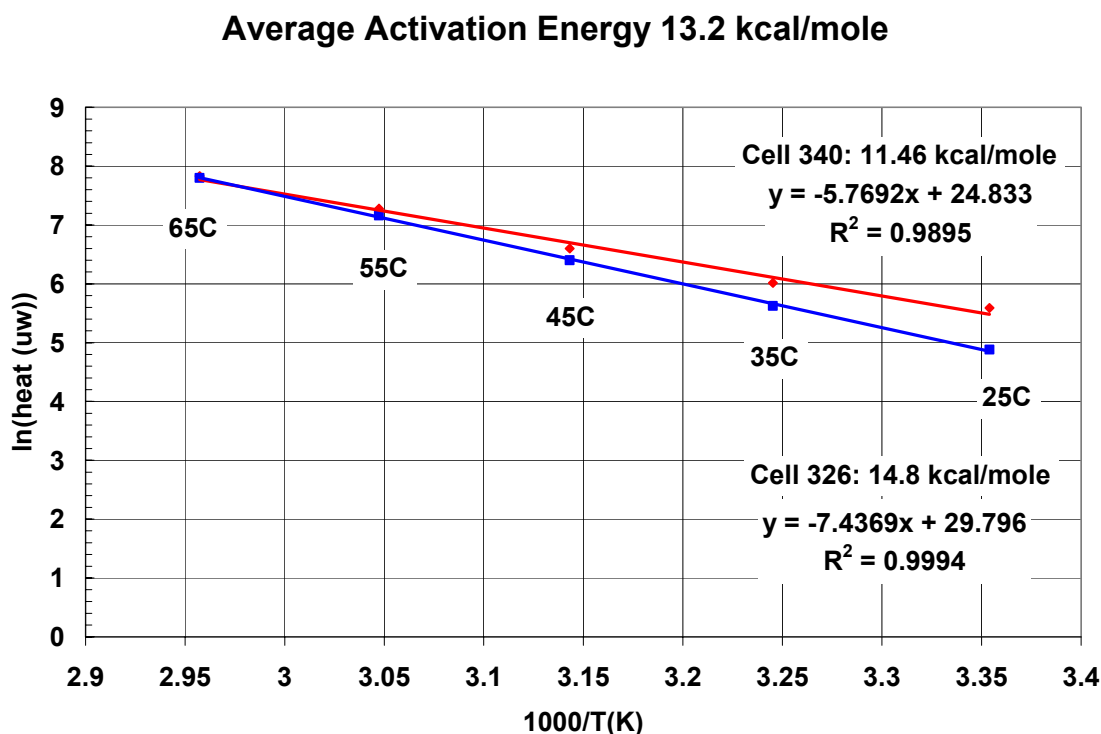
Figure 5-101.   Arrhenius plot of Gen2 microcalorimetry data.

6.0 XRD Studies of Thermal Degradation of Cathode Materials

With the success of lithium-ion cells in commercial electronics, this technology seems poised to move into aerospace, military, and hybrid electric vehicle applications. Problems of power-fade and safety in high power lithium-ion cells are the major technical barriers that have to be overcome for these more demanding applications. Safety is related to the occurrence of exothermic reactions in charged batteries at elevated temperatures that ultimately results in thermal runaway and catastrophic failure of the battery. The thermal runaway has been ascribed to reactions between the charged electrodes and the electrolyte. There is a lot of information on the reactions that occur in the electrolyte as the battery is heated. Calorimetric analysis (DSC, ARC and microcalorimetry) and analysis of electrolyte and evolved gasses have been utilized to understand the cell and component reactions that contribute to the complex thermal responses of Li-ion cells. However, there is very little information on reactions in the electrodes. Most temperature dependent diffraction studies of the structure of the charged electrodes have been performed in the absence of electrolyte/solvents. In order to understand thermal degradation of the electrodes in Li-ion cells, we have monitored the structural changes of the charged cathode material in the presence of electrolyte using both high resolution and time resolved x-ray diffraction (XRD).

116

6.1   High Resolution XRD

The high resolution XRD studies were done at Beam Line X7A at the National Synchrotron Light Source (NSLS) at BNL. The experimental setup of the diffractometer is shown in Figure 6-1.
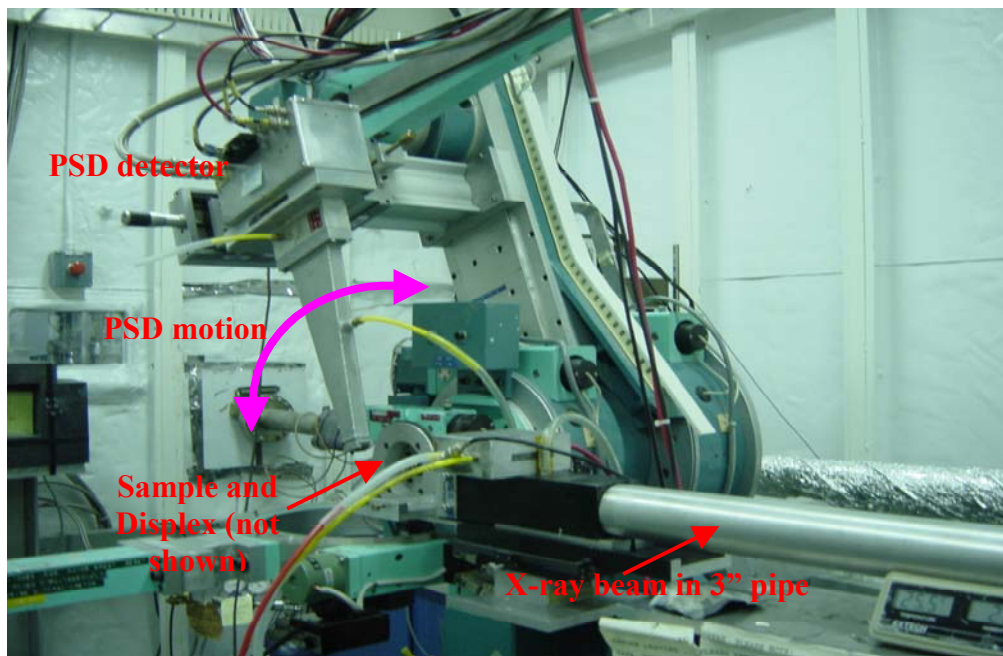
Figure 6-1.   Diffractometer at Beam Line X7A for high resolution XRD.

Cells with a coin cell configuration were used. Disc cathodes (2.82 cm2) were punched from cathode sheets with the Gen-2 chemistry. These were obtained from Quallion, via ANL, and only one side of the Al foil current collector was coated. The cells had a Li foil anode, a Celgard separator and a 1 M $LiPF_6$ in 1:1 EC:DMC electrolyte. Charged cathode samples were extracted from cells and were sealed in either 0.3 or 0.5mm quartz capillaries. The samples included wet samples from the cell or samples that were washed in tetrahydrofuran (THF) in an inert atmosphere. In some cases excess electrolyte was added before sealing the capillaries. These capillaries could withstand the pressure generated. The excess electrolyte case is more representative of the conditions in a battery, where there is a large reservoir of electrolyte in the anode.   The capillaries were mounted in the thermal stage of a diffractometer on Beam Line X7A at NSLS. The measurements were done, using 0.7044 Å x-rays. A position sensitive detector (PSD) was used to monitor the diffracted x-rays. At this Beam Line the thermal stage was a Displex, an apparatus capable of controlling temperature from liquid He temperatures up to 300ºC. We used the Displex to control temperatures from 25º to 300ºC. The temperature was increased in 25ºC increments and XRD patterns were recorded. The total time to do an experiment on a single sample was ~32 h.

117

Data were obtained for Gen-2 cathodes ($Li_{1-x}Ni_{0.8}Co_{0.15}Al_{0.05}O_2$) charged to three SOC levels (92 mAh/g, x = 0.33; 185 mAh/g, x = 0.60; and 220 mAh/g, x = 0.80). Figure 6-2 shows a complete XRD spectrum of material from an electrode charged to x = 0.33, before heating. The Q range of the data is equivalent to going to 140° with Cu K_α x-rays. Figure 6-3 shows the structural evolution on heating from ambient temperature to 300°C. The small peak, in the top panel at $2\theta = 8.62°$, indicates phase changes occurring at temperatures as low as 100°C. This peak can only be detected with a high resolution diffractometer. Figure 6-4 gives details of the XRD patterns for the initial material and the material heated to 300°C and cooled down to ambient temperature. The major product has a NiO rock salt structure. In addition to the NiO-like peak there was evidence for the presence of Li_2CO_3 and a spinel or cubic phase. XRD peaks for Li_2CO_3 appear at about 250°C. Li_2CO_3 is only seen at low states of charge.
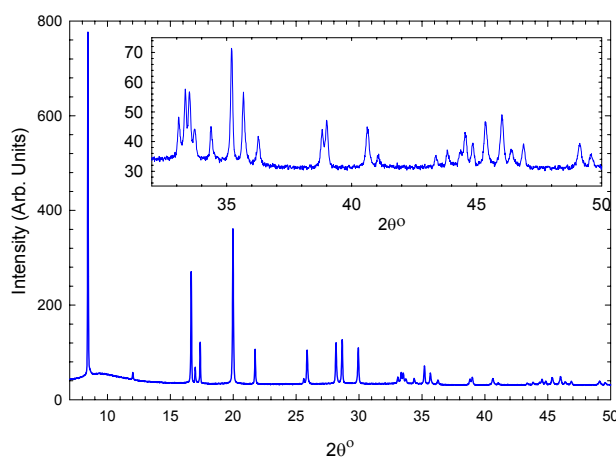
Figure 6-2. **XRD pattern for $Li_{1-x}Ni_{0.8}Co_{0.15}Al_{0.05}O_2$ from an electrode charged to x = 0.33, before heating. $\lambda = 0.7044$ Å. Insert shows expanded view of data at high angles.**
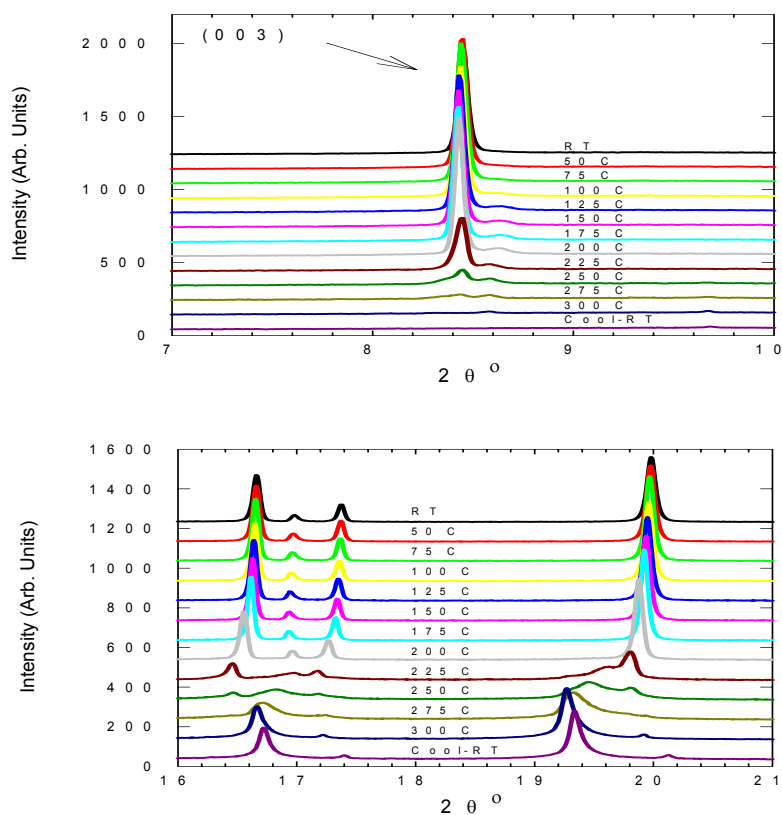
Figure 6-3. Evolution of the XRD patterns for $Li_{1-x}Ni_{0.8}Co_{0.15}Al_{0.05}O_2$ from an electrode charged to x = 0.33 on being heated to 300°C and on cooling to ambient temperature.
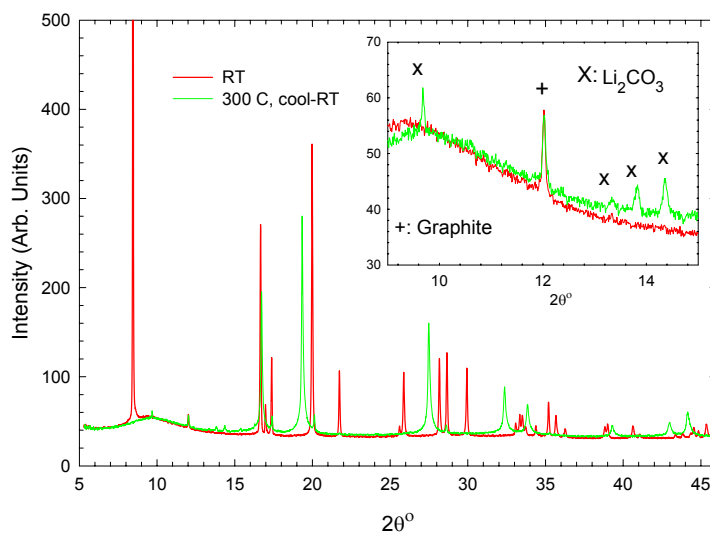
Figure 6-4. XRD patterns for $Li_{1-x}Ni_{0.8}Co_{0.15}Al_{0.05}O_2$ from an electrode charged to x = 0.33, after heating to 300°C and cooling down to ambient temperature. Inset shows XRD peaks for graphite and Li_2CO_3.

6.2 Time Resolved XRD

At Beam Line X7B, at NSLS, it was possible to do time resolved XRD. Figure 6-5 shows the experimental setup at Beam Line X7B. XRD patterns were recorded with a Mar 345-image plate detector. The typical time to obtain a complete individual diffraction pattern was of the order of 2.6 min. During XRD data collection the temperature of the sample was typically ramped by 2°C/min up to 450°C. So a complete set of data can be obtained on a sample in about 4h. The x-ray wavelength was 0.92252 Å.
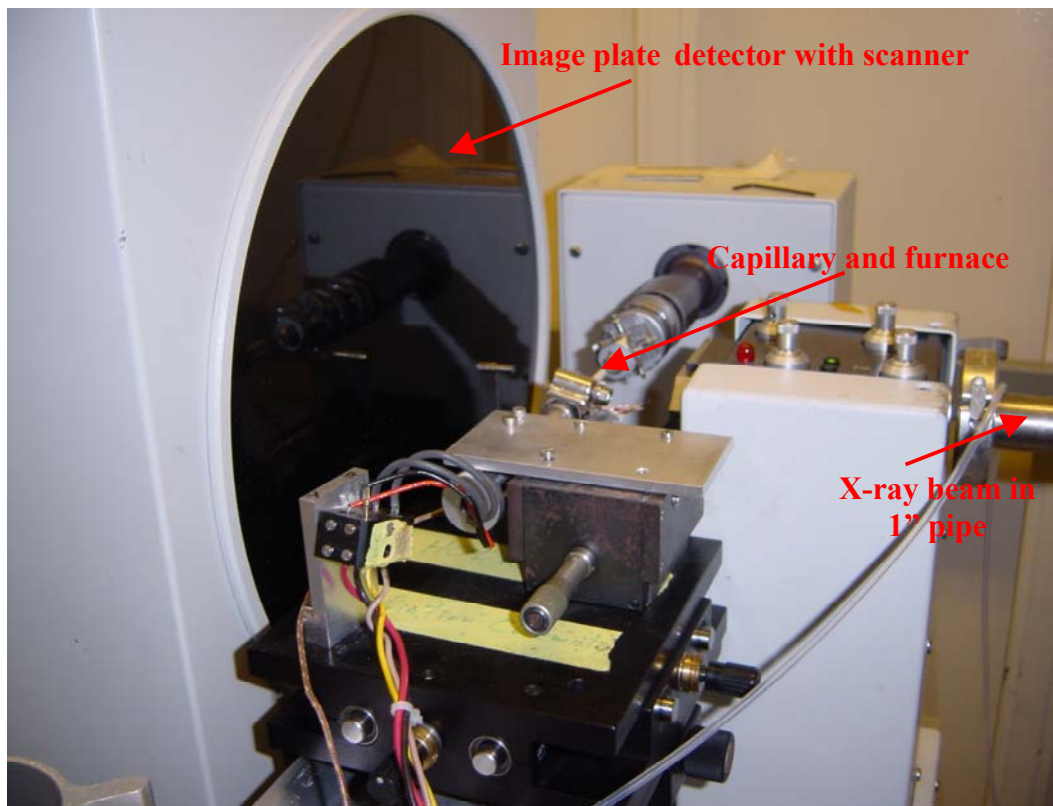
Figure 6-5.   Arrangement at Beam Line X7B for time resolved XRD.

Initially the results were irreproducible. Eventually, we found that the reaction pathway and the final products depended on the ratio of electrolyte to active material. The results depended on the time it took to transfer samples to the capillaries in the glove box. By adding electrolyte in the capillary we were able to get reproducible results. The excess electrolyte case is more representative of the conditions in a cell, where there is a large reservoir of electrolyte in the anode.

Figure 6-6 shows typical results for $Li_{0.31}Ni_{0.8}Co_{0.15}Al_{0.05}O_2$ with excess electrolyte. Decomposition of the layered structure starts at about 195˚C. In the interval between 195˚C and ~300˚C a disordered spinel phase is formed. There is some evidence for the formation of a second spinel phase, just below 300˚C. Above 300˚C we see a rock salt structure, consistent with the formation of NiO.
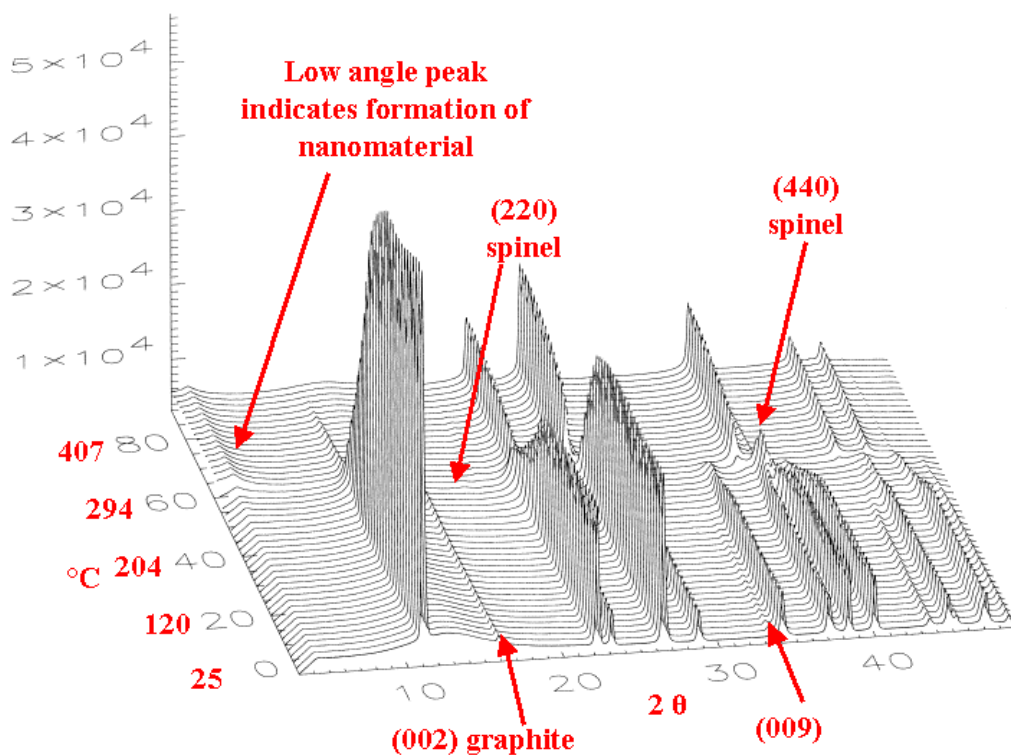
Figure 6-6. Temperature dependent XRD pattern of $Li_{0.33}Ni_{0.8}Co_{0.15}Al_{0.05}O_2$ cathode material in the presence of excess electrolyte (1 M $LiPF_6$ in 1:1 EC:DMC) obtained using an image plate detector at beam line X-7B at NSLS. The x-ray wavelength was 0.92252 Å. The temperature was ramped from room temperature to 450° C in 4 hours at a constant rate. A total of 91 XRD scans were performed during the temperature ramp.

At lower states of charge formation of the spinel phase occurs at higher temperatures. The respective temperatures are 195°C for $Li_{0.31}$, 225°C for $Li_{0.69}$ and 255°C for $Li_{0.77}$. In the presence of excess electrolyte the conversion of the spinel to the rock salt structure proceeds rapidly by a first order phase transformation. This reaction occurs close to 300ºC, irrespective of the degree of charge. Figure 6-7 shows an expanded view of the 2θ range 35-45º. It clearly shows the development of the (440) spinel peak and the final formation of the cubic NiO rock salt structure. At low states of charge diffraction peaks for Li_2CO_3 are also observed at elevated temperatures. Figure 6-8 shows typical results for $Li_{0.34}Ni_{0.8}Co_{0.15}Al_{0.05}O_2$ without excess electrolyte. The disordered spinel phase forms at about 200˚C. However, conversion of the spinel phase does not proceed via a first order phase transformation. Formation of the NiO appears to occur by a solid solution process, by loss of oxygen, in the spinel. This shows that the reaction path depends in the ratio of electrolyte to charged active material
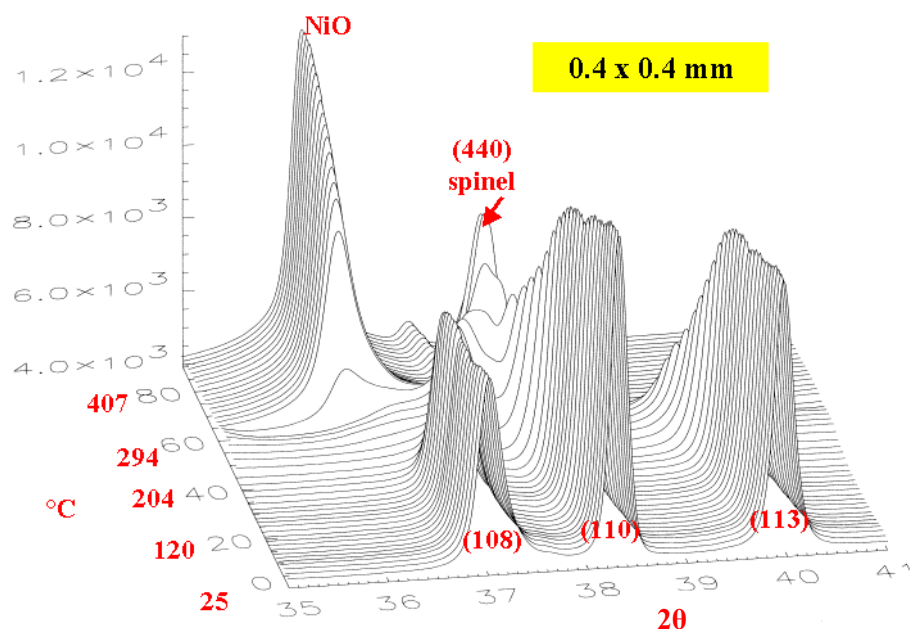
Figure 6-7. An expanded view of the region covering the (108), (110) and (113) peaks of the $Li_{0.33}Ni_{0.8}Co_{0.15}Al_{0.05}O_2$ cathode material. The arrow indicates the merger of the (108) and (110) peaks to form a spinel-like phase. The major final product has the rock salt structure. The rapid change in structure of the cathode material (around scans 55-60) is seen only in the presence of excess electrolyte.
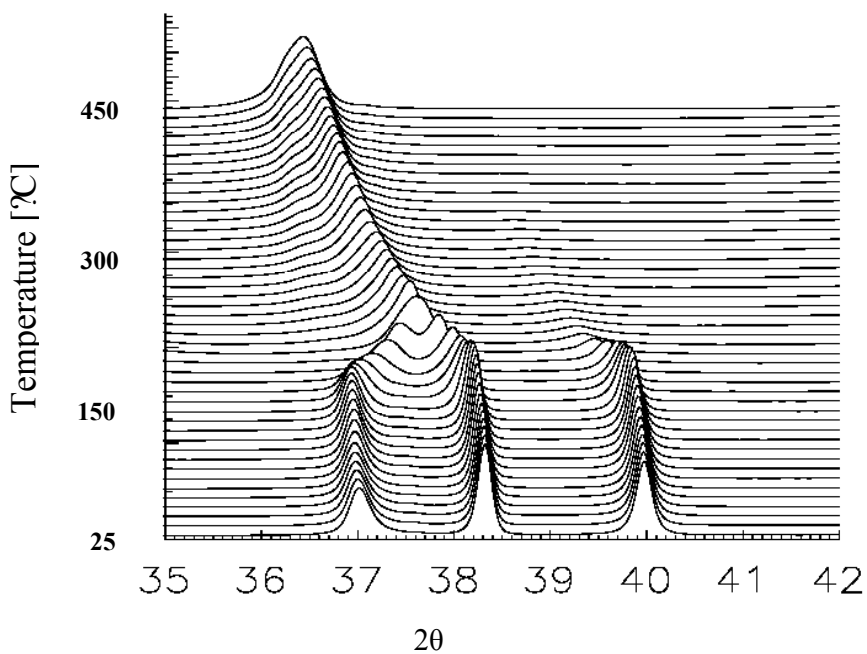
Figure 6-8. XRD results for $Li_{0.34}Ni_{0.8}Co_{0.15}Al_{0.05}O_2$ without excess electrolyte.

Our experiments, so far, show that the overall reactions at elevated temperatures depend on the state of charge as well as on the presence/absence of electrolyte. A strong interaction between the electrolyte and charged cathodes at elevated temperatures is evident. The methodology for doing this work has been worked out and will be applied to studies of electrodes from cycled and abused cells.

7.0   Thermal Abuse Conclusions

Our thermal abuse studies have allowed detailed measurement and characterization of the thermal abuse performance of Li-ion cells under a wide range of operational and abuse conditions. The extremes of cell response have been monitored and recorded to provide a safety performance reference for handling and testing of these cells. Quantitative analysis of the cells and cell materials have revealed details of the contributing decomposition reactions, which has allowed an understanding of many of the basic reaction mechanisms. Cell thermal abuse performance has been classified into three basic temperature regimes and the roles of the cell constituents identified in each of these regimes. The following sections summarize and discuss the materials and mechanisms active in these basic regimes.

7.1   Thermal Response Regimes

The thermal runaway response of Li-ion cells can be described as occurring in three stages divided into the major temperature regimes as shown in Figure 7-1:

Stage 1: Room Temperature to 125°C – Onset of thermal runaway
Stage 2: 125°C – 180°C – Venting and accelerated heating (smoke)
Stage 3: 180°C and above – Explosive decomposition (flame)
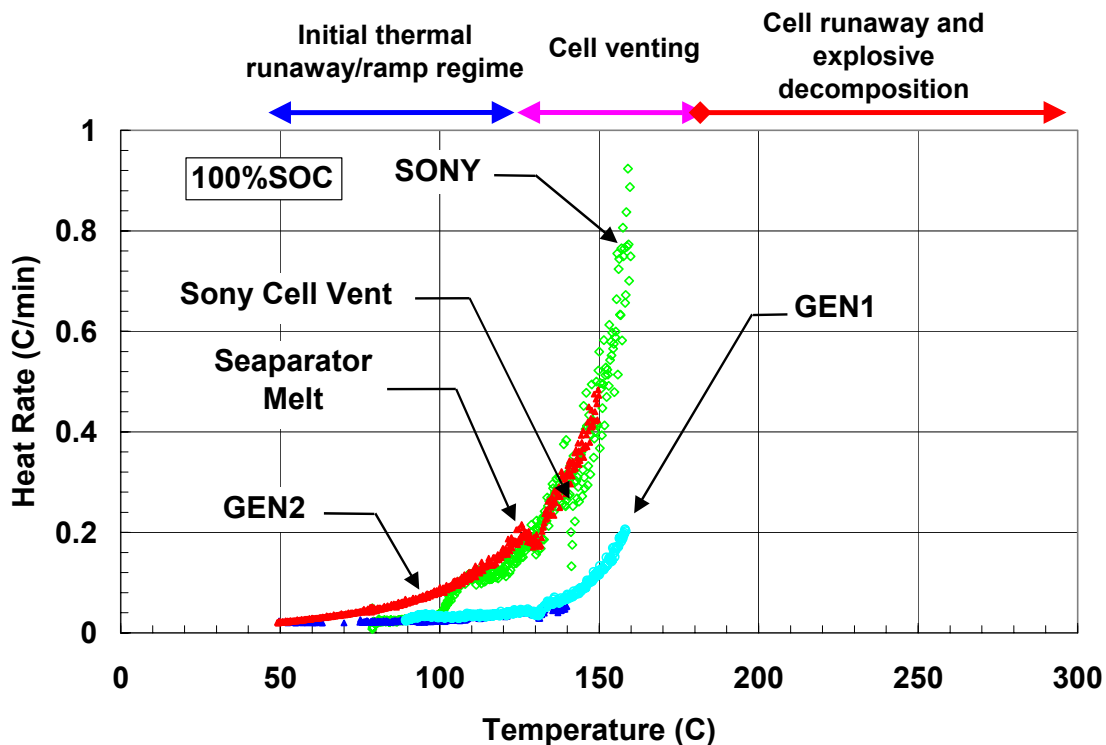
Figure 7-1.   Major temperature regimes corresponding to the three stages of thermal runaway.

124

Cell Thermal Abuse Response Summary

Stage 1. Room Temperature to 125°C Onset of Thermal Runaway

- Exotherms begin at anode due to SEI reactions and decomposition
- Low-level heat output starts as low as 50°C (possibly due to incomplete formation)
- Magnitude and onset of thermal response is highly influenced by morphology of anode carbon particles
- SEI decomposition leads to exothermic reduction of electrolyte at exposed lithiated carbon surface
- Gas generation slowly increases with increasing temperature (primarily from EMC)
- Aging reduces carbon reactivity (more stable, well developed SEI layer) leading to more thermally stable cell

Stage 2. Venting and Accelerated Heating (smoke) 125°C - 180°C

- Rate of gas generation increases above 125°C
- CO_2 is the main decomposition gas followed by CO, C_2H_4, H_2
- Cathode appears to be the major source of early gas generation along with EMC decomposition gases
- Anode reactions are the source of H_2
- Self-heating rate increases above 140°C
- Both anode and cathode participate in exothermic reactions that create a complex chemical environment within the cell.
- Electrolyte amount is critical to overall rates of heat and gas generation and ultimately dictates the full cell response
- For electrolyte decomposition reactions:
  - $EMC/LiPF_6$ source of main gas generation but not a source of heat
  - $EC/LiPF_6$ reaction is the main source of heat generation
  - Increased concentration of either $LiPF_6$ or EC greatly increase rate of EMC decomposition.

Stage 3. Explosive Decomposition (flame) 180°C and Above

- In full cells, very rapid increase in heat and gas generation rate is observed, with explosive decomposition around 200°C
- Several exothermic, gas-producing reactions over narrow temperature range from 180°C to 225°C are responsible for this dramatic cell response.
  - High-rate decomposition reactions occur between the cathode and electrolyte materials in the 140°C -200°C range with peak in heating rate at 190°C
  - High-rate decomposition reactions occur between the anode and electrolyte materials in the 200°C -225°C range with peak in heating rate at 225°C
  - Electrolyte decomposition rate peaks in the 180°C -200°C range
  - Sudden increase in gas evolution from anode above 200°C in addition to continued gas evolution from cathode and electrolyte decomposition
- Gases serve as propellant to eject any remaining electrolyte
- Expelled electrolyte and some of the gasses generated in the cell are flammable and can be ignited by external spark source.

7.2   Thermal Abuse Mechanisms

The mechanisms of thermal abuse response relate to the contributions of each cell component and the interactions between the components. The response of a full cell is dependent on each of these contributions but the full cell response can only be determined from a detailed modeling of the constituent masses and their measured reactions. We report here on the contributions of the individual component reactions and make only approximate evaluations of the relative contributions in a full cell. The following sections describe what we believe are the main thermal reaction mechanisms of the anode, cathode and electrolyte of the Li-ion chemistries studied in the ATD program.

7.2.1   Anode Reaction Mechanisms

Anode reactions begin immediately upon initial cycling of the cells during manufacturing. The anode carbon particles develop an SEI layer from reaction of the lithiated carbon with the electrolyte that serves as a barrier to further reactions while allowing Li ion diffusion during charge/discharge. This SEI layer consists of both organic and inorganic components resulting from reduction of the electrolyte. The exact composition depends on the salt and solvent species composing the electrolyte. $LiPF_6$ was the only salt used in all of the ATD Li-Ion cells measured and EC was a common constituent of all of the solvents. DEC and EMC were the linear carbonates used with the EC while the commercial Sony cells contained DMC. The main products of the reduction reactions have been reported by several researchers to be [7,22]:

$$(EC):\ 2(CH_2O)_2CO + 2e^- + 2Li^+\ \rightarrow\ (CH_2OCOOLi)_2 \downarrow + CH_2=CH_2 \uparrow\quad (2)$$

$$(CH_2O)_2CO + 2e^- + 2Li^+\ \rightarrow\ Li_2CO_3 \downarrow + CH_2=CH_2 \uparrow\qquad (3)$$

$$(DEC):\ (C_2H_5O)_2CO + e^- + Li^+\ \rightarrow\ C_2H_5OCOOLi \downarrow + C_2H_5{}^\bullet \uparrow\qquad (4)$$

$$(DMC):\ (CH_3O)_2CO + e^- + Li^+\ \rightarrow\ CH_3OCOOLi \downarrow + CH_3{}^\bullet \uparrow\qquad (5)$$
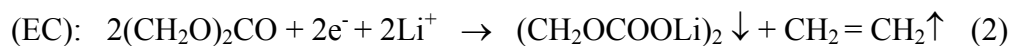
The radical species will continue to react and form other solid and gaseous species. Other workers have also shown reduction reactions leading to R-OLi products on the anode carbon such as [20,23]:

$$(EC):\quad (CH_2O)_2CO + 2e^- + 2Li^+\ \rightarrow\ (CH_2OLi)_2\ +\ CO \uparrow\qquad (6)$$

$$(DMC):\quad (CH_3O)_2CO + 2e^- + 2Li^+\ \rightarrow\ 2CH_3OLi\ +\ CO \uparrow\qquad (7)$$
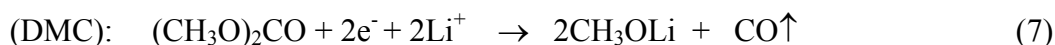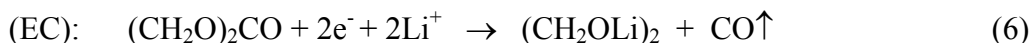
Reactions of binary solvents containing EC with DEC or DMC have been shown to have passive films resulting primarily from EC reduction products [24]. Similar selectivity is expected with the EMC solvent.

The electrolyte salt can also undergo decomposition and reduction to form:

$$LiPF_6 \quad \rightarrow \quad LiF\downarrow \; + PF5\uparrow \qquad\qquad (8)$$

$$LiPF_6 + ne^- + nLi^+ \quad \rightarrow \quad LiF\downarrow + Li_xPF_y\downarrow \qquad\qquad (9)$$

Many other reactions have been proposed of both the primary components and the secondary products resulting in solid products such as LiF and Li_2O as well as additional gas species such as CO_2, H_2, CH_4, C_2H_6, HF, and POF_3 [17, 25]. In particular any trace water will react with the PF_5 to form HF and POF_3. The resulting HF can react with many of the solid SEI products to further complicate the composition of the SEI layer.

The initial SEI layer consists primarily of the lithium alkyl carbonates and inorganic compounds such as Li_2CO_3. However, this layer is considered metastable that converts exothermically to a more stable inorganic layer with time [5,6]. This reaction takes place at a rate dependent on temperature and SOC and 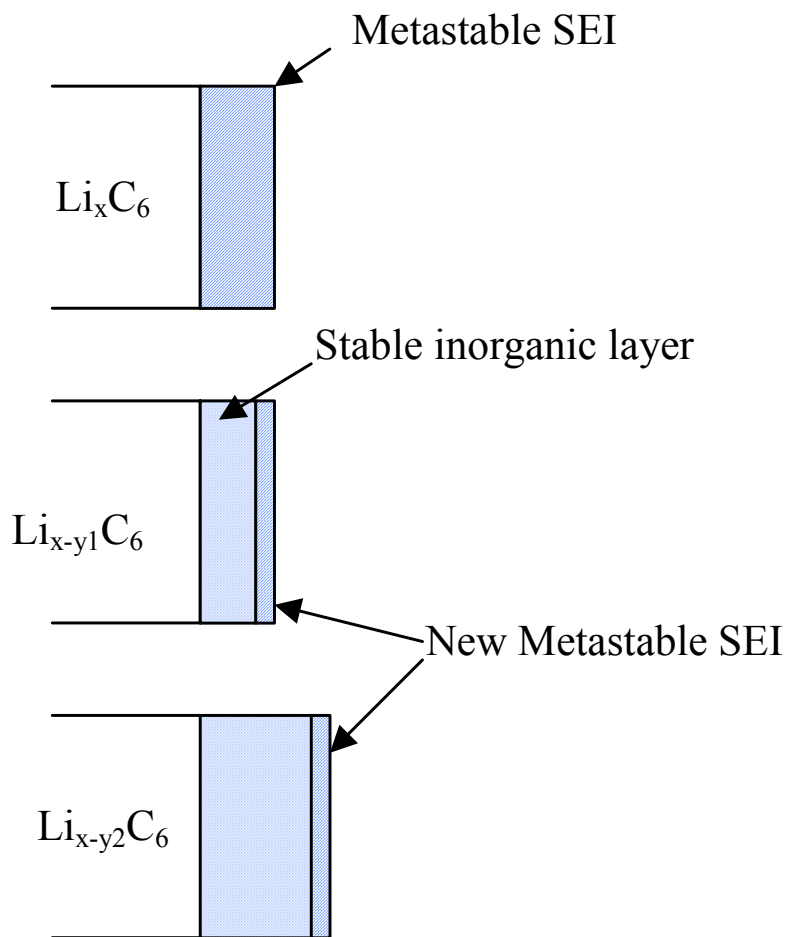is believed to be responsible for the low temperature heat output that initially drives the cell towards uncontrolled thermal runaway. As this SEI develops in time, it becomes thicker and provides greater coverage over the entire carbon particle surfaces. The exothermic reactions decay with time as we saw with our microcalorimetry measurements and result in a more stable cell as we saw from our ARC runs of aged cells. The effectiveness of this SEI layer in preventing reduction of the electrolyte depends on the particular chemistry of a given cell and also on the morphology of the carbon particles. Figure 7-2 illustrates this process. The metastable layer converts to a more stable inorganic layer but Li diffusion through the SEI layer still forms an outer surface metastable layer that can undergo further reaction.

The development of the SEI layer with time is also complicated by the development of polymeric hydrocarbons that form a porous coating on both anode and cathode. This polymer film can result from decomposition of the electrolyte to give poly(ether/carbonate) chains that we measured in the electrolyte by LC/MS. This film can affect cell performance and also contribute to exothermic decomposition at higher temperatures. With time and increased temperature these polymer films decompose to form PEO-type polymers with a resultant generation of CO_2 gas [8].

Heating of the anode initially results in increased reaction of the SEI formation process. At higher temperatures the SEI layer decomposes exothermically and then allows further exothermic reduction of the electrolyte. We have shown by DSC measurements that the electrolyte reacts exothermically with the SEI layer. Rinsing the anode carbons removed part of the SEI layer and resulted in increased reaction. The exposed SEI film was reactive with both the solvent and the salt electrolyte species but the salt greatly increased the magnitude of the reaction. This reaction even occurred for delithiated carbon indicating that the base-level SEI components (possibly carbonates and other salt products) are highly reactive. The SEI decomposition reaction occurs around 125°C but can occur anywhere between 100°C and 140°C depending on the development of the film and the carbon particle morphology. Gas generation below 125°C is limited primarily to heating of the formation gases and increased vaporization of the volatile linear carbonate species.

SEI Decomposition Reactions

Metastable SEI

Li_xC_6

Stable inorganic layer

$Li_{x-y1}C_6$

New Metastable SEI

$Li_{x-y2}C_6$

Initial cycling

Li_xC_6 + alkyl carbonate/$LiPF_6$ $\longrightarrow$ $ROCO_2Li$ + parent alkene

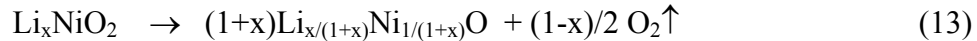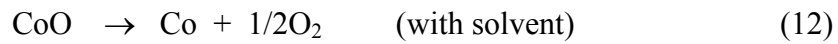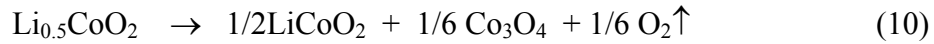**Figure 7-2.   Proposed mechanism of SEI formation and development**

Above the SEI decomposition temperature the electrolyte is reduced by the lithiated anode. This exothermic reaction increases with increasing temperature during which the lithium in the anode is consumed and the electrolyte is decomposed. The anode film is quite porous and allows from 60wt% and 100wt% of electrolyte to penetrate the pores and react with the high surface area carbon particles. The salt is quite reactive, as we have already reported and as has been reported by other researchers [8,10]. The result of this reaction is a reduction in the molarity of the electrolyte in the pores and reduced gas generation by the unreacted electrolyte with increasing temperature. The reacted anode layer eventually breaks down completely around 225°C with a resultant peak in heat and gas generation. The evolved gas products are very similar to the pure electrolyte decomposition gases with additional generation of H_2 and CO. Measurement of the anode decomposition products at these temperatures indicate that a thick non-conducting layer has developed consisting primarily of salt decomposition products such as LiF and possibly Li_2O [8]. Thus, the thermal stability of the anode is largely determined by salt decomposition reactions.

7.2.2 Cathode Reaction Mechanisms

Cathode contributions to cell thermal runaway primarily occur at higher temperatures and do not contribute to the initial exothermic output that can drive the cell to more reactive temperatures. Below 125°C the cathode structures for all of the cells studied here are stable and do not react significantly with the electrolyte. At high SOCs some oxidation of the electrolyte may occur and contribute to the SEI-like polymer film that has been measured on the oxide particles. However, no significant heat generation has been reported.

Cathode decomposition has been observed as low as 140°C accompanied by heat and gas generation. The delithiated metal oxide particles can undergo decomposition to generate O_2 and reduced metal oxides. The nickelate and cobaltate cathode materials have been reported to undergo the following reactions [13,14]:

$$Li_{0.5}CoO_2 \;\; \rightarrow \;\; 1/2LiCoO_2 \; + \; 1/6\, Co_3O_4 \; + 1/6\, O_2\uparrow \qquad\qquad (10)$$

$$Co_3O_4 \;\; \rightarrow \;\; 3CoO \; + 1/2O_2\uparrow \qquad\qquad (11)$$

$$CoO \;\; \rightarrow \;\; Co \; + \; 1/2O_2 \qquad \text{(with solvent)} \qquad\qquad (12)$$

$$Li_xNiO_2 \;\; \rightarrow \;\; (1+x)Li_{x/(1+x)}Ni_{1/(1+x)}O \; + (1-x)/2\, O_2\uparrow \qquad\qquad (13)$$

The $Li_xNi_{0.85}Co_{0.15}O_2$ and the Al doped oxide most likely undergo reaction similar to the nickelate. The generated oxygen results in combustion of the solvent according to the reaction:

$$\text{(EC): } CH_2OCOOCH_2 + 5/2\, O_2 \;\; \rightarrow \;\; 3CO_2 \; + \; 2H_2O \qquad\qquad (14)$$

The exothermic reaction of the cathode oxide in the presence of electrolyte results from this combustion as we measured by DSC and ARC. The reaction rate increases with increasing temperature and drops suddenly when the cathode decomposition reaction no longer produces oxygen. Increasing the ratio of electrolyte to oxide film weight does not increase this combustion reaction. However, excess electrolyte can result in a higher temperature

129

exotherm corresponding to the complete reduction of the metal oxide to the metallic phase as shown in Eq. 11. We also believe that the decomposition reaction of the cathode oxide is itself exothermic since we measured considerable heat output in the ARC bombs without the presence of added electrolyte. The degree of the exothermic reaction is highly SOC dependent largely as a result of the SOC dependent gas generation as indicated in Eq. 12. However, the peak reaction temperature was seen to shift to higher temperatures with decreasing SOC indicating that there may be oxidation state dependent decomposition of the electrolyte.

Gas generation from cathode/electrolyte reaction showed essentially the same gas species as for the straight electrolyte decomposition. No excess oxygen generation was measured indicating that all of the oxygen was consumed by solvent combustion yielding only CO_2, which is already a major electrolyte decomposition gas.
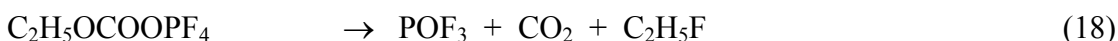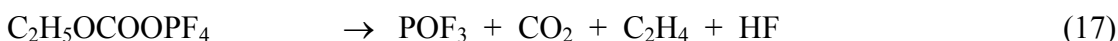
7.2.3   *Electrolyte Decomposition*

The electrolyte has been shown to be a significant source of heat and gas generation. As we have just discussed, the electrolyte can have significant reactions with the anode and cathode materials. We have also shown that the electrolyte can decompose at elevated temperatures to yield further heat and gas as a part of the overall thermal runaway reaction.

The electrolyte can also undergo decomposition reactions at low temperatures to yield both gaseous and solid products that can affect the performance of the electrode materials. EC reactions are responsible for the formation of the SEI layer on the anode and are critical to developing an operable Li-ion cell. The reactions with the EC component are also responsible for the exothermic decomposition of the full electrolyte and increase the gas generation by the EMC. The $LiPF_6$ is know to be unstable and reacts to produce PF_5, which acts as a strong Lewis acid. LBNL has proposed that EC can undergo a ring-opening reaction with PF_5 according to the reaction shown in Figure 7-3. The terminal radicals in this opened structure can continue to react with other EC molecules resulting in further ring opening and the formation of oligo-ether carbonates chains. These chains can then decompose through a de-carboxylation process to form PEO polymer chains and CO_2. This PEO film has been reported to form part of the chemical coatings on anodes and cathodes [8].

The ring-opened EC can also react with the linear EMC molecules to yield EMDOHC as shown in Figure 7-4. As was stated earlier, the EMC, unsymmetrical chain alkyl carbonate solvent has been shown to be inherently unstable and forms an equilibrium balance with the symmetrical linear alkyl carbonates through an alkyl exchange reaction to yield DMC and DEC. Thus, the ring opened EC will also react with these linear molecules to produce DMDOHC and DEDOHC. These dimers can also undergo de-carboxylation to form oligo-ether carbonate chains and eventually polyethers (like PEO) as indicated in Figure 7-5

Higher temperature greatly increases the rate of the low-temperature reactions and leads to new reaction paths and products. We have shown that gas generation begins above 150°C likely arising from reaction of $LiPF_6$ products such as PF_5 with the linear alkyl carbonate component. This reaction is enhanced by the presence of the EC component, which may have already reacted with the PF_5. The 1.2M $LiPF_6$ salt concentration is sufficient to cause maximum decomposition of the EMC in the presence of EC. Higher molarities do not increase the amount of gas generated. The decomposition gases consist of CO_2, ethylene, and

ethyl fluoride. No CO or CH_4 are generated. Figure 7-6 illustrates the possible bond breaking reactions that can lead to these gas species. PF_5 is a strong Lewis acid that attacks regions of higher electron density. The oxygen bond with the ethyl group will have greater electron density than will the bond with the methyl group and thus will preferentially dissociate from the EMC molecule. The gas species can be either C_2H_4 or it can react with the PF_5 to give ethyl fluoride both of which have been measured. The remaining gas species is CO_2 that is the dominant gas species at all temperatures and conditions. Reactions have been proposed for the $LiPF_6$/DEC electrolyte leading to these gaseous products that are probably valid for other ethyl-group carbonate solvents [17].

$$C_2H_5OCOOC_2H_5 + PF_5 \rightarrow C_2H_5OCOOPF_4 + HF + C_2H_4 \qquad (15)$$

$$C_2H_5OCOOC_2H_5 + PF_5 \rightarrow C_2H_5OCOOPF_4 + C_2H_5F \qquad (16)$$

$$C_2H_5OCOOPF_4 \rightarrow POF_3 + CO_2 + C_2H_4 + HF \qquad (17)$$

$$C_2H_5OCOOPF_4 \rightarrow POF_3 + CO_2 + C_2H_5F \qquad (18)$$

All of these gas species have been measured as part of the electrolyte decomposition products.

The electrolyte thus plays a critical role in the thermal response of the cell and is a major source of the exothermic reactions that lead to cell thermal runaway and gas generation. Any improvement in cell thermal stability needs to address improvements in electrolyte reactivity and in particular improvements in salt stability.

$$LiPF_6 \longrightarrow LiF + PF_5$$

✔ CO_2 production is enhanced.

✔ H_2 and C_2H_4 productions are also enhanced.

✔ No CO

✔ Thermally activated.
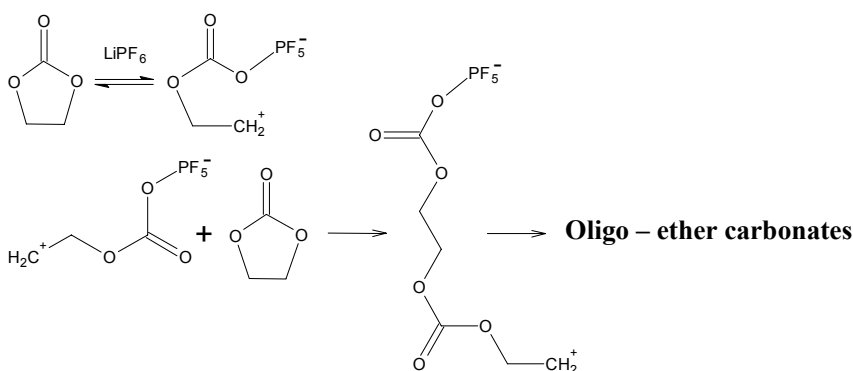
Figure 7-3. **LiPF₆ assisted EC ring opening reaction leading to PEO polymer and CO₂ products.**
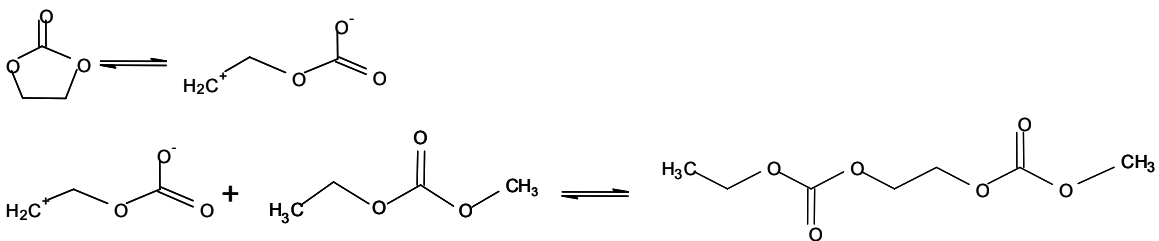
Figure 7-4. Reaction of a linear carbonate with EC to produce dimeric species, EMDOHC.

"DEDOHC"
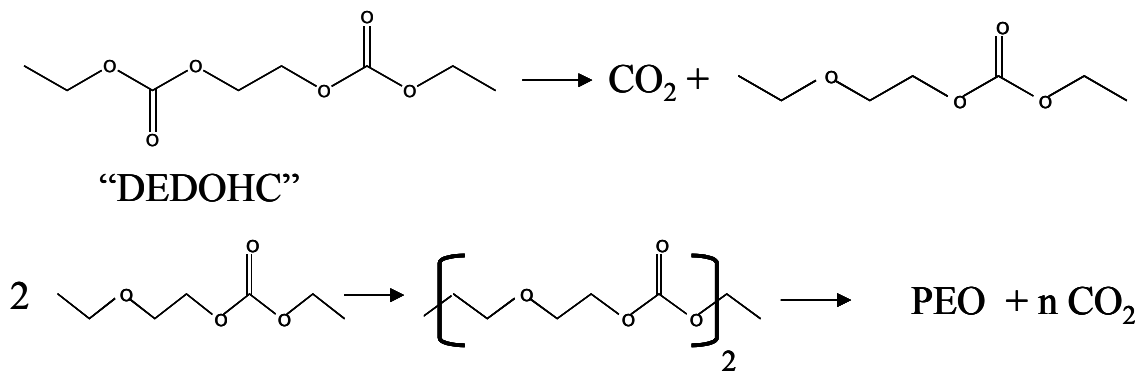
Figure 7-5. Elimination of CO2 from poly(carbonates) produces poly(ether-carbonates) and eventually polyethers (like PEO).

Thermal Decomposition of Solvents
- assisted by LiPF$_6$ and ring-opened EC

Monomers, Dimers and Trimers seen by LC/MS

EMC

CO$_2$ CH$_3$OH, etc.

C$_2$H$_2$
C$_2$H$_5$F   Minimal CH$_4$
C$_2$H$_6$

Figure 7-6.   Thermal decomposition of EMC assisted by LiPF$_6$ and EC.

8.0　References

1.　Manager: Tien Duong, Department of Energy, Office of FreedomCAR & Vehicle Technologies, Office of Energy Efficiency and Renewable Energy, http://www.eere.energy.gov/vehiclesandfuels/pdfs/program/2002_energy_storage.pdf
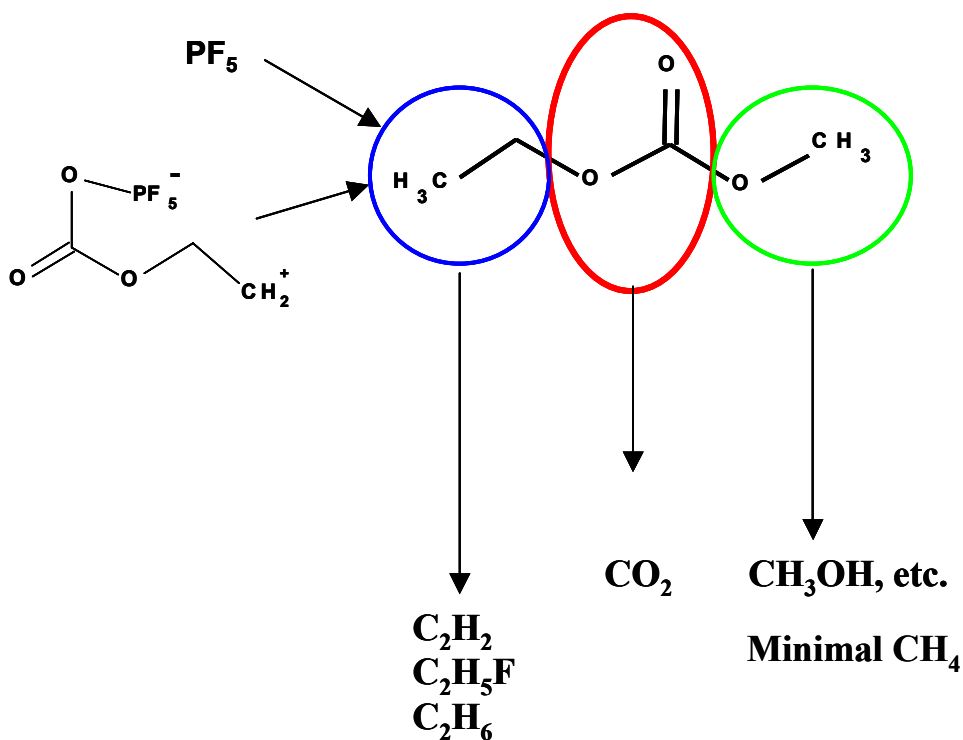2.　PolyStor Corp., 230 S. Vasco Road, Livermore, CA 94550.
3.　Quallion LLC, PO Box 923127, Sylmar, CA 91392-3127.
4.　U. von Sacken, E. Nodwell, A. Sundher, and J. R. Dahn, *J. Power Sources*, **54**, 240-245 (1995).
5.　M. N. Richard and J. R. Dahn, *J. Electrochem. Soc.*, **146**, 2068-2077 (1999).
6.　M. N. Richard and J. R. Dahn, *J. Electrochem. Soc.*, **146**, 2078-2084 (1999).
7.　P. Arora, R. White, and M. Doyle, *J. Electrochem. Soc.*, **145**, 3647-3667 (1998).
8.　A. M. Andersson, M. Herstedt, A. G. Bishop, K. Edstrom, Electrochimica Acta **47**, 1885-1898 (2002).
9.　A. Du Pasquier, F. Disma, T. Bowmer, A. S. Gozdz, G. Amatucci, and J-M Tarascon, *J. Electrochem. Soc.*, **145**, 472-477 (1998).
10.　Z. Zhang, D. Fouchard, J. R. Rea, J. Power Sources **70**, 16-20 (1998).
11.　J. Yamaki, H. Takatsuji, T. Kawamura, and M. Egashira, Solid State Ionics **148**, 241-245 (2002).
12.　D. D. MacNeil, T. D. Hatchard, and J. R. Dahn, *J. Electrochem. Soc.*, **148**, A663-A667 (2001).
13.　H. Arai, M. Tsuda, K. Saito, M. Hayashi, and Y. Sakurai, *J. Electrochem. Soc.*, **149**, A401-A406 (2002).
14.　D. D. MacNeil, T. D. Hatchard, and J. R. Dahn, *J. Electrochem. Soc.*, **149**, A912-A919 (2002).
15.　Y. Baba, S. Okada, and J. Yamaki, Solid State Ionics 148, 311-316 (2002).
16.　G. Botte, R. White, Z. Zhang, J. Power Sources **97-98**, 570-575 (2001).
17.　T. Kawamura, A. Kimura, M. Egashira, S. Okada, and J. Yamaki, , J. Power Sources **104**, 260-264 (2002).
18.　"PNGV Battery Test Manual", DOE/ID-10597 Rev. 3 (Feb. 2001).
19.　SEM micrographs provided by Argonne National Laboratory.
20.　H. Yoshida, T. Fukunaga, T. Hazama, M. Terasaki, M. Mizutani, and M. Yamachi, J. Power Sources **68**, 311-315 (1997).
21.　 X. Zhang, P.N. Ross, Jr., R. Kostecki, F. Kong, S. Sloop, J. Kerr, K. Streibel, E.J. Cairns, and F. McLarnon, *J. Electrochem. Soc.*, **148**, A463-A470 (2001).
22.　D. Aurbach, , J. Power Sources **89,** 206-218 (2000).
23.　K. Kumai, H. Miyashiro, Y. Kobayashi, K. Takei, and R. Ishikawa, J. Power Sources **81-82,** 715-719 (1999).
24.　C. R. Yang, Y. Y. Yang, and C. C. Wan, , J. Power Sources **72,** 66-70 (1998).
25.　C. Lee, B. Munn, and P. N. Ross, Jr., *J. Electrochem. Soc.*, **149**, A1286-A1292 (2002).

9.0 Distribution List

Vince Battaglia
Agronne National Lab
955 L'Enfant Plaza SW
Suite 6000
Washington, DC 20024

Khalil Amine
Argonne National Laboratory
9700 South Cass Ave.
Bldg. 205
Argonne, IL 60439-4837

Ira Bloom
Argonne National Laboratories
9700 South Cass Avenue
CTD, Bldg. 205
Lemont, IL 60439-4837

Dennis W. Dees
Argonne National Laboratory
9700 South Cass Avenue, Bldg. 205
Argonne, IL 60439-4837

Gary L. Henriksen
Argonne National Laboratory
9700 South Cass Avenue, Bldg.
205
Argonne, IL 60439-4837

Daniel Abraham
Argonne National Laboratory
9700 South Cass Avenue, Bldg. 205
Argonne, IL 60439-4837

Andrew Jansen
Argonnne National Lab
9700 S. Cass Ave.
Argonne, IL 60439-

T. Richard Jow
Army Research Lab
AMSRL-SE-DE
2800 Powder Mill Rd
Adelphi, MD 20783-1197

George Blomgren
Blomgren Consulting Services,
Ltd.
1554 Clarence Avenue
Lakewood, OH 44107

Ralph J. Brodd
Broddarp of Nevada, Inc.
2161 Fountain Springs Dr.
Henderson, NV 89074

James McBreen
Brookhaven National Lab
Energy Sciences and Technology
Dept.
Bldg. 555
Upton, NY 11973-5000

Enoch I. Wang
CIA
Central Intelligence Agency
2R4502 NHB
Washington, DC 20505

Mohamed Alamgir
Compact Power, Inc.
1200 South Synthes Avenue
Monument, CO 80132

Robert W. Minck
Consultant
24161 Becard Drive
Laguna Beach, CA 92677

William H. Tiedemann
Consultant
394 Douglas
Cedarburg, WI 53012

Cyrus N. Ashtiani
DaimlerChrysler Corp.
2730 Research Drive
Rochester, MI 48309

Vesselin G. Manev
Delphi Automotive Systems
Mail Code 485-220-130
1601 N. Averill Avenue
Flint, MI 48556

Tien Q. Duong
Department of Energy
1000 Independence Ave. SW
EE-32 FORSTL, Rm. 5F-034
Washington, DC 20585

David Howell
Department of Energy
1000 Independence Ave. SW
EE-32 FORSTL, Rm. 5F-034
Washington, DC 20585

Bijayendra (BJ) Kumar
Energetics, Inc.
7164 Gateway Drive
Columbia, MD 21046

Harold J. Haskins
Engineering Consultant
3569 NW Thrush Drive
Corvallis, OR 97330

Keith D. Kepler
Farasis Energy, Inc.
851 West Midway Avenue
Alameda, CA 94501

Theodore J. Miller
FORD Motor Corp.
Alternative Fuel Vehicle Center
15050 Commerce Drive North
Dearborn, MI 48120

William H. Schank
FORD Motor Company
Sustainable Mobility Technology Lab-1
15050 Commerce Drive North
Dearborn, MI 48120

M. Ahsan Habib
General Motors Corporation
Research & Development Center
Mail Code 480-106-224
30500 Mound Road
Warren, MI 48090-9055

Harshad S. Tataria
General Motors Corporation
Mail Code: 480-111-S52
P.O. Box 9010
30200 Mound Road
Warren, MI 48090-9010

Kevin Leslie Gering
Idaho Nat'l Eng & Env. Lab
MS 3830
P.O. Box 1625
Idaho Falls, ID 83415-3830

Chet Motloch
Idaho Nat'l Eng & Env. Lab
MS 3830
P.O. Box 1625
Idaho Falls, ID 83415-3830

John B. Deppe
Independent Consultant
2522 Hobbits Lane
Davidsonville, MD 21035

Jon P. Christophersen
INEEL
P.O. Box 1625
MS-3830
Idaho Falls, ID 83415-3830

Michael G. Andrew
Johnson Controls, Inc.
Automotive Systems Group
5757 North Green Bay Avenue
P.O. Box 591
Milwaukee, WI 53201-0591

John B. Kerr
Lawrence Berkeley Nat'l Lab
One Cyclotron Rd.
MS62-203
Berkeley, CA 94720

Frank McLarnon
Lawrence Berkeley National Lab
University of California
One Cyclotron Road
Berkeley, CA 94720

K. M. Abraham
Lithion Inc.
82 Mechanic Street
Pawcatuck, CT 06379-2154

Joe DiCarlo
Lithion/Yardney
82 Mechanic Street
Pawcatuck, CT 06379

Ahmad A. Pesaran
National Renewable Energy Laboratory
1617 Cole Boulevard
Golden, CO 80401-3393

Joseph Stockel
National Reconnaissance Office
14675 Lee Rd.
Chantilly, VA 20151

Peter B. Keller
Naval Surface Warfare Center
Code-683 Carderock Div.
9500 MacArthur Blvd.
West Bethesda, MD 20817-5700

Azzam N. Mansour
Naval Surface Warfare Center-
Carderock
9500 MacArthur Boulevard
Code 644
West Bethesda, MD 20817-5700

Hisashi Tsukamoto
Quallion, LLC
12744 San Fernando Rd.
Bldg. 4
Sylmar, CA 91392-3127

Thanh N. Tran
Sentech, Inc.
4733 Bethesda Avenue
Suite 608
Bethesda, MD 20814

Irwin Weinstock
Sentech, Inc.
4733 Bethesda Avenue
Suite 608
Bethesda, MD 20814

Joseph E. Doninger
Superior Graphite Company
Department of Technology
10 South Riverside Plaza
Suite 1600
Chicago, IL 60606

James A. Barnes
US Department of Energy
1000 Independence Avenue SW
Office of FreedomCAR & Vehicle Tech
Washington, DC 20585

MS-0512/02500	Tom Blejwas
MS-0521/02501	Wendy Cieslak
MS-0613/02521	Daniel H. Doughty
MS-0613/02521	Chris Crafts
MS-0613/02521	Emanuel Pete Roth
MS-0613/02521	Ganesan Nagasubramanian
MS-0829/12323	Edward V. Thomas
MS-0899/09616	Technical Library (2)
MS-9018/08945-1	Central Technical Files